

*LRP4 Regulates Dendritic Arborization and  
Synapse Formation in the Central Nervous System  
Neurons.*

**Dissertation**

Zur Erlangung des Doktorgrades (Dr.rer.nat) der Fakultät für Biologie an  
der Ludwig-Maximilians Universität München



Angefertigt in der Arbeitsgruppe von Prof. Dr. Magdalena Götz am Institut  
für Physiologische Genomik, LMU München

**Andromachi Karakatsani**

2015





## Eidesstattliche Erklärung

Ich versichere hiermit an Eides statt, dass die vorgelegte Dissertation von mir selbstständig und ohne unerlaubte Hilfe angefertigt worden ist. Des Weiteren erkläre ich, dass die Dissertation nicht ganz oder in wesentlichen Teilen einer anderen Prüfungskommission vorgelegt worden ist und dass ich mich nicht anderweitig einer Doktorprüfung ohne Erfolg unterzogen habe.

München, den 08.12.2015

1. Gutachter: Prof. Dr. Hans Straka

2. Gutachter: Prof. Dr. Anja Horn-Bochtler

Tag der Abgabe: 08.12.2015

Tag der mündlichen Prüfung: 25.04.2016

**For my parents**





# Table of Contents

<b>Abstract.....</b>	<b>10</b>
<b>Zusammenfassung .....</b>	<b>11</b>
<b>1 Introduction .....</b>	<b>13</b>
<b>1.1 Neurons and synapses .....</b>	<b>13</b>
1.1.1 Historical perspective .....	13
<b>1.2 Neurons: the basic functional units of the brain.....</b>	<b>13</b>
<b>1.3 Overview of dendrite and spine development .....</b>	<b>14</b>
1.3.1 Spines .....	15
<b>1.4 Overview of synapse formation.....</b>	<b>17</b>
1.4.1 Synaptic specializations of dendrites/Synaptic structure and function.....	17
<b>1.5 The neuromuscular junction .....</b>	<b>18</b>
1.5.1 Development of the neuromuscular junction .....	18
1.5.2 The family of low-density lipoprotein receptors and LRP4.....	21
<b>Aim of the study .....</b>	<b>27</b>
<b>2 Materials and Methods.....</b>	<b>29</b>
<b>2.1 Materials.....</b>	<b>29</b>
2.1.1 Primary antibodies.....	29
2.1.2 Secondary antibodies .....	31
2.1.3 Buffers and solutions .....	31
2.1.4 Media.....	35
2.1.5 Cell lines .....	35
2.1.6 Oligonucleotides .....	35
2.1.7 Plasmids.....	36
<b>2.2 Methods .....</b>	<b>37</b>
2.2.1 DNA/RNA methods .....	37
2.2.2 Biochemical methods.....	38
2.2.3 Cell culture methods .....	39
2.2.4 Animals .....	41
2.2.5 Image collection and quantitative analysis .....	42
<b>3 Results .....</b>	<b>43</b>
<b>3.1 Antibodies against LRP4 .....</b>	<b>43</b>
3.1.1 Immunocytochemistry of HEK293 cells .....	44
3.1.2 Western blotting.....	45
3.1.3 Immunohistochemistry of the NMJ .....	46
<b>3.2 LRP4 expression and localization in the adult murine brain.....</b>	<b>48</b>
3.2.1 Reverse transcription PCR.....	48
3.2.2 Western blotting.....	48
3.2.3 Immunohistochemistry .....	49
<b>3.3 LRP4 distribution in neuronal cultures .....</b>	<b>55</b>
3.3.1 LRP4 is localized in somas, dendrites and axons of cultured hippocampal neurons	56
3.3.2 Both glutamatergic and GABAergic neurons express LRP4.....	58
3.3.3 LRP4 in astrocytes.....	59
<b>3.4 Function of LRP4 in neuronal cultures .....</b>	<b>60</b>
3.4.1 Overexpression of LRP4 in neurons.....	60
3.4.2 Overexpression of LRP4 affects dendritic development and synapse formation in vitro	61
3.4.3 Time lapse analysis of E14 cortical neurons overexpressing LRP4 .....	63
3.4.4 Overexpression of LRP4 increases the number of synapses .....	64
3.4.5 Generation of microRNAs for the knockdown of LRP4 in vitro.....	66

3.4.6	Knockdown of LRP4 affects dendritic development and synapse formation in vitro	68
3.4.7	Knockdown of LRP4 reduces the number of direct presynaptic partners in dissociated neuronal cultures.....	69
3.5	<b>TM-agrin is required for the LRP4-mediated effect on dendritic development ..</b>	70
3.6	<b>LRP4-mediated effects on dendritic development are ameliorated by soluble agrin and are independent of MuSK .....</b>	73
4	<b>Discussion.....</b>	75
4.1	Expression of LRP4 in the murine brain.....	76
4.2	The role of LRP4 in dendrite formation .....	77
4.3	The role of LRP4 in spine and synapse formation .....	78
4.4	Agrin and LRP4 might act together to regulate dendritic development.....	79
4.5	Functional consequences of LRP4 knockdown in CNS neurons .....	80
4.6	Conclusions and future prospects.....	80
5	<b>Bibliography .....</b>	82
6	<b>Appendix .....</b>	93
6.1	Appendix 1: List of abbreviations .....	93
6.2	Appendix 2: List of figures .....	95
6.3	Appendix 3: List of tables .....	97
6.4	Appendix 3: Plasmid maps.....	99
6.4.1	pCMV-LRP4-IRES-eGFP .....	99
6.4.2	pSYN-LRP4.....	99
6.4.3	pcDNA6.2-GW/EmGFP.....	100
6.4.4	pcDNA6.2-GW/mir1232 .....	100
6.4.5	pcDNA6.2-GW/mir1544 .....	101
6.4.6	pcDNA6.2-GW/mir6854 .....	101
6.4.7	pcDNA6.2-GW/mir7072 .....	102
6.4.8	pcDNA6.2-GW/mir1232_1544 .....	102
6.4.9	pENTR1A_mir1232_1544.....	103
6.4.10	pCAG-miR-RFP .....	103
	<b>List of publications .....</b>	105
	<b>Acknowledgements .....</b>	107
	<b>Curriculum Vitae.....</b>	109



## Abstract

The formation, maintenance and plasticity of synapses are essential for neural circuit development and the functionality of the central nervous system (CNS). While synaptogenesis is relatively well characterized at the neuromuscular junction (NMJ; Wu et al., 2010), the molecular determinants orchestrating synapse formation in the CNS are complex and not fully understood. The existence of organizational proteins common to both the NMJ and CNS synapses, however, suggests that the development of both synapses might share common pathways.

A key regulator for synapse development at the NMJ is the low-density lipoprotein receptor-related protein 4 (LRP4; Weatherbee et al., 2006; Yumoto et al., 2012; Wu et al., 2012). At the NMJ LRP4 forms a complex with the muscle-specific tyrosine kinase MuSK, which serves as the receptor for the extracellular matrix protein agrin (Kim et al., 2008; Zhang et al., 2008). This interaction leads to the formation of most if not all pre- and postsynaptic specializations and the establishment of synaptic connectivity.

Recent studies suggest functions for LRP4 in the adult CNS, including hippocampal synaptic plasticity, fear-conditioning, associative and spatial learning, and LTP as well as maintenance of excitatory synaptic transmission (Gomez et al., 2014; Pohlkamp et al., 2015). Accordingly, *lrp4* mRNA is present in the neocortex, hippocampus, cerebellum and olfactory bulb (Tian et al., 2006; Lein et al., 2007). However, the localization of LRP4 protein and the molecular mechanisms underlying its function in the CNS have not been investigated.

In my thesis I analyzed the role of LRP4 in the CNS. I generated two rabbit antibodies against an intracellular and an extracellular epitope and determined the distribution of LRP4 in the CNS. I show that LRP4 is expressed in the adult CNS and is concentrated at synapses of many, but not all, neurons. Glial cells, as well as neurons generated during adult neurogenesis, do not express LRP4. Overexpression of LRP4 in embryonic cortical and hippocampal neuronal cultures resulted in the formation of more and shorter primary dendrites with an increased density of synapse-like specializations, whereas knockdown of LRP4 in these neurons resulted in reduced number of spine-like protrusions and in fewer presynaptic specializations but increased the length of the dendrites. Virus-mediated transsynaptic tracing revealed a reduced number of functional synaptic contacts in cortical neurons after knockdown of LRP4. These effects could be inhibited by soluble agrin as well as by anti-agrin antibodies. The effect on dendritogenesis was independent of MuSK since it also occurred in neurons from MuSK *-/-* mice. My results demonstrate an important role of LRP4 in dendritic arborization and synaptogenesis in developing CNS neurons and suggest different mechanisms of action of LRP4 at interneuronal synapses compared to the neuromuscular junction.



## Zusammenfassung

Die Bildung, Aufrechterhaltung und Plastizität von Synapsen ist essentiell für die Entwicklung von neuronalen Schaltkreisen und die Funktionalität des Zentralen Nervensystems (ZNS). Während die Bildung von Synapsen an der Neuromuskulären Endplatte (NMJ) bereits relativ gut charakterisiert wurde (Wu et al., 2010), ist der Kenntnisstand über die Synaptogenese im ZNS nur rudimentär. Allerdings deutet die Existenz von Schlüsselorganisatoren, die bei der Bildung von beiden Synapsentypen eine wichtige Rolle spielen, auf gemeinsame Mechanismen hin.

Ein Schlüsselregulator der Synapsenbildung an der NMJ ist LRP4 („low-density lipoprotein receptor-like protein-4“; Weatherbee et al., 2006; Yumoto et al., 2012; Wu et al., 2012). An der NMJ bildet LRP4 einen Komplex mit der Tyrosinkinase MuSK („muscle-specific kinase“), welcher als Rezeptor für das extrazelluläre Matrixprotein Agrin dient (Kim et al., 2008; Zhang et al., 2008). Diese Interaktion führt letztendlich zur Bildung von allen prä- und postsynaptischen Spezialisierungen und folgend zur Etablierung der synaptischen Transmission.

Kürzlich konnte gezeigt werden, dass LRP4 zusätzlich Funktionen im adulten ZNS besitzt, zum Beispiel bei der Regulierung synaptischer Plastizität im Hippocampus, bei Furcht-Konditionierung, assoziativem und räumlichem Lernen, bei LTP und bei der Etablierung der synaptischen Kommunikation (Gomez et al., 2014; Pohlkamp et al., 2015). Dementsprechend wird *lrp4* mRNA im Neokortex, Hippocampus, Kleinhirn und Bulbus olfactorius exprimiert (Tian et al., 2006; Lein et al., 2007). Die Verteilung des LRP4 Proteins und die molekularen Mechanismen, die der Funktion von LRP4 im sich entwickelnden und adulten ZNS zugrunde liegen, wurden allerdings noch nicht analysiert.

In meiner Arbeit habe ich die Rolle von LRP4 im sich entwickelnden ZNS untersucht. Ich habe zwei Antiseren aus Kaninchen gegen den intrazellulären- respektive den extrazellulären Teil von LRP4 hergestellt und mit ihnen die Verteilung von LRP4 im Gehirn untersucht. Ich zeige in meiner Arbeit, dass LRP4 im adulten Gehirn exprimiert wird und an vielen, aber nicht allen Synapsen konzentriert ist. Gliazellen sowie Nervenzellen, die während der adulten Neurogenese gebildet werden, exprimieren LRP4 nicht. Überexpression von LRP4 in Nervenzellen des embryonalen Hippocampus und Kortex bewirkt die Bildung von mehr, aber kürzeren primären Dendriten, die eine höhere Dichte von Synapsen-ähnlichen Spezialisierungen besitzen. Im Gegensatz dazu bewirkt eine stark reduzierte LRP4 Expression die Bildung von weniger Dornen-ähnlichen Fortsätzen und einer geringeren Anzahl von präsynaptischen Spezialisierungen, aber eine größere Dendritenlänge. Virus-vermittelte transsynaptische Markierungen zeigen eine reduzierte Anzahl von funktionellen synaptischen Kontakten in Kulturen von kortikalen

Nervenzellen nach knockdown der LRP4 Expression. Dieser Effekt konnte durch Zugabe von löslichem Agrin oder von funktionshemmenden anti-Agrin Antiseren gehemmt werden. Der Effekt von LRP4 knockdown war unabhängig von MuSK, da er auch in Neuronen aus MuSK  $-/-$  Mäusen auftrat.

Diese Ergebnisse zeigen eine wesentliche Funktion von LRP4 während der Bildung des Dendritenbaumes und der Synaptogenese im ZNS und deuten darauf hin, dass der molekulare Mechanismus der LRP4 Funktion während der Synaptogenese von interneuronalen Synapsen des ZNS anders ist, als an der NMJ.

# 1 Introduction

## 1.1 Neurons and synapses

### 1.1.1 Historical perspective

“... the nerve elements possess reciprocal relationships *in contiguity* but not *in continuity*. It is confirmed also that those more or less intimate contacts are always established, not between the nerve arborizations alone, but between these ramifications on the one hand, and the body and protoplasmic processes on the other. A granular cement, or special conducting substance would serve to keep the neuron surfaces very intimately in contact.” (Cajal, 1906).

The discovery of how the nervous system is organized and works at the cellular level is one of the most fascinating in the history of science. One of the great pioneers of neuroscience was Santiago Ramon y Cajal, the first to demonstrate that the nervous system consists of individual neurons among which information flows at sites of contacts.

Cajal’s histological findings were complemented by the electrophysiological work of Sir Charles S. Sherrington. In 1907, the British physiologist had shown that there is an electrical discontinuity in the circuitry of the nervous system, a “discrete gap” between nerve cells, and named this gap the ‘synapse’, from the Greek words *syn*, meaning ‘together’, and *haptein*, meaning ‘to clasp’.

Three decades later, Otto Loewi published his famous experiment, which provided the first reliable evidence for existence of chemical transmission in a synapse. By the 1920s, the scientific community was convinced that nerve signals were electrical, and that nerves behaved like wires. Loewi used two frog hearts to demonstrate, in favor of Cajal’s theory, that the vagus nerve produced its effect on the heart by secreting a chemical substance. It was later found that this substance was acetylcholine.

However, although most scientists accepted the neuron doctrine of Cajal, the definitive morphological proof for the synapse came only in the 1950s with the invention of the electron microscope that allowed the examination of the nervous tissue in higher magnification and revealed the synaptic ultrastructure.

## 1.2 Neurons: the basic functional units of the brain

The human brain is the most complex and sophisticated organ of all biological systems. It consists of approximately  $10^{11}$  neurons associated with 5-10 times as many glial cells (Noctor et al., 2007). Even though glia outnumbers neurons by tenfold, neurons are the elementary units of the brain that perform the bulk of information processing. Despite the large number of different neuronal subtypes, all neurons share some common features: the cell body (*soma*), the dendrites, the axon, and the axon terminal. The cell body contains the nucleus and the cytoplasm

(*perikaryon*) and is involved in the neurons' main metabolic functions, as it ensures the synthesis of macromolecules required for the morphology and function of a neuron. The dendrites are cellular extensions emerging from the soma that successively branch to form a dendritic tree. Together with the soma they constitute the main receptive area of neurons, as they receive numerous synaptic contacts from other neurons. Almost every neuron has only one long and thin axon extending from the soma that undergoes extensive branching at the distal end thus enabling communication with other cells. Research in the 1950s showed that action potentials in neurons of the CNS originate at the axon hillock, a specialized unmyelinated region of the soma, which forms the beginning of the axon (Stuart et al., 1997). Following initiation, action potentials can be either transmitted away from the neuron's cell body to other neurons over long distances or backpropagate into the dendrites, thus providing a retrograde signal of neuronal output to the dendritic tree (Stuart et al., 1997).

### 1.3 Overview of dendrite and spine development

Neurons are highly polarized cells. Their two types of processes, axons and dendrites, exhibit great differences in morphology, molecular composition, microtubule polarity, and function. Primary cell cultures of neurons from the murine embryonic cortex and hippocampus provide a valuable model for studying mammalian neuronal development and polarity, as in this experimental system neurons adopt spatially and functionally distinct dendritic and axonal domains. The observation of single neurons *in vitro* revealed that they undergo morphological changes, which can be divided into five stages (**Figure 1.1**; Dotti et al., 1988). First, shortly after plating, neurons form lamellipodia in their periphery that several hours later are transformed into immature neurites, the so-called "minor processes" (stages 1 and 2). During stage 2 to 3, one of the minor processes begins to extend rapidly and differentiates into an axon, constituting the first evidence of neuronal polarity. Stage 4 is characterized by the elongation of the other minor processes, which will become dendrites, while in stage 5 the maturation of the axonal and dendritic arbors continues including dendritic branching, formation of dendritic spines and synaptogenesis.

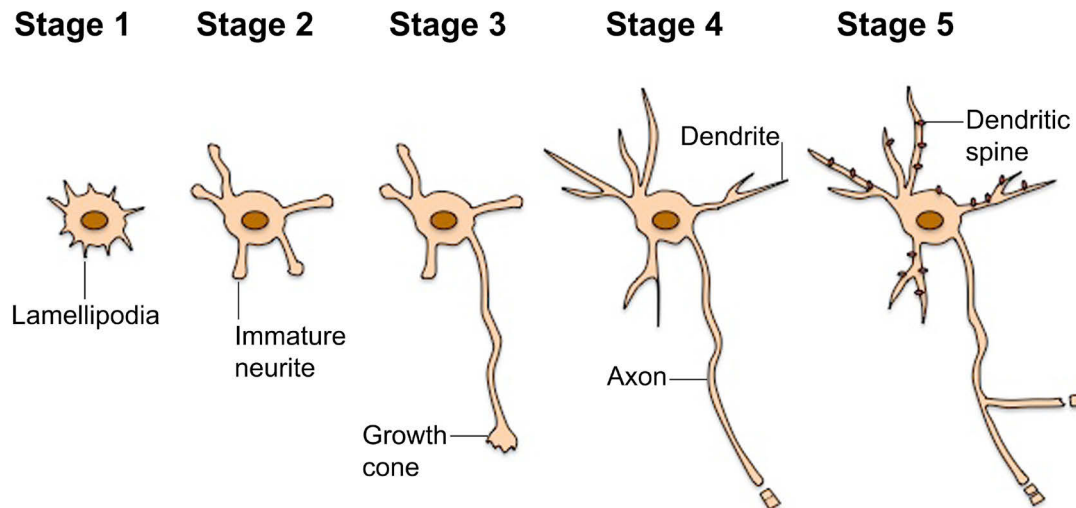


**Figure 1.1. Stages of neuronal polarization**

Schematic representation of neuronal polarization of neurons *in vitro*. Shortly after plating, the neurons form small protrusions called lamellipodia (stage 1), that develop into several immature neurites (stage 2). One neurite then breaks the initial morphological symmetry, extending at a rapid rate and establishing polarity (stage 3). The remaining neurites elongate and acquire the characteristics of dendrites (stage 4). Approximately seven days after plating, neurons form synaptic contacts through dendritic spines and axon terminals, and establish a neuronal network (stage 5). (Adapted from Arimura and Kaibuchi, 2007)

The dendritic branching patterns are hallmarks of specific neuronal cell types and constitute the major site of information processing and integration of synaptic inputs. However, the cellular and molecular mechanisms that shape the dendritic arbors and regulate dendritic field formation remain largely unknown. Transcription factors play important roles in regulating dendrite arbor development, but little is known about specific target genes that they regulate (Parrish et al., 2006, 2007). A variety of extracellular cues and their receptors are involved in dendritic outgrowth and branching. However, which intracellular signaling cascades mediate the effects of extrinsic signals that shape dendritic arbors remain unexplored (Parrish et al., 2007). Dendro-dendritic self-avoidance, tiling and coexistence contribute to the organization of the dendritic fields, but the molecular mechanisms underlying dendritic organization remain unknown (Parrish et al., 2007). Therefore, it is crucial to determine the mechanisms involved in the establishment, maintenance and remodeling of dendritic fields and to what extent defects in all the aspects of dendritic development contribute to neurological diseases.

### 1.3.1 Spines

The dendrites of most projection neurons are covered with specialized structures called dendritic spines. Dendritic spines are tiny protrusions that emerge from the dendritic shaft and represent the main unitary postsynaptic compartment for excitatory synaptic input. Dendritic spines can be categorized in five groups according to their morphology: filopodia, thin spines, short and

stubby spines, mushroom-shaped spines, and cup-shaped spines (**Figure 1.2**; Hering and Sheng, 2001). Filopodia are long ( $>2\ \mu\text{m}$ ), thin and immature protrusions, whereas mature spines typically have a round head and a narrow neck and the total spine volume ranges from less than  $0.01\ \mu\text{m}^3$  to  $0.8\ \mu\text{m}^3$  (Harris, 1994, 1999). The shape and size of spines is not static and can alter during development, but also due to neuronal activity and plasticity. For example, during early developmental stages filopodia, which are considered to be the precursors of spines, are more abundant, and later on can convert into stubby and further into the even more stable mushroom-shaped spines. According to the density of spines on dendritic processes, neurons can be classified as spiny, sparsely spiny, and aspiny (smooth; Kriegstein and Dichter, 1983). Spines contain the postsynaptic components of the synapse. These postsynaptic structures not only include AMPA- and NMDA-type glutamate receptors but also receptor interacting proteins, signal transduction molecules, and scaffolding proteins anchored in a matrix of cytoskeletal and signaling molecules. This protein dense specialization appears as an electron-dense thickening of the membrane at the synaptic junction and is therefore called postsynaptic density (PSD). Most spines contain a single, continuous PSD that corresponds to one synaptic contact. However, some PSDs appear to be intermittent or 'segmented', a condition that reflects a transition phase during spine division and the generation of two synapses from one (Hering and Sheng, 2001). This form of plasticity appears necessary for memory formation and learning. In a recent study, the dynamics of spines localized on the basal dendrites of CA1 pyramidal neurons was monitored, revealing a single population of dendritic spines with a mean lifetime of approximately 1-2 weeks (Attardo et al., 2015). This rapid turnover supports the idea that the transience of hippocampal-dependent memory directly reflects the turnover dynamics of hippocampal synapses (Attardo et al., 2015).

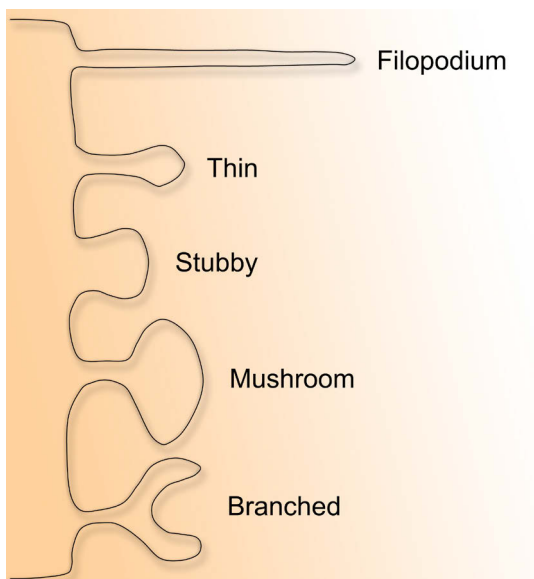


**Figure 1.2. Morphology of dendritic spines**

Different morphology of dendritic spines can be grouped into five categories: filopodia, thin spines, stubby spines, mushroom spines and branched spines. (Modified from Hering and Sheng, 2001).

## 1.4 Overview of synapse formation

### 1.4.1 Synaptic specializations of dendrites/Synaptic structure and function

Neurons are the functional units of the nervous system that interconnect into the functional neural networks underlying behavior. The capacity of a neuron to innervate and function within a network is mediated via specialized cell junctions known as synapses. There are two basic types of synapses, chemical and electrical, that are morphologically and functionally different. At chemical synapses, information flows in one direction: from one neuron via the release of neurotransmitters to an adjacent cell that detects the neurotransmitters (Pereda, 2014).

Chemical synaptic transmission occurs between an axon terminal and a dendrite or soma of a cell that can be a neuron, muscle fiber, or gland cell (Pereda, 2014). Morphologically, all types of chemical synapses share some features as they basically consist of three components: the presynapse, the synaptic cleft and the postsynapse (**Figure 1.3**). Successful chemical transmission requires elaborate presynaptic molecular machinery (collectively named presynaptic specializations) and also a similarly complex postsynaptic molecular machinery (postsynaptic specializations). The presynaptic terminal is an area within the axon characterized by the presence of neurotransmitter-filled vesicles docked and primed at the active zone, as well as the machinery for the calcium-dependent exocytosis. Structurally, the postsynapse is characterized by an electron-dense zone (PSD), which corresponds to the region where neurotransmitter receptors and many associated proteins are concentrated and anchored to the cytoskeleton. The synaptic cleft is a 50 nm (neuromuscular junction) and 20 nm- wide (CNS synapses) gap between the pre- and the postsynaptic cell. Transmission at chemical synapses is initiated when an action potential invades the synaptic terminal and induces a depolarization of the presynaptic membrane. This results in a rapid and local increase of the intracellular  $\text{Ca}^{2+}$  concentration, which subsequently triggers exocytosis of synaptic vesicles and release of the neurotransmitter into the synaptic cleft. Subsequently, the neurotransmitter can bind to ionotropic (ligand-gated ion channels) and metabotropic (G protein-coupled) receptors located at the postsynaptic site (Sheng and Kim, 2011; Pereda, 2014).

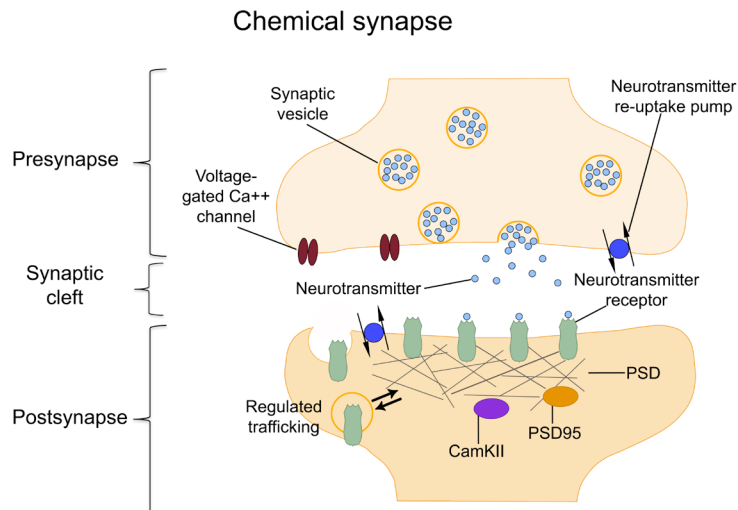


**Figure 1.3. Structure of the chemical synapse**

Chemical synapses consist of three components: the presynaptic terminal, the synaptic cleft and the postsynaptic terminal. The key feature of chemical synapses is the presence of synaptic vesicles filled with the neurotransmitters within the presynaptic terminal. It is these chemical agents that mediate

the communication between neurons. (Modified from Pereda, 2014).

In the CNS, two main categories of synapses are found: inhibitory (GABAergic and glycinergic) and excitatory (glutamatergic) synapses. Inhibitory synapses use gamma-aminobutyric acid (GABA) or glycine as their neurotransmitter. Binding to the corresponding neurotransmitter receptor leads to hyperpolarization of the postsynaptic site usually by chloride influx. They are often found at dendritic shafts close to the soma or directly at the cell body. In contrast, excitatory synapses are localized at dendritic spines. Glutamatergic synapses are the main type of excitatory synapses in the mammalian CNS. The depolarizing response to glutamate is mediated by three neurotransmitter-gated ion channels; AMPA, kainate and NMDA receptors. The establishment of all pre- and postsynaptic specializations during development is the hallmark of synaptogenesis and is required for successful synaptic transmission.

## 1.5 The neuromuscular junction

The neuromuscular junction (NMJ) is a specialized cholinergic synapse formed between presynaptic motoneurons and skeletal muscle fibers. Due to its large size and accessibility, this peripheral synapse has provided essential insight into synaptic transmission as well as the molecular mechanisms of synapse formation and maintenance (Wu et al., 2010). Defects in the signaling pathways associated with the development and function of the NMJ lead to a variety of neuromuscular disorders all characterized by use-dependent muscle weakness and fatigue, including congenital myasthenic syndromes (CMS) or myasthenia gravis (McConville and Vincent, 2002; Ferraro et al., 2012; Punga and Ruegg, 2012).

### 1.5.1 Development of the neuromuscular junction

The neuromuscular junction is by far the best-characterized synapse in the entire nervous system (Tintignac et al., 2015). During embryonic development motoneuron axons grow long distances to reach and innervate the striated muscle fibers, which constitute their distal targets. Prior to



motor innervation, muscle fibers already show a certain level of maturation as indicated by the presence of acetylcholine receptors (aneural AChRs) in the central region of the muscle. This phenomenon, called muscle prepatternning, appears to be nerve independent as it also occurs in mutant mice that lack phrenic or motor nerves (Yang et al., 2001). The muscle prepatternning is a transient process and is not involved in synapse formation, since it is not sufficient to establish neuromuscular transmission. Once the motoneuron interacts with the muscle fiber, mature AChR clusters (neural AChRs), form at the postsynaptic areas exactly apposed to the nerve terminals.

The agrin/LRP4/MuSK pathway is the only pathway that regulates AChR aggregation and synapse formation *in vivo*. The master organizer of synaptogenesis at the NMJ is the extracellular matrix protein agrin. Agrin is a heparan sulfate proteoglycan (HSPG) with a molecular mass of >500 kD that has been originally isolated from the electric organ of *Torpedo californica*, where it is enriched in the basal lamina (Nitkin et al., 1987). Agrin was originally identified from its AChR clustering activity in cultured myotubes (Nitkin et al., 1987). According to the ‘agrin hypothesis’ (McMahan, 1990) agrin is synthesized by motoneurons, transported along the axons to the terminal where it is released into the synaptic cleft. In the cleft agrin becomes stably associated with the basal lamina by binding to laminin alpha chain and to alpha-dystroglycan. Basement membrane-associated agrin binds to its receptor complex consisting of dimers of LRP4 (Kim et al., 2008; Zhang et al., 2008) and MuSK (Glass et al., 1996). This interaction initiates an intracellular signaling cascade leading to the formation of most if not all pre- and post-synaptic specializations (Tintignac et al., 2015). Consistent with the agrin hypothesis, mice which are deficient for either agrin, MuSK or LRP4 fail to form NMJs and die at birth due to respiratory musculature failure and complete immobility (Gautam et al., 1996; Glass et al., 1996; Zhang et al., 2008; Kim et al., 2008). Moreover, ectopic expression of agrin is sufficient to induce locally the formation of AChR clusters in adult muscles and to elicit the formation of a postsynaptic apparatus in denervated muscles (Jones et al., 1997; Rimer et al., 1997) indicating that agrin is not only required but also sufficient for postsynaptic development.

### 1.5.1.1 Agrin cDNA and isoforms

The full-length agrin cDNA has been cloned from several species and the amino acid sequences show a high degree of homology. The cDNA predicts a number of structural domains, including a C-terminal domain with similarity to the laminin alpha chain. This part of agrin is required and sufficient for its synaptogenic role at the NMJ. Alternative first exon usage generates two N-terminal isoforms of agrin: the matrix-associated agrin (NtA-agrin), which is concentrated in the basal lamina of the NMJ, and the transmembrane isoform (TM-agrin), which is primarily expressed in the CNS. These two forms of agrin can also be alternatively spliced at two additional positions close to the C-terminal known as A/y and B/z sites (Kröger and Schröder, 2002), generating multiple isoforms that differ dramatically in their distribution, in their biological functions, in their LRP4 binding affinity and in their ability to activate MuSK (Kim et al., 2008; Zhang et al., 2008). Only isoforms which contain inserts of 8, 11 or 19 amino acids at splice site B/z are able to interact with LRP4 and have synaptogenic function (Gesemann et al., 1996).

The agrin receptor complex consists of two proteins: the tyrosine kinase MuSK and the agrin binding protein LRP4. MuSK is a member of the large receptor tyrosine kinase (RTK) family that was originally discovered in a screen for tyrosine kinases in the synapse-rich electric organ of *Torpedo* (Jennings et al., 1993) and co-localizes with AChRs at NMJs (DeChiara et al., 1996). The role of MuSK in NMJ formation is evident in MuSK deficient mice (MuSK<sup>-/-</sup>) that, similar to agrin-mutant mice, lack mature NMJs, AChR clusters and other muscle-derived synaptic proteins and die perinatally (DeChiara et al., 1996; Gautam et al., 1996).

Like other RTKs, MuSK is a type I transmembrane protein consisting of a glycosylated extracellular domain, a single transmembrane helix, and a cytoplasmic region containing a tyrosine kinase domain. MuSK is an atypical receptor tyrosine kinase. Typically, receptor tyrosine kinases are activated by ligands that bind directly to the receptor ectodomain, inducing dimerization and trans-autophosphorylation, thereby stimulating the catalytic kinase activity of the receptor (Schlessinger, 2000). However, MuSK does not bind directly to neural agrin (Glass et al., 1996). Instead, agrin binds to LRP4 and ligand-binding is relayed to activate the kinase (Kim et al., 2008; Zhang et al., 2008). MuSK and LRP4 comprise a scaffold for a plethora of proteins that constitute downstream signaling cascades and, more specifically, are implicated in NMJ assembly and the regulation of synapse-specific gene expression (**Figure 1.4**).

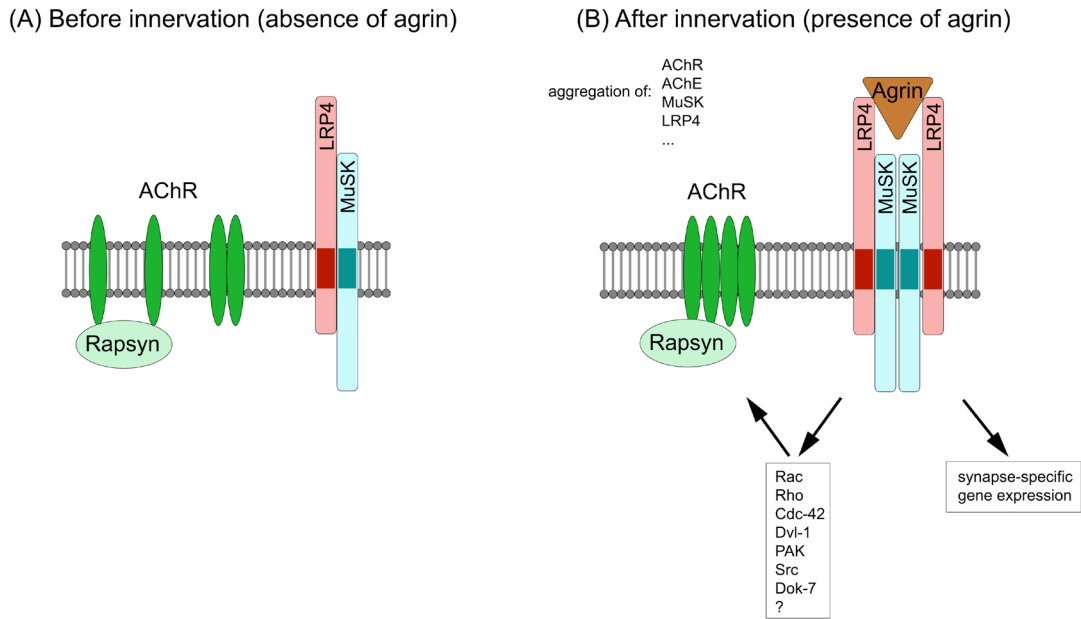


**Figure 1.4. A working model for the agrin/LRP4/MuSK signaling pathway at the NMJ**

(A) Prior to innervation, LRP4 interacts with MuSK at basal levels to activate the pathway necessary for forming aneural clusters and for guiding motoneuron growth cones to the middle regions of muscle fibers. (B) Upon innervation, neural agrin binds to LRP4 and activates MuSK. Activation of MuSK induces an intracellular signaling cascade that involves the phosphorylation of several molecules leading to the aggregation of AChR, AChE and other protein at the synapse. Activation of MuSK induces also the synapse-specific gene expression via a different pathway.

### 1.5.2 The family of low-density lipoprotein receptors and LRP4

The low-density-lipoprotein receptor (LDLR) family is an ancient gene family of structurally closely related cell-surface receptors that have been highly conserved throughout evolution. In mammals, the core members of the LDLR family include the low-density-lipoprotein receptor (LDLR), the very-low-density-lipoprotein receptor (VLDLR), the apolipoprotein E receptor 2 (ApoER2/LRP8), the LDL-related protein (LRP1), the LDL-related protein-1B (LRP1B), megalin (LRP2), and the low-density lipoprotein receptor-related protein 4 (LRP4/MEGF7) (Lane-Donovan et al., 2014). All core members of the LDLR family share common structural domains that include ligand binding domains, epidermal growth factor (EGF) homology domains, a membrane anchoring domain, and a cytoplasmic tail containing at least one consensus amino acid NPxY motif that facilitates endocytotic trafficking and signal transduction (**Figure 1.5**). Besides the core members of the LDLR family, there are several more distantly related LRP4s that share some but not all of the structural elements that characterize the core members. These include LR11 (SORLA), LRP5 and LRP6 (Lane-Donovan et al., 2014).

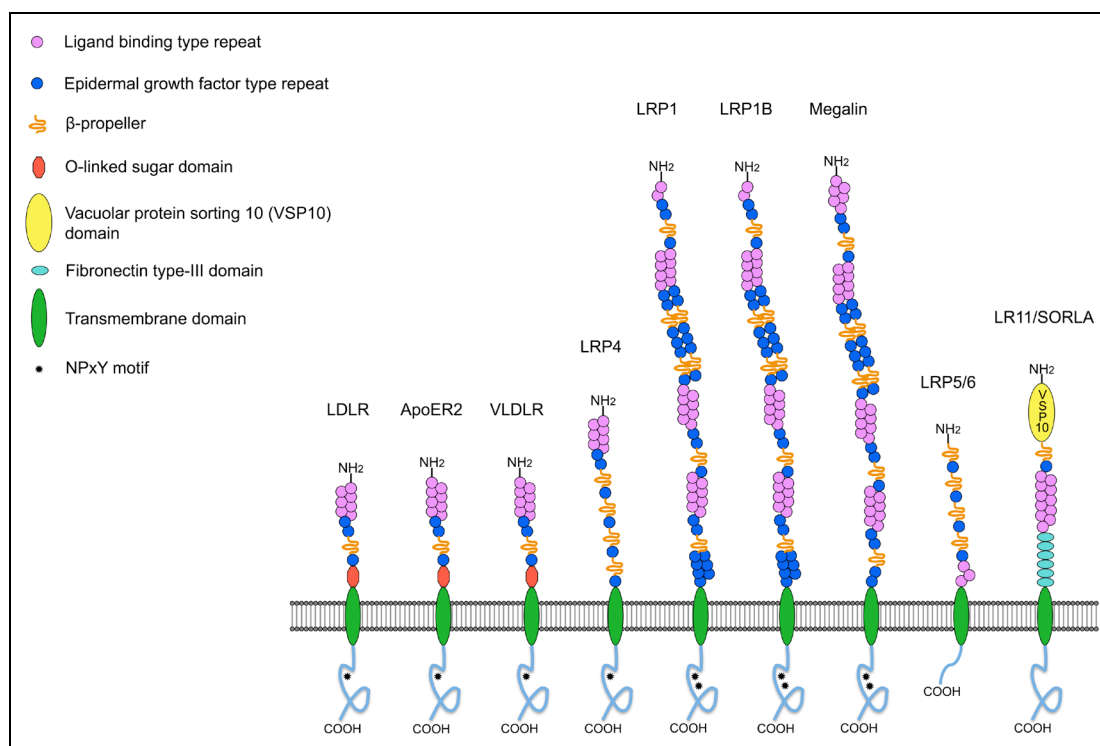


**Figure 1.5. The LDL receptor family**

Each member of the LDL receptor family contains a ligand-binding domain, an EGF homology domain, a single transmembrane segment, and at least one cytoplasmic NPxY motif. This motif serves as a docking site for intracellular adaptor proteins that mediate the endocytosis and signal transduction of these receptors (adapted from Qiu et al., 2006).

The core members of the family are involved in the cellular uptake of extracellular ligands and regulate diverse biological processes including lipid and vitamin metabolism as well as cell-surface protease activity (Lane-Donovan et al., 2014). Some members of the family also participate in cellular signaling and regulate the development and functional maintenance of the nervous system (Herz and Bock, 2002). Historically, most research studies have focused on the importance of LDLR family members in cholesterol homeostasis. However, the discoveries that LDL receptors are involved in modulation of hippocampal synaptic plasticity and necessary for normal learning and memory have forced neurobiologists to recognize the importance of LDLRs in CNS function (Lane-Donovan et al., 2014).

### 1.5.2.1 LRP4

The low-density lipoprotein-related receptor 4 (LRP4; also called MEGF7) is a relatively recent member of the LDLR family. This protein was initially identified during a motif-trap screening for large mRNAs that are expressed in the human brain and contain multiple EGF-like motifs (MEGFs; Nakayama et al., 1998; see **Figure 1.5**).

LRP4 is a type I single transmembrane protein with about 90% of the protein being extracellular and only 8% intracellular. The full-length cDNA sequence of LRP4 (7784 bp; GenBank<sup>TM</sup> accession number AB073317) contains a 5718-nucleotide (1905 amino acid residues in human and rodents) open reading frame and predicts a number of domains also found in other core members of the LDLR family, including: a) eight cysteine-rich repeats where the (lipoprotein) ligands bind (LDLa), b) six domains with similarity to the epidermal growth factor (EGF-like), c) four type “B” repeats that contain a conserved YWTD motif and are critical for ligand release and recycling of the receptor (LY), d) a hydrophobic transmembrane region, and e) a cytoplasmic tail containing an ‘NPxY’ (Asp-Pro-any amino acid-Tyr) motif that serves as an internalization signal (Chen et al., 1990; see **Figure 1.6**). LRP4 also contains a 15-amino acid signal peptide sequence at the N-terminal and a PDZ domain-binding consensus sequence, -ESQV, at the C-terminal end. The LDLa domains 6-8, the first two EGF-like domains, and the first of four  $\beta$ -propeller domains constitute an approximately 50-kDa fragment that is necessary and sufficient to bind the appropriate agrin isoform (Zhang et al., 2011; Zong et al., 2012; see **Figure 1.6**). LDLa repeats 4-8, the first three  $\beta$ -propeller domains, and the two intervening EGF-like domains of LRP4 are sufficient to bind MuSK (Zhang et al., 2011; Zong et al., 2012; see **Figure 1.6**). The LRP4 gene and its protein domain structure are conserved across species including frogs, birds, rodents and primates, with the exception of the *Drosophila* LRP4, which does not contain the NPxY and the PDZ binding C-terminus, and may not be a typical LRP4 (Shen et al., 2015).

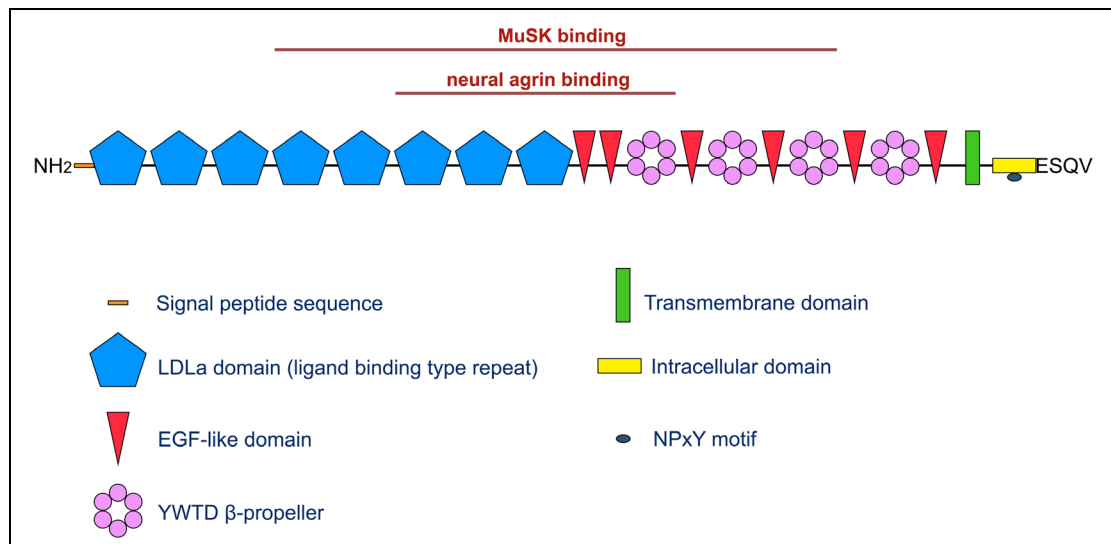


**Figure 1.6. Domain structure of LRP4**

The different structural domains of LRP4 and their interaction partners are indicated. LRP4 contains a large extracellular domain at the N-terminus, a transmembrane domain and short intracellular C-terminal part. The domains of LRP4 where the agrin and MuSK bind to are also indicated. For more details see text.

### 1.5.2.1.1 Developmental functions of LRP4

LRP4 expression was shown to have a widespread distribution during mouse organogenesis. More specifically, LRP4 mRNA has been shown to be widely expressed in multiple tissues and organs including kidney, lungs, limb and ectodermal organs (Ohazama et al., 2008; Weatherbee et al., 2006). Several studies have described hypomorphic and also null mutations of LRP4 (LRP4<sup>mitt</sup>, LRP4<sup>mte</sup>, LRP4<sup>dan</sup>, LRP4<sup>mdig</sup>, LRP4<sup>ECD/ECD</sup>) that cause a common limb phenotype mainly characterized by polysyndactyly in both fore and hind limbs and a mild form of craniofacial and tooth development abnormalities in mice and mulefoot disease in cattle (Johnson et al., 2006; Simon-Chazottes et al., 2006; Duchesne et al., 2006; Drögemüller et al., 2007). In human patients more than ten point mutations in LRP4 gene have been identified which lead to the Cenani-Lenz syndrome, an autosomal recessive disorder characterized by defects in limbs and kidneys (Li et al., 2010). Moreover, mutations in LRP4 have been identified in patients with sclerosteosis, a disease with abnormal bone mineral density (BMD; Choi et al., 2009). All of these data show that LRP4 plays an essential role as a modulator of the signaling pathways that control limb development, digit formation, and bone homeostasis.

### 1.5.2.1.2 The role of LRP4 during neuromuscular junction development

LRP4 is a key regulator for synapse development at the neuromuscular junction (NMJ). A few years ago, in an N-ethyl-N-nitrosourea (ENU) mutagenesis screen in mice two kinds of mutations of LRP4 were identified, named *mitt* and *mte* (Weatherbee et al., 2006). These are complete loss-of-function mutations and in both homozygous LRP4<sup>mitt</sup> and LRP4<sup>mte</sup> mice, NMJs do not form, motor nerve terminals fail to stop in the central region of muscle fibers and instead arborize extensively and AChR aggregates do not form at all. These mice die at birth due to respiratory musculature failure (Weatherbee et al., 2006). It was subsequently discovered that LRP4 interacts with MuSK and forms a tetrameric complex which serves as the receptor for agrin (**Figure 1.7**; Kim et al., 2008; Zhang et al., 2008; Zong et al., 2012).

In the absence of agrin, LRP4 self-associates and interacts with MuSK at basal levels, resulting in the activation of the latter and subsequently in the pre patterning of the muscle (**Figure 1.7**; Kim et al., 2008). The binding of agrin to LRP4 triggers a reorganization of the preexisting tetrameric complex, promoting *trans*-phosphorylation and kinase activation of MuSK. Activation of MuSK stimulates intracellular signaling pathways that results in the formation of most, if not all, postsynaptic specializations including (1) clustering and anchoring of AChRs and additional muscle proteins that are critical for synaptic transmission, and (2) elevated transcription of ‘synapse-specific’ genes in myofibre synaptic nuclei (**Figure 1.7**; Tintignac et al., 2015). LRP4 is

required for the relay of agrin signaling to MuSK and in the absence of LRP4, agrin's ability to induce MuSK phosphorylation is minimal (Kim et al., 2008; Zhang et al., 2008).

In addition to its role in postsynaptic differentiation of the NMJ, LRP4 has also an essential and early role in presynaptic differentiation *in vivo*. Recent studies have shown that muscle-derived LRP4 acts as a direct retrograde stop signal for  $\alpha$ -motoneuron growth and promotes the formation of presynaptic specializations (Figure 1.7; Yumoto et al., 2012; Wu et al., 2012).

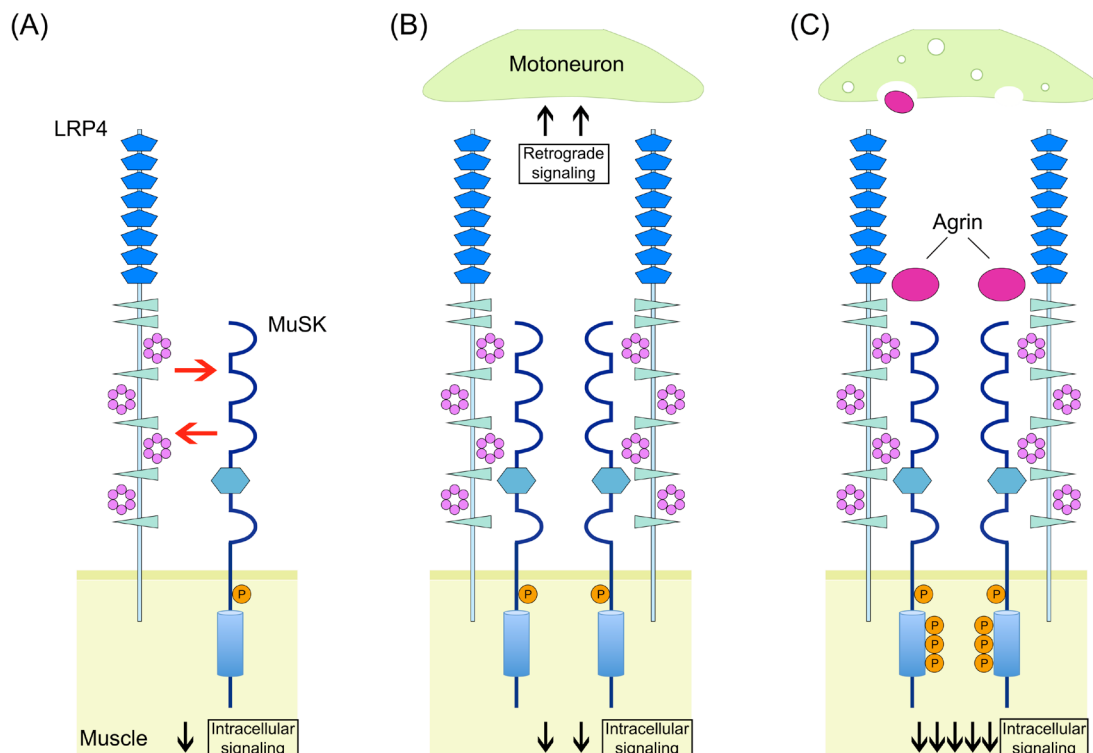


**Figure 1.7. The agrin/LRP4/MuSK complex at the neuromuscular junction**

At the neuromuscular junction, LRP4 serves as a receptor for agrin and a coreceptor for the muscle-specific tyrosine kinase MuSK. In the absence of agrin, LRP4 interacts with MuSK at basal levels resulting in the prepaterning of the muscle (A). When agrin is present, it binds to LRP4 and triggers a re-organization of the tetrameric complex and activation of MuSK that leads to the stimulation of the intracellular signaling involved in the formation of all postsynaptic specializations (B). Muscle-derived LRP4 can also act as a retrograde stop signal for  $\alpha$ -motoneurons and promoting the formation of presynaptic specializations (C). (Modified from <http://first.lifesciencedb.jp/archives/5676>).

#### 1.5.2.1.3 Role of LRP4 in the CNS

In the CNS, *lrp4* mRNA is prominently present in the neocortex, hippocampus, cerebellum, and olfactory bulb (Tian et al., 2006; Lein et al., 2007). Moreover, LRP4 protein has been detected in postsynaptic membrane fractions prepared from the adult rat forebrain where it interacts with the postsynaptic scaffold protein PSD95 (Tian et al., 2006; Gomez et al., 2014). Thus, in addition to its essential role at the NMJ, these studies suggested functions for LRP4 in the adult

CNS (Gomez et al., 2014; Pohlkamp et al., 2015). LRP4<sup>-/-</sup> mice rescued for LRP4 expression selectively in muscle but lacking LRP4 in the brain (LRP4<sup>-/-</sup>; LRP4<sup>m</sup>) exhibit impaired synaptic hippocampal plasticity, reduced LTP as well as excitatory synaptic transmission defects, and deficits in cognitive tasks that assess learning and memory, including fear-conditioning (Gomez et al., 2014). Similarly, mice expressing only the extracellular domain of LRP4 (LRP4<sup>ECD/ECD</sup>) show deficits in LTP, without exhibiting major changes in the general anatomy of the brain (Pohlkamp et al., 2015). The cellular and molecular basis of these deficits remains unknown.



## **Aim of the study**

While the aforementioned studies unequivocally show an essential role of LRP4 during formation and maintenance of the NMJ, its role during CNS development is unclear. In particular, the molecular basis of the altered behavior in LRP4-deficient mice is unclear. The aim of this thesis project therefore was:

1. To determine the overall localization of LRP4 in embryonic and adult mouse CNS, and more specifically to determine whether LRP4 is present in neurons.
2. To investigate the subcellular distribution of LRP4, in particular to determine if LRP4 is concentrated at CNS synapses, as it is at the NMJ and if yes, at which synapses.
3. To investigate the effect of an overexpression and knockdown of LRP4 in CNS neurons.



## 2 Materials and Methods

Use and care of animals was approved by German authorities and according to national law (TierSch§7). For this study, C57BL/6J wild-type mice were bred in the animal facility of the Institute of Physiology of LMU Munich. The day of the vaginal plug was considered embryonic day (E) 0. Mice with a targeted deletion of the MuSK gene have been described previously (DeChiara et al., 1996). Mice obtained from crosses between GLAST<sup>CreERT2</sup> and CAG-CAT-eGFP (GLAST::CreERT2/eGFP) have been previously characterized (Bardehle et al., 2013). All experimental procedures were performed in accordance with German and European Union guidelines.

### 2.1 Materials

#### 2.1.1 Primary antibodies

**Table 1. Primary antibodies**

Antigen	Host species	WB	ICC	IHC	Supplier	Cell type labelled
Agrin 204	rabbit	-	1:1000	1:500	Prof.M. Rüegg, Basel, Switzerland	NMJ, CNS synapses
$\alpha$ -tubulin	mouse IgG1	1:3000	-	-	Sigma, Hamburg, Germany	Major constituent of microtubules (loading control in Western blotting)
Bassoon	rabbit	-	1:1000	-	Dr. Wilko D. Altmann, Magdeburg, Germany	Presynaptic nerve terminals
beta-III-tubulin (Tuj1)	mouse IgG2b	-	1:500	-	Sigma, Hamburg, Germany	Immature neurons
Calbindin	mouse IgG1	-	1:500	1:500	Sigma, Hamburg, Germany	Short-axon cells, Purkinje neurons, DG granule neurons

CamKII	mouse IgG1	-	1:500	-	Abcam, Cambridge, UK	Glutamatergic neurons
Doublecortin (Dcx)	guinea pig	-	-	1:300	Millipore, Schwalbach, Germany	Immature DG granule neurons
$\gamma$ -Amino butyric acid (GABA)	rabbit	-	1:200	-	Sigma, Hamburg, Germany	GABAergic neurons (interneuron)
Glial fibrillary acidic protein (GFAP)	mouse IgG1	-	1:500	1:500	Sigma, Hamburg, Germany	aNSCs, astrocytes
Green fluorescent protein (GFP)	chicken	-	1:500	1:500	Abcam, Cambridge, UK	eGFP-labeled cells
Lrp4 (int.)	rabbit	1:10.000	1:1000	1:300	Self-made	
Lrp4 (int.)	rabbit	1:10.000	1:1000	1:300	Sigma, Hamburg, Germany	
Lrp4 (ext.)	rabbit	1:10.000	1:1000	1:300	Self-made	
Lrp4 (ext.)	rabbit	1:10.000	1:1000	1:300	Sigma, Hamburg, Germany	
MAP-2	mouse IgG1	-	1:500	-	Sigma, Hamburg, Germany	Dendritic processes
Neurofilament heavy chain (NFH)	chicken	-	-	1:300	Millipore, Schwalbach, Germany	Filaments in axons
Neuronal Nuclei (NeuN)	mouse IgG1a	-	-	1:300	Millipore, Schwalbach, Germany	Nuclei of postmitotic neurons
PSD95	mouse IgG2a	-	1:200	-	Thermo Fischer Scientific, Nidderau, Germany	Postsynaptic terminals
Red fluorescent protein (RFP)	rat IgG2a	-	1:400	-	Chromotek, Planegg-Martinsried, Germany	DsRed/RFP-labeled cells
S100 $\beta$	mouse	-	1:500	-	Sigma, Hamburg, Germany	Astrocytes (adult brain)

Synaptobrevin 2	mouse IgG1	-	1:1000	-	SySy, Göttingen, Germany	Presynaptic terminals
Tau	mouse IgG2a	-	1:200	-	Millipore, Schwalbach, Germany	Axonal processes
Vesicular Glutamate transporter 1 (Vglut1)	guinea pig	-	1:2.500	1:25.000	Millipore, Schwalbach, Germany	Presynaptic terminals

WB: dilution used for Western blotting, ICC: dilution used for Immunocytochemistry, IHC: dilution used for Immunohistochemistry.

### 2.1.2 Secondary antibodies

**Table 2. Secondary Antibodies**

Species specificity	Fluorescence tag	Dilution	Supplier
Goat $\alpha$ -mouse IgG	Alexa Fluor® 488	1:1000	Molecular Probes, Nidderau, Germany
Goat $\alpha$ -mouse IgG	Cy3	1:500	Jackson, Suffolk, UK
Goat $\alpha$ -mouse IgG	Alexa Fluor® 647	1:1000	Invitrogen, Darmstadt, Germany
Goat $\alpha$ -mouse HRP		1:3000	Invitrogen, Darmstadt, Germany
Goat $\alpha$ -mouse IgG1	Alexa Fluor® 488	1:1000	Invitrogen, Darmstadt, Germany
Goat $\alpha$ -mouse IgG1	biotin	1:200	Invitrogen, Darmstadt, Germany
Goat $\alpha$ -mouse IgG2a	Alexa Fluor® 488	1:1000	Invitrogen, Darmstadt, Germany
Goat $\alpha$ -mouse IgG2a	TRITC	1:1000	Invitrogen, Darmstadt, Germany
Goat $\alpha$ -rabbit IgG	Alexa Fluor® 488	1:1000	Invitrogen, Darmstadt, Germany
Goat $\alpha$ -rabbit IgG	Alexa Fluor® 647	1:1000	Invitrogen, Darmstadt, Germany
Biotinylated secondary	Streptavidin FITC	1:200	Invitrogen, Darmstadt, Germany
Biotinylated secondary	Streptavidin Cy3	1:200	Invitrogen, Darmstadt, Germany
$\alpha$ -bungarotoxin	Alexa Fluor® 594	1:1000	Invitrogen, Darmstadt, Germany

### 2.1.3 Buffers and solutions

**Table 3. Buffers and solutions**

Buffer/Solution	Components	Preparation	Use
Ampicillin stock, 100 mg/ml	1 g Ampicillin Autoclaved ddH <sub>2</sub> O	Dissolve powder in 10 ml autoclaved ddH <sub>2</sub> O. Make aliquots and store at -20°C.	To prepare agar plates for selecting bacterial colonies.
4', 6'-diamidino-2-	2 mg DAPI	Dissolve powder in 1 ml 1x	To visualize

phenylindole (DAPI) stock, 2 mg/ml	1 ml 1x PBS	PBS. Store at -20°C.	nuclei in IHC and ICC.
Ethylene-diamine-tetraacetic acid, disodium salt (EDTA), 0.5 M pH 8.0	18.6 g EDTA disodium salt powder 1 N NaOH ddH <sub>2</sub> O	Dissolve powder in 50 ml ddH <sub>2</sub> O and adjust the pH with NaOH. Top up the solution to a final volume of 100 ml. Autoclave.	To prepare 50x TAE buffer.
Kanamycin stock, 100 mg/ml	1 g Kanamycin Autoclaved ddH <sub>2</sub> O	Dissolve powder in 10 ml autoclaved ddH <sub>2</sub> O. Make aliquots and store at -20°C.	To prepare agar plates for selecting bacterial colonies.
Lysis buffer (10X)	5 ml Tris – HCl (1M) pH 7.5 10 ml EDTA (0.5M) ddH <sub>2</sub> O	Dissolve components in up to 50 ml ddH <sub>2</sub> O. Store at RT.	Diluting to 1X lysis buffer.
Paraformaldehyde, 20% (20% PFA)	134 g Na <sub>2</sub> HPO <sub>4</sub> ·2H <sub>2</sub> O 100 g PFA (Sigma) 10 ml NaOH, 32% 7 ml HCl, 37%	Dissolve Na <sub>2</sub> HPO <sub>4</sub> ·2H <sub>2</sub> O in 1600 ml autoclaved ddH <sub>2</sub> O and heat to 60°C while stirring. Stop heating and add PFA to the heated solution and dissolve completely by adding NaOH. Let the solution cool on ice and adjust pH to 7.4 with HCl. Store at -20°C.	Diluting to 4% PFA.
Paraformaldehyde, 4% (4% PFA)	20% PFA Autoclaved ddH <sub>2</sub> O	Dilute 50 ml 20% PFA in 200 ml ddH <sub>2</sub> O. Store at 4°C.	Fixative.
Phosphate buffered saline, 0.15 M (10x PBS)	400 g NaCl 10 g KCl 58.7g Na <sub>2</sub> HPO <sub>4</sub> ·2H <sub>2</sub> O 10 g K <sub>2</sub> HPO <sub>4</sub>	Dissolve components in up to 5 l ddH <sub>2</sub> O and autoclave. pH of the solution should be ca. 7.4. Store at RT.	Diluting to 1x PBS.
Phosphate buffered saline, 1x (1x PBS)	10x PBS Autoclaved ddH <sub>2</sub> O	Dilute 100 ml 10x PBS in 900 ml ddH <sub>2</sub> O. Store at RT.	Washing for IHC and ICC.
Phosphate-buffered saline, 0.1% Tween 20 (PBST)	100 ml PBS 1 ml Tween 20 900 ml ddH <sub>2</sub> O	Mix all components. Store at RT.	Washing membranes for Western blotting.
Phosphate buffer, 0.25	6.5 g	Dissolve Na <sub>2</sub> HPO <sub>4</sub> ·2H <sub>2</sub> O in	To prepare

M (10x PB)	Na <sub>2</sub> HPO <sub>4</sub> ·2H <sub>2</sub> O 1.5 g NaOH Autoclaved ddH <sub>2</sub> O	up to 40 ml autoclaved ddH <sub>2</sub> O. Adjust pH to 7.4 using NaOH and make up volume to 50 ml with ddH <sub>2</sub> O.	storing solution.
Poly-D-Lysine (PDL; molecular weight > 300 kDa) stock solution, 1 mg/ml	PDL powder ddH <sub>2</sub> O Concentration: 1 mg/ml	Dissolve 50 mg PDL powder in sterile ddH <sub>2</sub> O to make a stock solution of 1 mg/ml. Filter sterilize. Store 1 ml aliquots at -20°C.	Stock solution for coating of coverslips.
Poly-D-Lysine (PDL) working solution	1 ml PDL stock solution 50 ml 1x PBS	Add 1 ml stock solution in 49 ml sterile 1x PBS. Filter sterilize and use it immediately.	Coating of coverslips for cell culture.
RIPA buffer	50 mM Tris-HCl pH 8.0 150 mM NaCl 1% DOC (Sodium Deoxycholate) 1% NP-40 0.1% SDS Protease Inhibitors Autoclaved ddH <sub>2</sub> O	Dissolve DOC in autoclaved ddH <sub>2</sub> O. Add Tris-HCl, NaCl and NP-40 and ddH <sub>2</sub> O up to the final volume. Store at 4°C. Before use, add SDS and the protease inhibitors tablet (1 tablet/20 ml RIPA).	Lysis buffer for cells.
SDS running buffer (10x)	30.3 g Tris base (0.25 M) 144 g Glycine (1.92 M) 10 g SDS [1% (w/v)] Autoclaved ddH <sub>2</sub> O	Dissolve the components in 800 ml autoclaved ddH <sub>2</sub> O while stirring. Make up volume to 1 l with ddH <sub>2</sub> O. Store at RT.	To prepare running buffer (1x) for SDS-PAGE.
Storing solution (cryo-protectant)	30 ml Glycerol 30 ml Ethyleneglycol 10 ml 10x PB Autoclaved ddH <sub>2</sub> O	Dissolve the components in 30 ml autoclaved ddH <sub>2</sub> O while stirring. Adjust pH to 7.4. Store at 4°C.	To store free-floating tissue sections.
Sucrose solution, 30%	15 g Sucrose 50 ml 1x PBS	Dissolve the sucrose in 30 ml 1x PBS while stirring. Make up volume to 50 ml with 1x PBS. Store at 4°C.	To cryo-protect fixed tissue before cryo-sectioning.
Transfer buffer (10x)	2.42 g Tris base 11.52 g Glycine ddH <sub>2</sub> O	Dissolve the components in 800 ml autoclaved ddH <sub>2</sub> O while stirring. Make up volume to 1 l with ddH <sub>2</sub> O. Store at RT.	To prepare transfer buffer (1x) for Western blotting.
Transfer buffer (1x)	2.42 g Tris base	Dissolve the Tris base and	Transfer

	11.52 g Glycine 160 ml Methanol ddH <sub>2</sub> O	glycine in 700 ml ddH <sub>2</sub> O while stirring. Add methanol. Make up volume to 1 L with ddH <sub>2</sub> O. Store at 4°C.	buffer for Western blotting.
Transformation buffer I	1.47 g Kac (30 mM) 6.05 g RbCl (100 mM) 0.74 g CaCl <sub>2</sub> x 2H <sub>2</sub> O (10 mM) 75 ml Glycerin (15%) 4.95 g MnCl <sub>2</sub> x 4H <sub>2</sub> O (50 mM) conc. HCl Autoclaved ddH <sub>2</sub> O	Dissolve the components in 400 ml autoclaved ddH <sub>2</sub> O while stirring. Adjust pH to 5.8 using HCl and make up volume to 500 ml with ddH <sub>2</sub> O. Filter sterilize and store at 4°C.	To prepare chemo-competent <i>E. coli</i> .
Transformation buffer II	0.21 g MOPS (10 mM) 1.10 g CaCl <sub>2</sub> x 2H <sub>2</sub> O (75 mM) 0.12 g RbCl (10 mM) 15 ml Glycerin (15%) conc. HCl Autoclaved ddH <sub>2</sub> O	Dissolve the components in 70 ml autoclaved ddH <sub>2</sub> O while stirring. Adjust pH to 6.5 using HCl and make up volume to 100 ml with ddH <sub>2</sub> O. Filter sterilize and store at 4°C.	To prepare chemo-competent <i>E. coli</i> .
Tris-Acetate-EDTA buffer (TAE), 50x	242 g Tris base 57.1 ml glacial acetic acid 100 ml 0.5 M EDTA ddH <sub>2</sub> O	Dissolve the Tris base in ca. 750 ml ddH <sub>2</sub> O. Add glacial acetic acid and EDTA and make up volume to 1 l with ddH <sub>2</sub> O. pH should be ca. 8.5. Autoclave. Store at RT.	To prepare 1x TAE buffer for electrophoresis of agarose gels.
Tris-Acetate-EDTA buffer (TAE), 1x	20 ml 50x TAE ddH <sub>2</sub> O	Dilute 20 ml 50x TAE buffer in up to 1 l ddH <sub>2</sub> O. Store at RT.	Running buffer for agarose gels.
Tris-buffered saline (TBS), 10x	24 g Tris base 88 g NaCl conc. HCl ddH <sub>2</sub> O	Dissolve the components in 900 ml ddH <sub>2</sub> O while stirring. Adjust the pH to 7.6 using HCl and make up volume to 1 L with ddH <sub>2</sub> O.	Diluting to 1x TBS.
Tris-buffered saline, 0.1% Tween 20 (TBST)	100 ml TBS 10x 1 ml Tween 20 900 ml ddH <sub>2</sub> O	Mix all components. Store at RT.	Washing membranes for Western blotting.



### 2.1.4 Media

**Table 4. Media for cell and bacterial culture**

Medium	Components	Notes
LB Agar	Add 10 g Bacto-tryptone, 5 g Yeast extract, 10 g NaCl and 15 g Agar to 800 ml ddH <sub>2</sub> O. Mix until the components are dissolved. Adjust pH to 7.5 with NaOH. Adjust volume to 1 L with ddH <sub>2</sub> O. Autoclave. Add antibiotic when agar cools to ca. 50-60°C.	Growing bacteria for transformation/cloning. Makes ca. 20 x 10 cm plates.
LB Broth	Add 10 g Bacto-tryptone, 5 g Yeast extract and 10 g NaCl to 800 ml ddH <sub>2</sub> O. Mix until the components are dissolved. Adjust pH to 7.5 with NaOH. Adjust volume to 1 L with ddH <sub>2</sub> O. Autoclave.	Growing bacteria for transformation/cloning.
E14 differentiation medium	Neurobasal medium 1x PenStrep (100x; Sigma) 1x Glutamax (100x; Sigma) B27 supplement (Gibco)	Medium for differentiation of E14 cortical neuronal culture. Add 1 ml B27 supplement to a final volume of 50 ml medium.

### 2.1.5 Cell lines

**Table 5. Prokaryotic and eukaryotic cell lines**

Bacterial strains:	E. coli TOP10 (Invitrogen)
	E. coli BL21
	E. coli Dh5alpha (Invitrogen)
Eukaryotic cell lines:	HEK 293 cells (generous gift of Dr. Alex Lepier)

### 2.1.6 Oligonucleotides

Primer name	Sequence (5' → 3')	Description
mir1232 Top Strand	5'- TGCTGTTAACATTGCAGTTCTCCTCAGTTTTGGC CACTGACTGACTGAGGAGATGCAATGTTAA-3'	
mir1232 Bottom Strand	5'- CCTGTTAACATTGCATCTCCTCAGTCAGTCAGTG GCCAAACTGAGGAGAAGTCAATGTTAAC-3'	
mir1544 Top	5'- TGCTGTTCAGTAGCAGCGTGTACTCGGTTTTGG	

<b>Strand</b>	CCACTGACTGACCGAGTACACTGCTACTGAA -3'	<b>Linker</b> <b>microRNA target</b> <b>sequence</b> <b>(sense/antisense)</b> <b>Loop sequence</b>
<b>mir1544</b> <b>Bottom</b> <b>Strand</b>	5'- CCTGTTTCAGTAGCAGTGTACTCGGTCAGTCAGTG GCCAAAACCGAGTACACGCTGCTACTGAAC -3'	
<b>mir6854</b> <b>Top</b> <b>Strand</b>	5'- TGCTGTGTTGAGCCAGTCTTTGAAAGGTTTTGGC CACTGACTGACCTTTCAAAGTGGCTCAACA -3'	
<b>mir6854</b> <b>Bottom</b> <b>Strand</b>	5'- CCTGTGTTGAGCCAGTTTGAAAGGTCAGTCAGTG GCCAAAACCTTTCAAAGACTGGCTCAACAC -3'	
<b>mir7072</b> <b>Top</b> <b>Strand</b>	5'- TGCTGTAAAGGAGCATGAAGCTAATGGTTTTGGC CACTGACTGACCATTAGCTATGCTCCTTTA -3'	
<b>mir7072</b> <b>Bottom</b> <b>Strand</b>	5'- CCTGTAAAGGAGCATAGCTAATGGTCAGTCAGTG GCCAAAACCATTAGCTTCATGCTCCTTTAC -3'	

### 2.1.7 Plasmids

Plasmid	Source
pCR-LRP4-TOPO	ImaGenes
pCDNA3.1(-) Myc-His B	Invitrogen
pCMV-LRP4	Personally cloned
pCMV-LRP4-IRES-eGFP	Personally cloned
pCMV-LRP4ext.	Cloned by Katja Peters
pCAG-eGFP	Generous gift of Dr. Alex Lepier
pCAG-RFP	Generous gift of Dr. Alex Lepier
pSYN-GFP:actin	Generous gift of Dr. Sergio Gascon
pSYN-LRP4	Personally cloned
pcDNA <sup>TM</sup> 6.2-GW	Invitrogen
pcDNA <sup>TM</sup> 6.2-GW/EmGFP	Invitrogen
pcDNA <sup>TM</sup> 6.2-GW/mir1232	Personally cloned
pcDNA <sup>TM</sup> 6.2-GW/mir1544	Personally cloned
pcDNA <sup>TM</sup> 6.2-GW/mir6854	Personally cloned
pcDNA <sup>TM</sup> 6.2-GW/mir7072	Personally cloned
pcDNA <sup>TM</sup> 6.2-GW/mir1232_1544	Personally cloned
pENTR1A_Myc_DsRed+kozak_MCS	Generous gift of Dr. Sergio Gascon
pENTR1A_Myc_DsRed+kozak_mir1232_1544	Personally cloned
pCAGGS-Dest	Generous gift of Dr. Alex Lepier
pCAG-miRLRP4-RFP	Personally cloned
pSYN-TMAGrin	Cloned by Anna Schick
pCAG-DsRedExpress-T2A-Glyco-IRES-TVA	Cloned by Dr. Aditi Deshpande

## 2.2 Methods

### 2.2.1 DNA/RNA methods

#### 2.2.1.1 RNA extraction from tissue and cDNA synthesis

To extract RNA from tissue, 1 mL of Trizol was used per 50-100 mg of tissue and the tissue was homogenized in sterile homogenators. Samples were incubated for 5 min at room temperature and 200 µl of chloroform per 1 mL of Trizol was added. Samples were mixed by vortexing for 15 sec, incubated for 10 min at room temperature and centrifuged at 11300 rpm for 15 min at 4°C. After centrifugation, samples have separated into two phases: the upper aqueous phase is colorless and contains the RNA. The organic phase is reddish, contains DNA and proteins in the phenol/chloroform solution. For the RNA precipitation, the aqueous phase was carefully removed and 500 µl of isopropanol per 1 mL of initial Trizol volume was added. Samples were mixed by inverting the tubes 5-6 times and centrifuged at 11300 rpm for 8 min at 20°C. The precipitated RNA was washed with 75% ethanol (1 mL of ethanol per 1 mL of Trizol) and centrifuged at 8900 rpm for 5 min at 20°C. Supernatant was removed and the pellet (that contains the RNA) was air-dried and re-dissolved in H<sub>2</sub>O.

The protocol was performed under sterile conditions (all reagents were RNase-free). The purified RNA was subsequently used for cDNA synthesis.

To extract RNA from cells a similar procedure was followed as for tissue. The cells that were adherent and grew in a monolayer were mechanically lysed in the flask by adding Trizol, after removing the medium. The cells that were in solution were first centrifuged and then lysed by adding Trizol. The amount of Trizol added was 1 ml per 10-cm<sup>2</sup> surface or 1 ml per 5-10 x 10<sup>6</sup> cells. A homogenator or a 1 ml syringe was used for the homogenization of the cells.

In order to synthesize cDNA using the total RNA as template, the iScript cDNA synthesis kit (Bio-Rad, California, USA) was used according to the manufacturer's instructions. A typical cDNA synthesis reaction was prepared as follows:

5X cDNA synthesis kit buffer	4 µl
iScript enzyme mixture	1 µl
RNA sample	1 µg
Nuclease-free H <sub>2</sub> O	ad 20 µl

## 2.2.2 Biochemical methods

### 2.2.2.1 Cell/tissue lysis

For preparation of HEK293 and neuronal cell lysates, cells cultured in 6-well plates were lysed with RIPA buffer with the addition of complete protease inhibitor cocktail (ROCHE, Mannheim, Germany). An adequate amount of RIPA was added to the cells (e.g. 150  $\mu$ l per 35 mm dish of cultured cells) and cells were lysed using a cell scraper. Lysates were incubated on ice for 30 min and cleared by centrifugation at 13000 rpm for 15 min at 4°C. Supernatant was collected and protein concentration was determined using the Bradford assay.

For preparation of adult mouse brain protein, tissue was homogenized in 10 volumes w/v lysis buffer. After homogenization with a glass-Teflon homogenizer, lysates were centrifuged at 3500 rpm for 30 min at 4°C to remove cellular debris. For the membrane protein fractions, supernatant was centrifuged at 15000 rpm for 30 min at 4°C and the pellet was re-suspended in 10 mM Tris 7.4. Protein concentration was determined using the Bradford assay and samples were stored at -80°C.

### 2.2.2.2 Sodium dodecylsulfate poly-acrylamide gel electrophoresis and Western blotting

Separating gel:

Gel Percentage	Acrylamide (ml)	1.5 M Tris, pH 8.8 (ml)	20% SDS ( $\mu$ l)	ddH <sub>2</sub> O (ml)	10% APS ( $\mu$ l)	TEMED ( $\mu$ l)	Final volume (ml)
7%	1.87	2	40	3.97	80	6	8
10%	2.67	2	40	3.17	80	3	8
12%	3.2	2	40	2.64	80	3	8
15%	4	2	40	1.84	80	3	8

Stacking gel:

Acrylamide ( $\mu$ l)	0.5 M Tris, pH 6.8 ( $\mu$ l)	20% SDS ( $\mu$ l)	ddH <sub>2</sub> O (ml)	10% APS ( $\mu$ l)	TEMED ( $\mu$ l)	Final volume (ml)
850	625	25	3.4	50	5	5

Sodium dodecylsulfate poly-acrylamide gel electrophoresis (SDS-PAGE) was performed using the vertical Mini-PROTEAN 3 gel system (BIO-RAD). Gels were polymerized using the corresponding gel casting system. After pouring the separation gel, isopropanol was added on top to avoid dehydration of the gel and to obtain a sharp border between running and stacking gel.

As soon as the separating gel was polymerized, the isopropanol was removed and the stacking gel was poured, pushing at the same time a comb in the gel. After the stacking gel was polymerized, protein samples could be loaded and electrophoresis was performed in 1x running buffer first at 80V and then at 140-160V when probes had entered the separation gel.

Transfer buffer was stored at 4°C. Whatman sheets and a nitrocellulose membrane were cut to the size of the gel and soaked in transfer buffer, additionally to the sponge pads. The gel and the membrane were sandwiched between soaked pieces of sponge pads, Whatman paper and perforated plastic plates.

The transfer was performed in a blotting tank (Biorad) overnight at 4°C 30V constant current. After transfer of the proteins onto the nitrocellulose membrane, the membrane was washed in 1x PBST in order to completely remove the methanol. To avoid nonspecific binding, the membrane was incubated in blocking solution [1x PBST, 5% (w/v) skimmed milk] for 2-3 hours at RT. Incubation of the membrane with primary antibodies for 2-4 hours at RT or overnight at 4°C followed. Membranes were washed thrice in 1x PBST or TBST and incubated with specific secondary antibodies conjugated to horseradish-peroxidase (HRP, dilution 1:10.000 in blocking buffer) at RT for 1-2 hours. Immunoreactive proteins were visualized with a chemiluminescent substrate (ECL-kit; GE Healthcare, Little Chalfont, UK) on Hyperfilm ECL (Amersham, Amersham, UK) films.

### **2.2.3 Cell culture methods**

Before PDL coating, the glass coverslips were thoroughly washed in acetone for 1 h at 4 °C followed by 0.1 M HCl in 70% ethanol for 1 h at 4 °C. Finally, they were rinsed in 100% ethanol and dried on a paper towel under the laminar flow hood. For coating, coverslips were transferred to a 24-well plate and 500 µL poly-D-lysine (PDL) working solution was added in each well. Incubation for at least 2 h or overnight at 37 °C followed. PDL was aspirated and coverslips were thoroughly washed with sterile double distilled water. Plates were dried under the laminar flow hood and stored at 4 °C for up to one week.

#### **2.2.3.1 Preparation and transfection of embryonic cortical and hippocampal cultures**

Cultures were prepared from timed pregnant C57BL/6 female mice at E14-16. The day of vaginal plug detection was considered day 0. Females were sacrificed by cervical dislocation and the abdominal cavity was cut open to expose the uteri containing the embryos. After removal of the uterine tissue and placenta, embryos were transferred to a 60-cm dish containing ice-cold Hanks buffered salt solution with 10 mM Hepes buffer (HBSS-Hepes). Embryos were

decapitated and the brains were isolated in a 60-cm dish with HBSS-Hepes under a dissecting binocular microscope (Leica, Wetzlar, Germany). The hindbrain was removed, the hemispheres were separated and the meninges were stripped away. Cortices or hippocampi from both hemispheres were dissected out and transferred to a 15-mL tube filled with ice-cold HBSS-Hepes. Under a tissue culture flow hood, the HBSS-Hepes was carefully aspirated with a Pasteur pipette and 3 mL fresh HBSS-Hepes were added to the cortices. The tissue was then mechanically dissociated using a 1000- $\mu$ L pipette. The cell suspension was centrifuged at 1000 rpm for 5 minutes and the supernatant was discarded. The cell pellet was resuspended in 1 mL culturing medium and the total cell number was determined using an improved Neubauer chamber. Cells were seeded onto glass coverslips coated with PDL at a density of 200,000 cells/well (of a 24-well plate). The culturing medium used was Neurobasal medium with Glutamax, B27 supplements (Invitrogen, Darmstadt, Germany) and penicillin/streptomycin (1x; Invitrogen, Darmstadt, Germany). Transfections with Lipofectamine 2000 (Invitrogen, Darmstadt, Germany) were performed after 2-3 days *in vitro* (DIV). Each coverslip was incubated with 0.5  $\mu$ g total DNA and 0.5  $\mu$ L Lipofectamine 2000, mixed in Neurobasal media, according to manufacturer's instructions, for 2 h before being changed back to regular complete culturing media. Fixation of the neuronal cultures and immunocytochemistry was performed as described (Threadgill et al., 1997).

### 2.2.3.2 Rabies virus and G-TVA construct

The construct encoding for *DsRedExpress2*, the RABV *glycoprotein* (G) and the *TVA800* (the GPI anchored form of the TVA receptor), designed as CAG-DsRedExpress2-2A-G-IRES2-TVA (i.e., G-TVA construct), as well as the construction of the G gene-deleted *GFP*-expressing RABV (SAD $\Delta$ G-GFP) have been described previously (Deshpande et al., 2013; Wickersham et al., 2007a). Cells that express the G-TVA, as well as the SAD $\Delta$ G-GFP, synthesize the virus, which is able to transmit into all presynaptic neurons innervating the transfected neuron. This allows the identification of all neurons that synaptically connected to the transfected cell.

### 2.2.3.3 Immunocytochemistry

For immunocytochemistry, cells were fixed with 4% paraformaldehyde (PFA) in PBS, pH 7.4, for 10 min followed by blocking with 2% bovine serum albumin (BSA) and 0.2% Triton X-100 in PBS for 30 min prior to staining. Primary antibodies were applied in blocking solution overnight at 4°C. One day later, cells were thoroughly washed in PBS and fluorescent-conjugated secondary antibodies were applied in blocking solution for 2 hours at RT. To visualize nuclei,

cells were incubated for 10 min in 0.1 µg/ml DAPI (Sigma). Cells on coverslips were embedded in Mowiol mounting medium (Roth, Karlsruhe, Germany) and allowed to dry at RT.

#### **2.2.3.4 Time lapse video microscopy**

Time-lapse video microscopy of dissociated cultures from the embryonic cerebral cortex at E14 was performed with an AxioObserver Z1 (Zeiss, Oberkochen, Germany) at a constant temperature of 37°C and 8% CO<sub>2</sub>. Phase contrast images were acquired every 10 min and fluorescent images every 20 min for 8-9 hours using a 20x objective (Zeiss), an AxioCamHRm camera and a Zeiss AxioVision 4.7 software. Single-neurite tracing was performed in ImageJ using the Simple Neurite Tracer plugin (Longair et al., 2011). Movies were assembled using ImageJ 1.42q (National Institute of Health, USA) software with 1 frame per second.

#### **2.2.4 Animals**

Animals were anaesthetized by intraperitoneal injection of a solution containing 1.0 mL Ketamine hydrochloride, 10% (injected approximately 100mg/kg body weight), 0.25 ml 2% Xylazine hydrochloride (Rompun; injected at 5 mg/kg body weight) and 2.5 ml physiological saline solution (sodium chloride). A lethal dose is required to ensure that mice are sedated during perfusion. Per adult mouse about 200-250 µl Ketamine/Rompun was injected. To ensure the mouse was properly sedated after injection, the toes were pinched to determine the mouse's response to a painful stimulus.

Anaesthetized animals were subsequently transcardially perfused, first with 1x PBS for 2-3 min and then with 4% PFA for 18-23 min. Brains were dissected and post-fixed in 4% PFA for 10 - 15 min, thoroughly washed with 1x PBS and stored in 1x PBS at 4°C till sectioning. For histology, fixed brains were cryoprotected in 30% sucrose (in PBS), embedded in tissue-tek (OCT compound) and stored at -20°C. Thirty µm free-floating cryostat sections were stored in cryo-protectant solution at -20°C.

For immunohistochemistry, sections were blocked with 5% goat serum and 0.5% Triton X-100 in PBS for 30 min prior to staining. Primary antibodies were applied in blocking solution overnight at 4°C. The day after, sections were thoroughly washed in PBS and secondary antibodies conjugated to fluorescent dyes or biotin, were applied in blocking solution for 2 hours at RT. For biotinylated antibodies incubation with streptavidin linked to Alexa dyes followed. To visualize nuclei, cells were incubated for 10 min in 0.1 µg/ml DAPI (Sigma). Sections were embedded in Mowiol mounting medium (Roth) and allowed to dry at RT. Slides were stored at 4°C in boxes.

## 2.2.5 Image collection and quantitative analysis

### 2.2.5.1 Confocal imaging

Stainings were imaged using either a LSM10 (Zeiss) or a SP5 (Leica) laser-scanning confocal microscope. For overview pictures of whole brain sections the Zeiss AxioImager.M2 fluorescence microscope was used. High quality pictures (1024x1024 or 2048x2048 pixels) were taken using a 25x or 40x objective. Serial z-stacks were taken and collapsed to obtain a maximum-intensity projection of the scanned image. Laser power levels, photomultiplier gain levels, scanning speed, and the confocal pinhole size were kept constant within experimental and control specimens. Data were saved as .lsm or .lif files so that all information could be saved. For further processing pictures were exported as tiff files. Digital processing of entire images, including adjustment of brightness and contrast, was performed using Photoshop CS3 (Adobe, Munich, Germany).

High-resolution z-stacks of dendrites from cortical and hippocampal neurons were collected with the 40x lens and a 2x digital zoom factor (optical sections of 0.5-1  $\mu\text{m}$ ). The number of primary dendrites emerging from the soma was manually counted and the dendritic length in  $\mu\text{m}$  was determined using the Zen2009 software (Zeiss, Oberkochen, Germany) in cortical and hippocampal neurons after 10 DIV using the images obtained with the laser-scanning confocal microscope as detailed above. Spine density was manually determined in 20  $\mu\text{m}$  long dendritic segments. Bassoon and PSD95 puncta were also manually determined.

The number of presynaptic partners of double transduced cells (GFP+/DsRED+) was determined by counting the double transduced cells (GFP+/DsRED+) and the RABV-only single transduced cells (GFP+). Results were expressed as connectivity ratio, representing the number of GFP-positive cells per GFP- and DsRed-double positive cells as described by (Wickersham et al., 2007).

### 2.2.5.2 Statistical analysis

Results are presented as means  $\pm$  SD. Statistical significance was calculated with GraphPad Prism 5 (GraphPad Software, San Diego, California) using the One-way ANOVA test with Dunnett's posthoc test. For the experiments with the rabies virus we used the unpaired t-test with Welch's correction. A *p* level of <0.05 was set as the level of statistical significance.



### 3 Results

#### 3.1 Antibodies against LRP4

The distribution of the LRP4 protein in the CNS is unknown. In order to analyze the distribution of LRP4 in the CNS, I generated two polyclonal antibodies in rabbits. These antibodies together with two commercially available antibodies (see Materials and Methods section for details) were used throughout my study to determine the distribution and localization of LRP4. To generate antibodies against LRP4 a unique sequence of the protein was identified. Based on previous studies (Tian et al., 2006), two regions of the LRP4 protein were selected as antigens, an intracellular and an extracellular region, respectively. Additionally, to exclude possible cross-reactions of the antibodies with other proteins (in particular with other members of the LDL family) due to sequence similarities, a BlastP database search was performed. Two possible regions were selected as antigens: sequence 1 (intracellular part of the protein, amino acids: 1755-1905) with the length of 150 amino acids (DPGMGNLTYSNPSYRTSTQEVKLEAAPKPAVYNQLCYKKEGGPDHSYTKKIKIVEGIRLLAGDDAEWGDLKQLRSSRGGLLRDHVCMKTDTVSIQASSGSLDDTETEQLLQEEQSECSSVHTAATPERRGSLPDTGWKHERKLSSSEQV) and sequence 2 (juxtamembrane extracellular part of the protein, amino acids: 1383-1700) with the length of 317 amino acids (LNNVISLDYDSVHGKVYYTDVFLDVIRRADLNGSNMETVIGHGLKTTDGLAVDWVARNLYWTDGTGRNTIEASRLDGSCRKVLINNSLDEPRAIAVFPRKGYLFWTDWGHIAKIERANLDGSEKVLINTDLGWPNGLTLDYDTRRIYWVDAHLDRIESADLNGKLRQVLVSHVSHPFALTQQDRWIYWTDWQTKSIQRVDKYSGRNKETVLANVEGLMDIIVVSPQRQTGTNACGVNNGGCTHLCFARASDFVCACPDGHPCSLVPGLVPPAPRATSMNEKSPVLPNTLPTTLHSSTTKTRTSLEGAGGRCSER). Antibodies raised in rabbit were ordered from Pineda Antikörper Service, Berlin, Germany. For each sequence, serum of the animal was collected after three immunizations. IgGs were affinity-purified from the rabbit sera using the antigen in an affinity column method. To determine the selectivity and specificity of the anti-LRP4 antibodies, a selective staining pattern, the disappearance of staining after preabsorption of the antiserum with the purified corresponding antigen and a protein band of the expected size on Western blots are required. The criteria for the specificity of the antiserum include the absence of staining in mice that are deficient for the protein of interest, an identical staining pattern of antibodies raised against different epitopes on the same protein (not true if the protein is cleaved for example) and the correspondence between the staining pattern after in situ hybridization (ISH) and immunohistochemistry (IHC) in consecutive sections (Pradidarcheep et al., 2008).

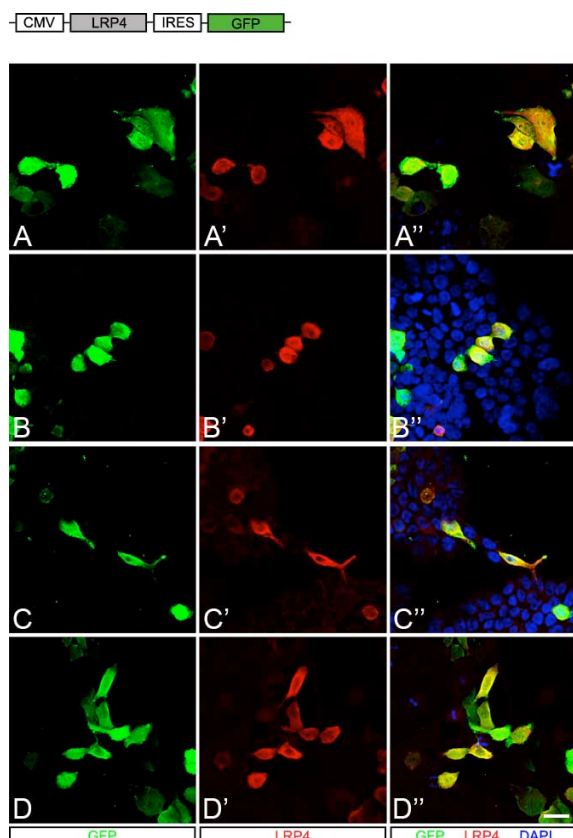


**Figure 3.1. Determination of antibody specificity using HEK293 cells transiently transfected with full-length LRP4**

Construct for overexpression of full-length LRP4 in HEK293 cells. Immunocytochemistry of HEK293 cells transiently transfected with pCMV-LRP4-IRES-GFP. Cells were fixed two days post transfection. (A-D) The transfected cells can be distinguished by GFP staining (green channel). (A'-D') Single channel images depicting the transfected cells stained for LRP4 (red channel) using the commercial antibody against the intracellular epitope (A'), the commercial antibody against the extracellular epitope (B'), the generated-in-house antibody against the intracellular epitope (C'), and the generated-in-house antibody against the extracellular epitope (D'). Note that all antibodies detect LRP4. (A''-D'') Merged images of the single channel images. Nuclei stained for DAPI (blue channel). Scale bar: 20  $\mu$ m.

### 3.1.1 Immunocytochemistry of HEK293 cells

As a first step to test the specificity/selectivity of the anti-LRP4 antibodies, I transiently overexpressed the full-length and the extracellular part of LRP4 in HEK293 cells. To this end, I cloned the LRP4 cDNA encoding the full-length protein into the pMES vector (Schröder et al., 2007), which contains an internal ribosomal entry site (IRES) sequence followed by the cDNA coding for eGFP (pCMV-LRP4-IRES-eGFP). The simultaneous expression of LRP4 and eGFP (due to the IRES sequence) allowed me to distinguish transfected from untransfected cells.

To overexpress specifically extracellular LRP4, the cDNA encoding the extracellular part of the protein was cloned into pEXPR-IBA42 vector under the CMV promoter generating the pCMV-LRP4ext vector. I co-transfected HEK293 cells with the pCMV-LRP4ext and a second vector encoding a CAG-driven eGFP protein, which allowed me to identify the transfected cells (pCAG-GFP+). I confirmed the presence of LRP4 in the transfected HEK293 cells using antibodies against LRP4 and GFP (Figure 3.1 and Figure 3.2). All of the antibodies selectively stained the HEK293 cells that were transfected with the full-length LRP4, but not untransfected cells (Figure 3.1). Immunocytochemistry of unfixed cells confirmed the presence of LRP4 on the cell surface and in the cytoplasm. The staining observed in the cytoplasm can be explained by the presence of LRP4 in the Golgi apparatus and the endoplasmic reticulum.

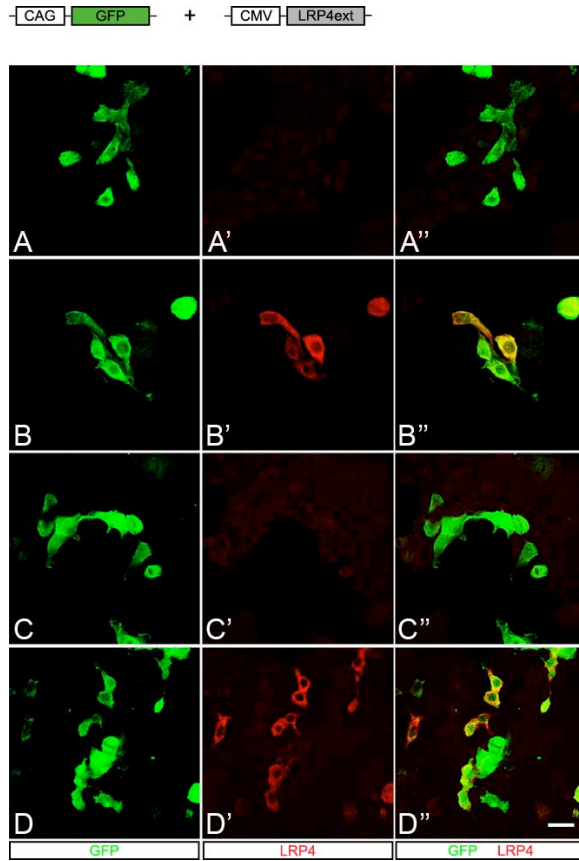


**Figure 3.2. Determination of antibody specificity using HEK293 cells transiently transfected with extracellular LRP4**

Constructs for the simultaneous expression of GFP and extracellular LRP4 in HEK293 cells. Immunocytochemistry of HEK293 cells transiently cotransfected with pCMV-LRP4ext and pCAG-GFP as a reporter. (A-D) The transfected cells can be distinguished by GFP staining (green channel). (A'-D') Single channel images depicting the transfected cells stained for LRP4 (red channel) using the commercial antibody against the intracellular epitope (A'), the commercial antibody against the extracellular epitope (B'), the generated-in-house antibody against the intracellular epitope (C'), and the generated-in-house antibody against the extracellular epitope (D'). Note that none of the

antibodies directed against the intracellular epitope detect the extracellular part of LRP4. (A''-D'') Merged images of the single channel images. Scale bar: 20  $\mu$ m.

Moreover, only the antibodies directed against the extracellular region of LRP4 stained HEK293 cells that were cotransfected with the pCMV-LRP4ext and the pCAG-GFP (**Figure 3.2**). These results show that the antibodies against both the intracellular and the extracellular epitopes selectively detect LRP4 in HEK293 cells that express LRP4.

### 3.1.2 Western blotting

To further test the specificity of the antibodies, SDS-PAGE followed by Western blotting was performed. The samples included protein lysates from transfected and untransfected HEK cells. Samples were separated on SDS-PAGE gels and analyzed by Western blotting. I detected a 250 kDa band (**Figure 3.3**) representing the expected size of the LRP4 protein after posttranslational modifications (Tian et al., 2006). However, transfection of LRP4 revealed different protein products at approximately 70-90 kDa, in addition to the 250 kDa full-length LRP4 band. These smaller bands might be processing products of the receptor, since there is evidence for proteolytic cleavage of LRP4 by ADAM10 and  $\gamma$ -secretase (Dietrich et al., 2010). There was no detectable signal in lysates from untransfected HEK cells. In addition, the pre-immune sera from both rabbits used at equivalent dilutions detected no band in LRP4-transfected HEK cells (data not

shown). These results further demonstrate the specificity of the antibodies. More Western blotting results will follow at later paragraphs showing the specificity of the antibodies also in different tissues.

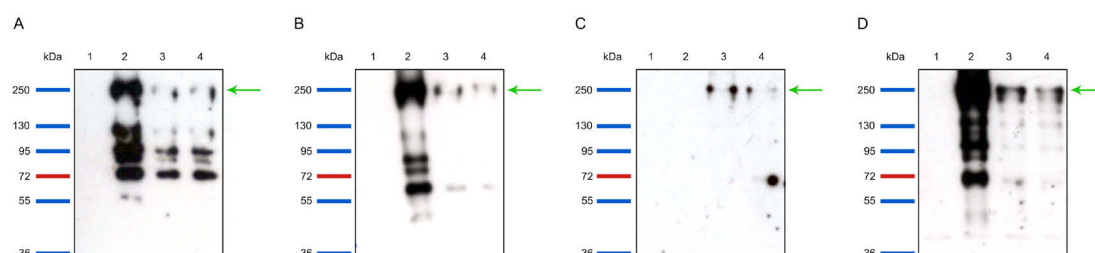


**Figure 3.3. Analysis of antibody specificity in Western blotting**

SDS-PAGE analysis and Western blot detection of HEK cells transfected with three different plasmids for overexpression of LRP4. The green arrows indicate the location of LRP4 at 250 kDa. Note that no signal can be detected in untransfected HEK cells. Samples from left to right are: lane M, molecular weight marker; lane 1, HEK cells transfected with empty vector; lane 2, HEK cells transfected with full-length human LRP4; lanes 3 and 4, HEK cells transfected with full-length mouse LRP4. The antibodies used are: the antibody generated-in-house against the intracellular epitope (A); the commercial antibody against the intracellular epitope (B); the antibody generated-in-house against the extracellular epitope (C); the commercial antibody against the extracellular epitope (D). Note the equivalent staining patterns with all four antibodies.

### 3.1.3 Immunohistochemistry of the NMJ

To further validate the ability of the antibodies to specifically detect LRP4 in tissue, I stained adult mouse skeletal muscle where it has previously been reported that LRP4 immunoreactivity is concentrated at the neuromuscular junction (Kim et al., 2008; Zhang et al., 2008). To this end, longitudinal sections of adult mouse leg muscles were double-labeled for AChRs using  $\alpha$ -bungarotoxin (selectively labeling the NMJ) and for LRP4. As a positive control, NMJs were stained for agrin and AChRs. As expected, the staining with the pre-immune sera was negative (data not shown). I confirmed using all four anti-LRP4 antibodies that in adult mouse skeletal muscle LRP4 was concentrated at the NMJ where it colocalized with the AChRs (**Figure 3.4**).

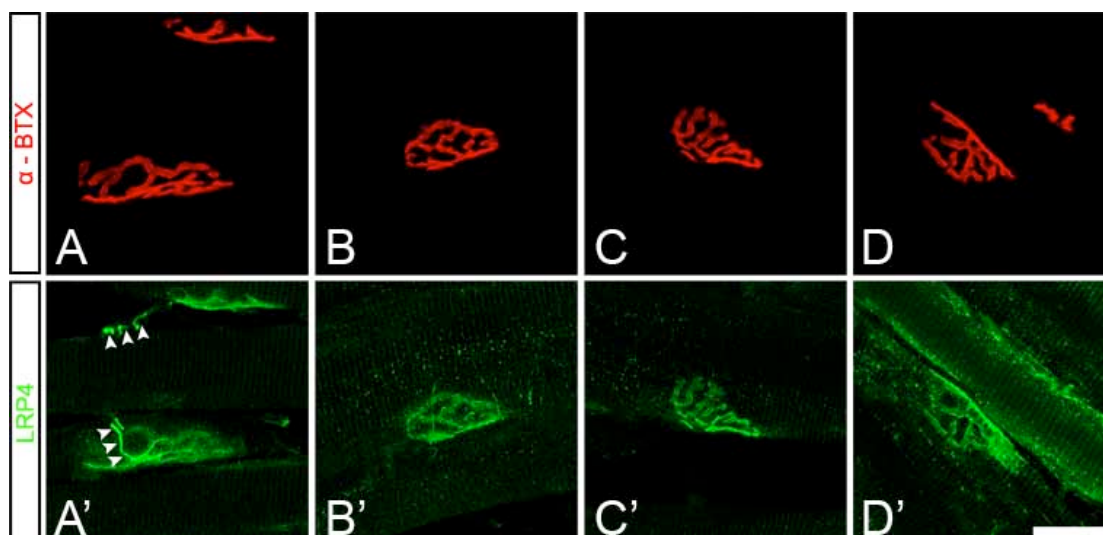


**Figure 3.4. Analysis of LRP4 localization at the adult NMJ and antibody specificity**

(A-D) Longitudinal sections of the adult mouse muscle stained with  $\alpha$ -bungarotoxin (red channel), a toxin that specifically binds to the AChR  $\alpha$ 1 subunit and thus labels the NMJ. (A'-D') Single channel images depicting the same NMJs stained for LRP4 (green channel) using the commercial antibody against the intracellular epitope (A'), the commercial against the extracellular epitope (B'), the generated-in-house antibody against the intracellular epitope (C'), and the generated-in-house against the extracellular epitope (D'). Note that all the antibodies detect LRP4 at the NMJ. The arrowheads in (A') indicate the motor neurons that are also positive for LRP4 but only the commercial antibody against the intracellular epitope can label them.  $\alpha$ -BTX:  $\alpha$ -bungarotoxin. Scale bar: 20  $\mu$ m.

To further rule out non-specific immunostaining signals, I performed an antibody-antigen competition experiment. To this end, the peptides against which the antibodies were raised were preincubated with the respective antibodies. This antibody-peptide mixture was then applied to cryostat sections from adult mouse skeletal muscle. Preabsorption process with the immunogen efficiently eliminated the staining of the NMJs demonstrating that the antibodies specifically recognized LRP4 (Figure 3.5).

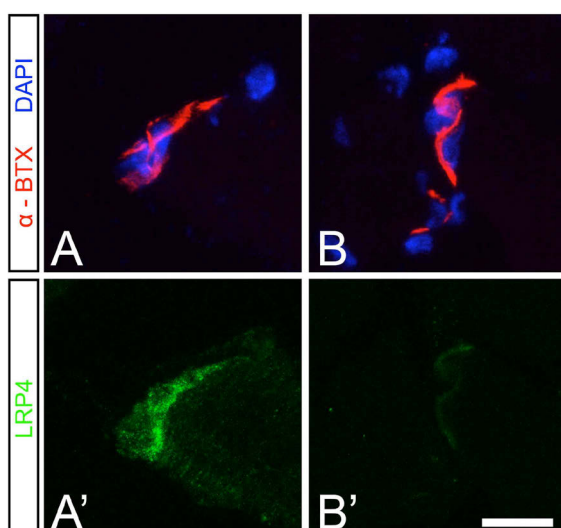


**Figure 3.5. Test of antibody specificity – antibody antigen competition experiment**

(A-B') Longitudinal sections of adult mouse skeletal muscle stained with  $\alpha$ -bungarotoxin (red channel; A and B) and with either LRP4 antibody against the intracellular epitope (green channel; A') or with LRP4 antibody pre-incubated with the peptide the antibody was raised against (green channel; B'). Note that staining with the LRP4 antibody specifically labeled the NMJ (A'), whereas the staining pattern is abolished when the antibody is pre-incubated with the peptide (B'). Thus,

preabsorption with the peptide was able to compete with the signal of immunostaining. Note that other antibody staining was likewise abolished in the presence of the peptide used as immunogen. Scale bar: 20  $\mu\text{m}$ .

These results confirm that the antibodies can specifically detect LRP4 in adult murine NMJs and can be used to analyze the distribution of LRP4 in other tissues, especially the brain.

## 3.2 LRP4 expression and localization in the adult murine brain

### 3.2.1 Reverse transcription PCR

After having confirmed the specificity and selectivity of the antibodies, I used them to determine the distribution of LRP4 in the CNS. To initially test whether LRP4 is expressed in the developing and adult murine CNS, I performed reverse transcription PCR. Specifically, total RNA was isolated from brain and eyes of four developmental stages (P5, P8, P15 and adult). As a positive control for the presence of *lrp4* mRNA, cDNA from adult brain was used since it has been previously reported that *lrp4* is expressed in the adult rat brain by *in situ* hybridization (Tian et al., 2006). As expected, no band was detected in the control reaction where water was used as a template. I detected *lrp4* mRNA in brain and eyes of the adult and of developmental stages (**Figure 3.6**), suggesting that LRP4 transcripts are present in the CNS before, during and after synaptogenesis which occurs between postnatal days 8-15.

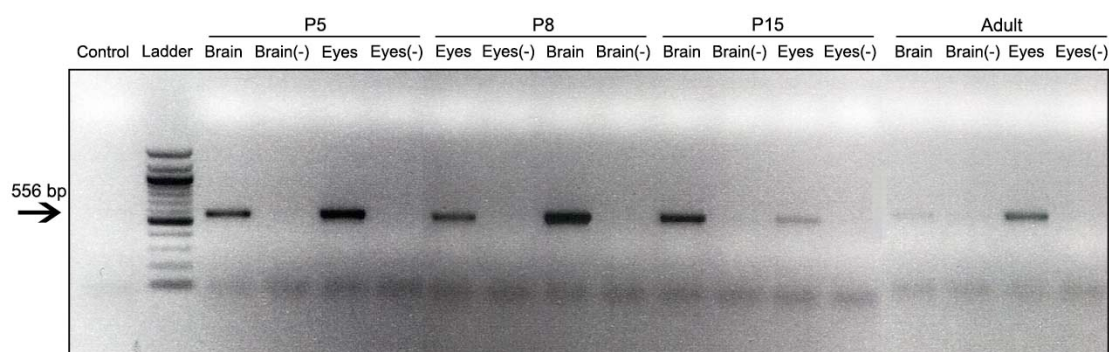


**Figure 3.6. *lrp4* mRNA is present in the murine brain and eyes during development and in adult stages**

Reverse transcription PCR of cDNA from mouse brain and eyes of different developmental stages using a set of intron/exon spanning primers. *lrp4* mRNA can be detected in the brain and eyes of P5, P8, P15 and adult mice. The size of the band is the size of the PCR product based on the designed primers. Note that no band can be detected in the reaction where water was used as a template (negative control).

### 3.2.2 Western blotting

To address if LRP4 protein can be detected in the adult mouse brain, I performed Western blotting using lysates from the adult brain. To this end, membrane protein fractions from the cerebral cortex, hippocampus, cerebellum and olfactory bulb were prepared and separated on SDS-PAGE gel and subsequently analyzed by Western blotting. A band with a molecular mass of



approximately 250 kDa was detected in all tissues (**Figure 3.7**). As a positive control, lysates from HEK cells transfected with the full-length LRP4 were used. I did not detect a specific signal in lysates from the untransfected HEK cells (**Figure 3.3**), demonstrating the specificity of the antibodies in Western blotting. These results show that LRP4 can be detected in the adult murine brain, not only at the mRNA, but also at the protein level.

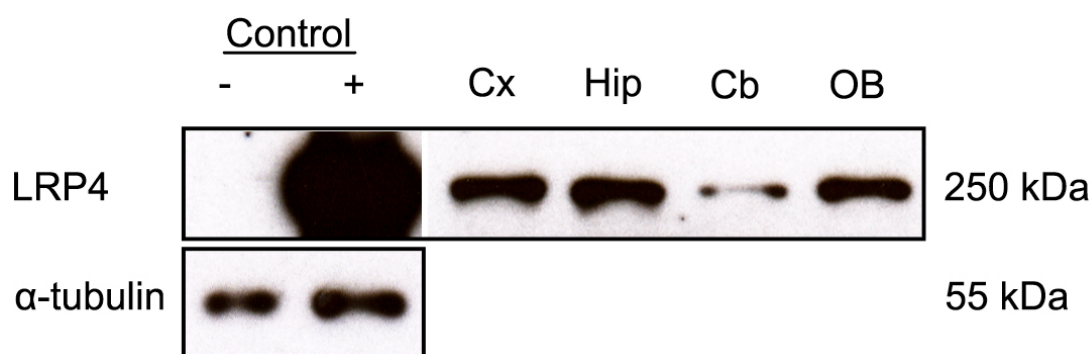


**Figure 3.7. LRP4 protein is present in the adult mouse brain**

Western blotting of protein lysates (1  $\mu$ g of protein) from the adult mouse cerebral cortex (Cx), hippocampus (Hip), cerebellum (Cb) and olfactory bulb (OB) probed with anti-LRP4 antibodies. Lysates from HEK cells transfected with full-length mouse LRP4 (+ control) and untransfected HEK cells (- control) were used to determine the specificity of the antisera. Anti- $\alpha$ -tubulin antibodies were used as loading control. The antibodies reacted with a band of 250 kDa, corresponding to the molecular mass of LRP4.

### 3.2.3 Immunohistochemistry

Previous studies have shown that *lrp4* mRNA is expressed in the adult rat brain, including the neocortical and hippocampal areas, the neurogenic niches, the olfactory bulb (OB) and the cerebellum (Tian et al., 2006). In order to characterize the distribution of LRP4 protein in the adult mouse brain, I performed immunohistochemical analyses using both the commercially available and the generated in-house antibodies. All antibodies exhibited a similar if not identical distribution pattern in all the brain areas tested, but the commercial antibodies had a lower background. For this reason, the distribution of LRP4 is described in the following sections using the commercial antibody against the intracellular epitope.

#### 3.2.3.1 Cerebral cortex

To determine the cellular and subcellular localization of LRP4 in the adult mouse cortex I performed immunohistochemical analysis. The staining revealed a wide distribution of LRP4 throughout the sub-cortical areas – motor, somatosensory and visual cortex (**Figure 3.8**). Double labeling with NeuN, which is a specific marker for postmitotic neurons (Mullen et al., 1992), revealed that LRP4 is localized in most, if not all, postmitotic (i.e. NeuN-positive) neurons in all

cortical layers (I-VI), particularly in neuronal cell bodies and dendrites, as well as in axons (Figure 3.8).

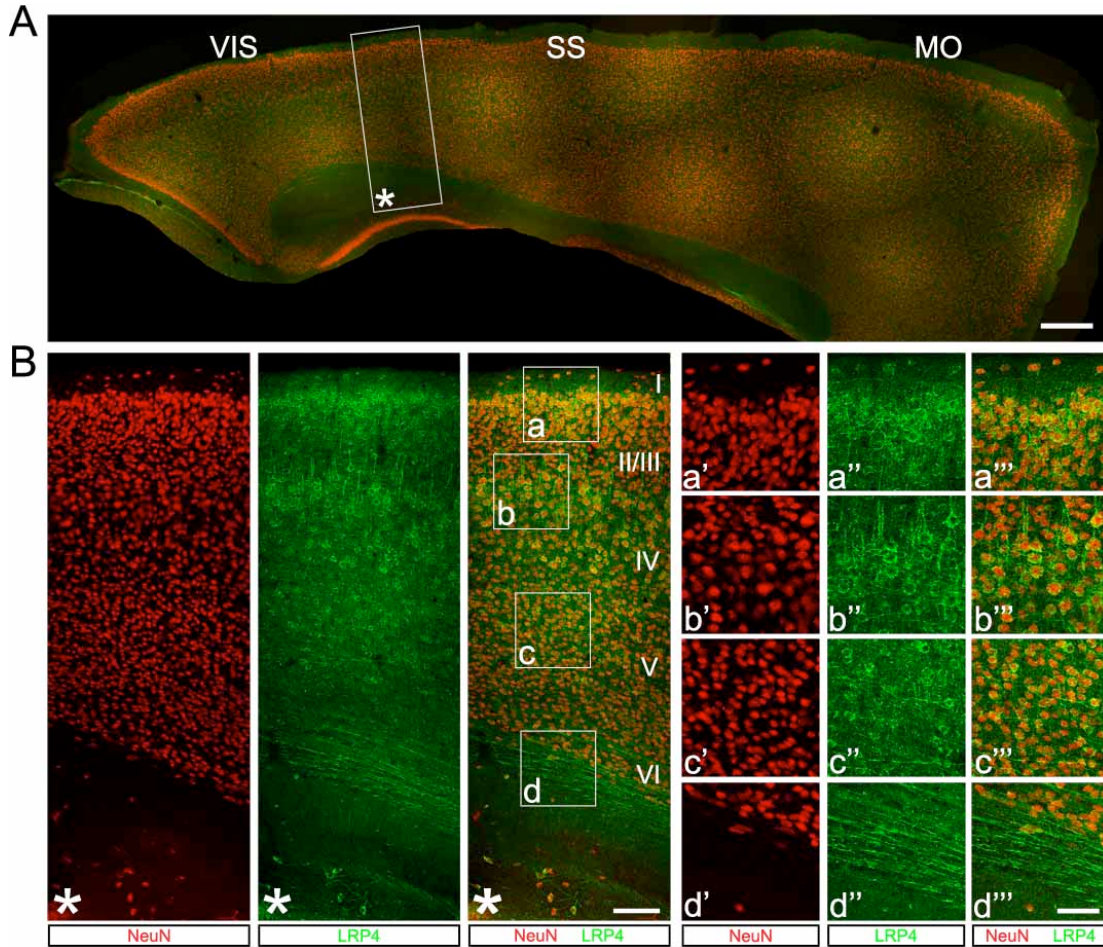


**Figure 3.8. Distribution of LRP4 in the neurons of the adult murine cortex**

(A) Overview of NeuN (red channel) and LRP4 (green channel) distribution in a sagittal reconstruction of the adult murine cerebral cortex. (B) Confocal z-stack of adult somatosensory cortex. (a'-d''') Insets depict the boxed areas from panel B, representing high magnifications of different layers of the cortex. The different cortical layers are indicated on the right side of the merged picture. Note that LRP4 is associated with the cell bodies and processes of neurons of all cortical layers (layer I/II a'-a'''; layer III/IV b'-b'''; layer V c'-c'''; layer VI d'-d'''). VIS: visual cortex; SS: somatosensory cortex; MO: motor cortex. Scale bars: 500  $\mu$ m (A), 100  $\mu$ m (B), and 50  $\mu$ m (insets in B).

To further examine whether the distribution of LRP4 in the cortex is restricted to neurons or if it is also present in the astroglial population, I immunolabeled adult mouse cerebral cortex with antibodies against GFAP/S100 $\beta$ , which are specific astrocytic markers (Jacque et al., 1978; Walz, 2000), and against LRP4. This analysis revealed that the levels of LRP4 protein were below the detection limits in astrocytes of the adult mouse cerebral cortex (Figure 3.9)

In summary, these results demonstrate that little, if any, LRP4 protein is present in astroglial cells, but high expression is detectable in neurons within all layers of the adult cortex.



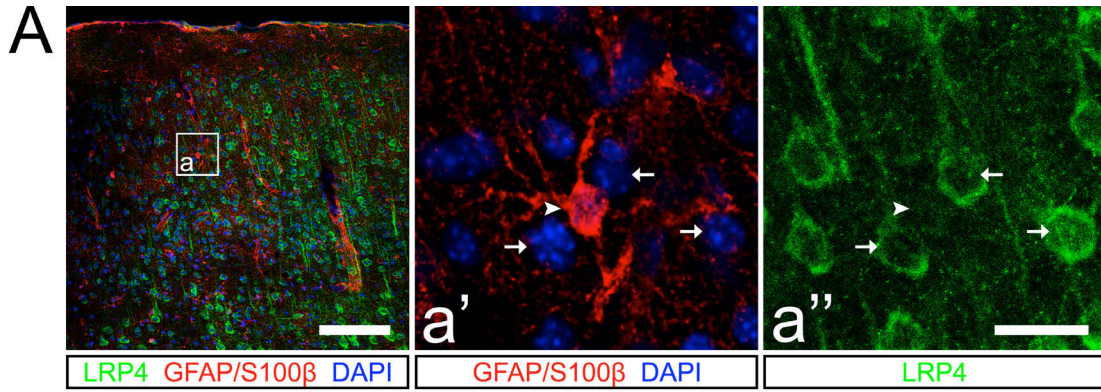


**Figure 3.9. Distribution of LRP4 in astrocytes of the adult murine cortex**

(A) Maximum projection of 10 confocal planes of the adult cerebral cortex labeled for LRP4 (green channel), GFAP and S100β (red channel). Nuclei were labeled with DAPI (blue channel). Enlarged single confocal planes of the boxed area depicting an astrocyte (arrowhead in a') surrounded by a number of neurons (arrows in a'). While the neuronal cell bodies appear strongly labeled by anti-LRP4 antibodies (arrows in a''), the levels of LRP4 in the astrocyte appear much lower and are close to the detection limits (arrowhead in a''). Scale bars: 100 μm (A), 20 μm (a' and a'').

### 3.2.3.2 Hippocampus

Staining of the adult murine hippocampus with the anti-LRP4 antibody revealed a widespread distribution of LRP4 within the hippocampus, with higher expression levels in the CA1, CA2 and CA3 regions and lower levels in the dentate gyrus (DG; **Figure 3.10**). Double labeling with anti-NeuN antibody showed that LRP4 is highly concentrated in hippocampal neurons of the CA1, CA2 and CA3 regions particularly around their soma and in their processes (**Figure 3.10**). In addition, LRP4 was highly concentrated in the axons of the entorhinal cortical neurons which give rise to the perforant path and project to the dentate gyrus and the hippocampal fields CA1 and CA3. In contrast to what has been reported (Tian et al., 2006), only low levels of LRP4 protein were detected in the dentate gyrus compared to the CA1-CA3 hippocampal regions. Furthermore, double labeling with anti-Doublecortin (Dcx) antibody, that specifically marks newly generated neurons, revealed that in adult-born, Dcx-positive cells the levels of LRP4 protein were below the detection limits (**Figure 3.10**).

Taken together, these data indicate that in the adult murine hippocampus LRP4 is predominantly localized in neurons of the CA1-CA3 regions, and at lower levels in the granule cells of the dentate gyrus, excluding the adult-born cells. The differential levels of LRP4 expression in the dentate gyrus compared to the CA1-CA3 region might suggest that LRP4 is primarily expressed in neurons generated during embryonic and early postnatal stages.

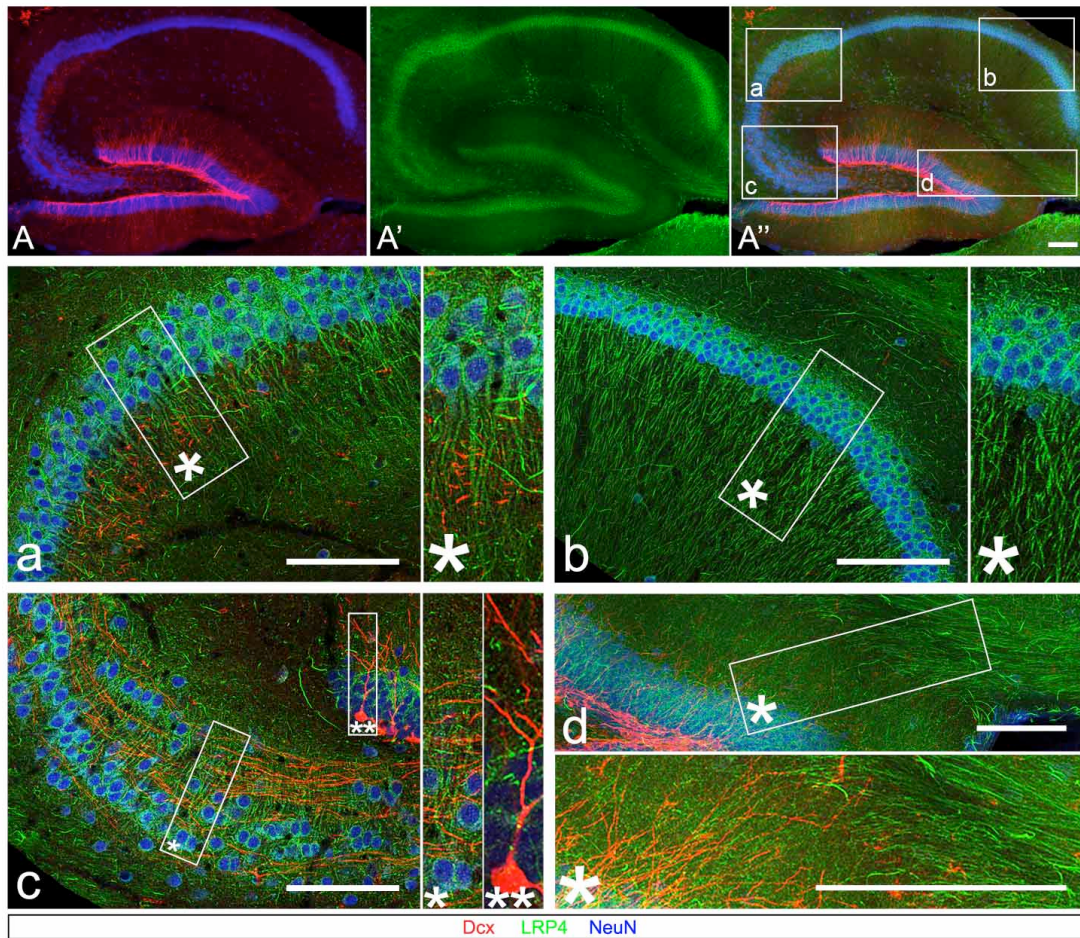


**Figure 3.10. Distribution of LRP4 in the adult murine hippocampus**

(A-A'') Reconstruction of a sagittal confocal section of the adult hippocampus labeled for LRP4 (green channel), Dcx (red channel) and NeuN (blue channel). (a-c) Panels that represent high magnifications of single confocal sections and panel d is a maximum projection of 12 confocal planes of the areas indicated by white boxes in panel A''. Note the presence of LRP4 in somas and processes of hippocampal neurons of the CA1- (inset b) and CA3- (insets a and c) regions and in the axons of the perforant path (inset d). Note that the Dcx-positive cells of the dentate gyrus (c, inset with two asterisks) are not labeled by anti-LRP4 antibodies. Scale bars: 100  $\mu\text{m}$  (A''), and 50  $\mu\text{m}$  (insets).

### 3.2.3.3 LRP4 localization in the adult-born neurons

To more directly investigate if LRP4 is expressed by neurons recently generated during adult neurogenesis, I used a transgenic mouse line in which GFP expression can be induced in adult neural stem cells from the dentate gyrus and subependymal zone (SEZ) (GLAST::Cre<sup>ERT2</sup>/eGFP; Mori et al., 2006; Nakamura et al., 2006) and is subsequently inherited by their progeny. In this mouse line the tamoxifen inducible form of Cre recombinase (Cre<sup>ERT2</sup>) is expressed in the locus of the astroglia/astrocyte-specific glutamate transporter (GLAST) and tamoxifen administration can induce the Cre-mediated recombination of the reporter locus (eGFP). GFP expression is induced in astroglia, including cells with astroglial features in the lateral wall of the lateral ventricle (LV), the subependymal zone, as well as in the subgranular layer (SGL) of the dentate



gyrus and is maintained also in their neuronal progeny. Forty-five days after tamoxifen-induced transgene expression, neither the recombined newly generated neurons (GFP+ Dcx+) nor the recombined mature neurons (GFP+ Dcx-) could be labeled with anti-LRP4 antibodies, confirming the very low levels of LRP4 protein in the granule neurons of the dentate gyrus (**Figure 3.11**). In agreement with the results described by Burk et al. (2012), recombined (GFP+) neuroblasts and postmitotic neurons that were generated in the SEZ and migrated to the olfactory bulb along the rostral migratory stream were also not labeled by anti-LRP4 antibodies, confirming that neurons generated during adult neurogenesis initially do not express LRP4 (**Figure 3.11**).

Taken together, these results demonstrate that little, if any, LRP4 protein is present in adult-born neurons, but high expression is detectable in a subpopulation of neurons of the olfactory bulb.

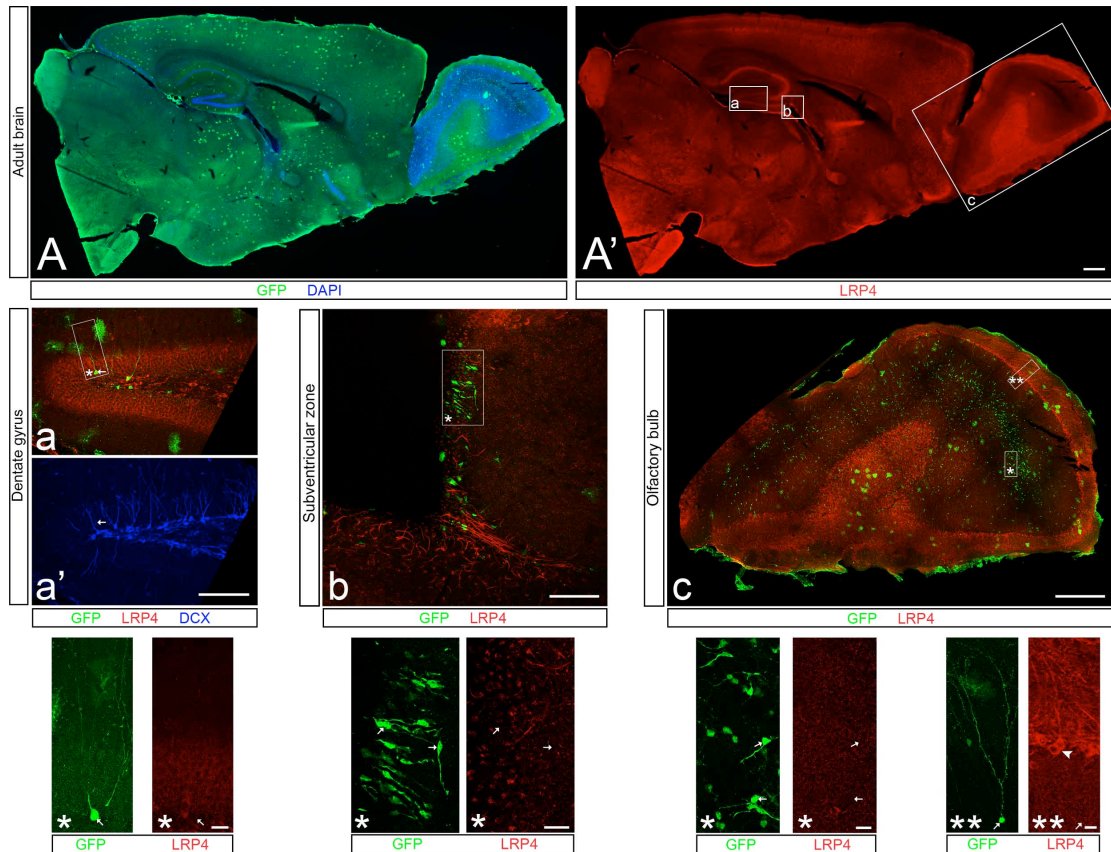


**Figure 3.11. Overview of LRP4 distribution in the adult-born neurons**

(A-A') Reconstruction of a sagittal confocal section of the adult hippocampus of the GLAST::CreERT2/eGFP transgenic mouse line labeled for LRP4 (red channel) and GFP to label the recombined cells (green channel). Nuclei are labeled with DAPI (blue channel). (a-c) Panels that represent high magnifications of the areas indicated by white boxes in panel A'. (a-a') Enlarged image of the DG. Note the absence of LRP4 in the DCX-labeled (blue channel) newly generated neurons of the DG (a, a'). Note also the absence of LRP4 immunoreactivity in the newly generated neurons that are not DCX-labeled (i.e. are more mature; white boxed area with one asterisk, white arrow). (b) Enlarged image of the SEZ. Note the absence of LRP4 immunoreactivity in the adult-born generated cells (white boxed area with

one asterisk, white arrows). (c) Enlarged image of the OB. GFP-recombined neurons do not show immunoreactivity for LRP4 (white boxed areas with one and two asterisks, white arrows). However, in the OB, the mitral cells are immunoreactive for LRP4 (white boxed area with two asterisks, white arrowhead). DG: Dentate gyrus; DCX: Doublecortin; SVZ: Subventricular zone; OB: Olfactory bulb. Scale bars: 500  $\mu\text{m}$  (A'), 100  $\mu\text{m}$  (a; b; c), 50  $\mu\text{m}$  (panels with asterisks).

### 3.2.3.4 Cerebellum

To determine the distribution of LRP4 in the cerebellum, I immunolabeled cryostat sections from adult mouse cerebellum with antibodies against calbindin D28k, which is a specific marker for mature Purkinje neurons (Jande et al., 1981), NeuN and GFAP (**Figure 3.12**). Double staining with anti-LRP4 antibody revealed that in the cerebellum LRP4 was exclusively localized in calbindin-positive Purkinje cells, particularly in their cell bodies and primary, secondary and tertiary dendrites. Hardly any NeuN-positive cells in the granule cell layer showed expression of LRP4, indicating a distribution of LRP4 in specific subsets of neurons in this area of the CNS. Double staining using antibodies against neurofilament heavy, a specific marker for neuronal axons, and LRP4 revealed that in addition to the cell bodies and dendrites LRP4 was also present in axons extending from the Purkinje neurons (**Figure 3.12 E-E''**).

To examine if LRP4 was present in the Bergmann glia of the cerebellum, I immunolabeled adult mouse cerebellum with antibodies against GFAP. Double labeling revealed that in this specific glial population of the cerebellum the level of LRP4 protein was below the detection limits (**Figure 3.12 D-D''**).

Taken together, these results show that in the adult mouse cerebellum LRP4 is predominantly localized in Purkinje neurons.

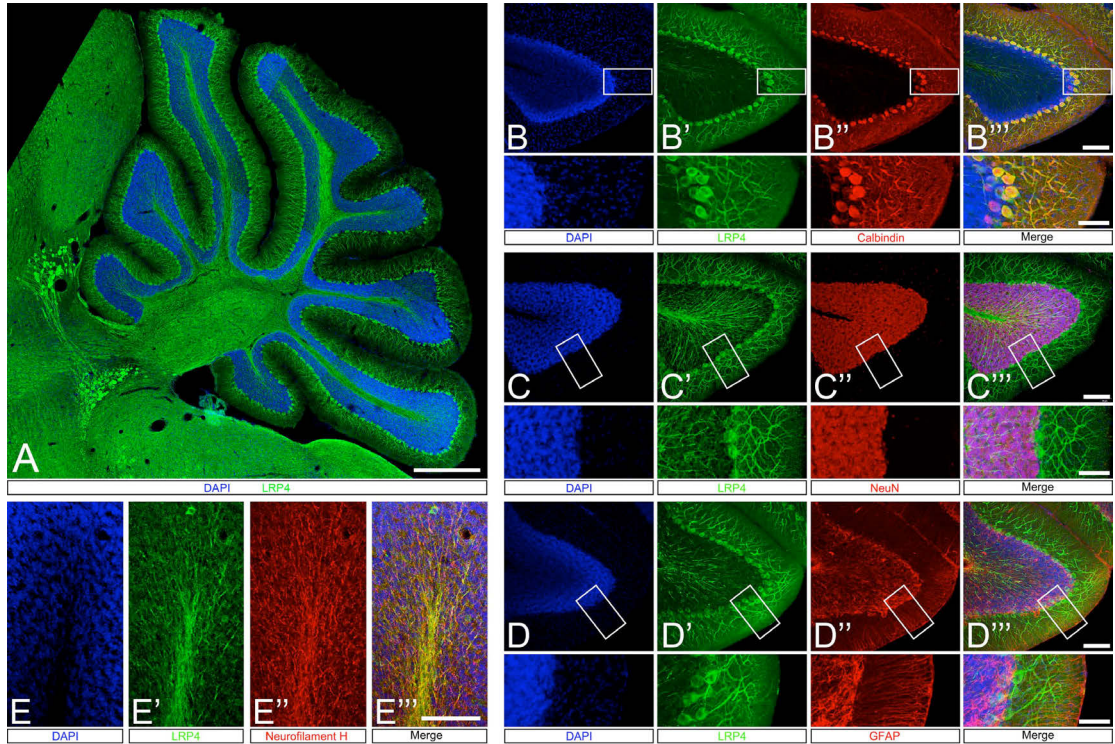


**Figure 3.12. Distribution of LRP4 in the adult murine cerebellum**

(A) Overview of LRP4 distribution in the adult murine cerebellum. Reconstruction of a sagittal section using Zeiss LSM710 “ZEN-tilescan”. (B-E”) Sagittal sections of single folia of the adult cerebellum labeled with antibodies against LRP4 (green channel; B’, C’, D’ and E’) and calbindin D28k (red channel; B”), NeuN (red channel; C”), GFAP (red channel; D”) or Neurofilament heavy (red channel; E”). Nuclei were labeled with DAPI (blue channel). Note the colocalization of LRP4 immunoreactivity with the Purkinje neuron-specific marker calbindin. Scale bars: 500  $\mu$ m (A), 100  $\mu$ m (B-E”) and 50  $\mu$ m (insets).

### 3.3 LRP4 distribution in neuronal cultures

As a first step to investigate the function of LRP4 in the CNS I used cultures of hippocampus and cortex. Low-density cultures are far less complex than neural tissue, making them an ideal model for investigating the subcellular localization and trafficking of neuronal proteins (Kaeck and Banker, 2006). Moreover, these cultures are suitable for the overexpression and knockdown of proteins, allowing the functional analysis of proteins by interfering with their concentration.

To determine the spatial and temporal localization of LRP4, I immunolabeled dissociated cells from the embryonic cerebral cortex and hippocampus at different time points (days) *in vitro* (DIV3, 6, 8, 10 and 12) with the same anti-LRP4 antibody previously used for the detection of LRP4 *in vivo* and in combination with antibodies against the microtubule associated protein (MAP2) that localizes to the soma and the dendrites (Caceres et al., 1984). I detected LRP4 in cortical neurons of all stages analyzed (Figure 3.13). Similar results were obtained in cultured hippocampal neurons (Figure 3.13). These results show that LRP4 is expressed in both cortical and hippocampal neurons at all stages analyzed.



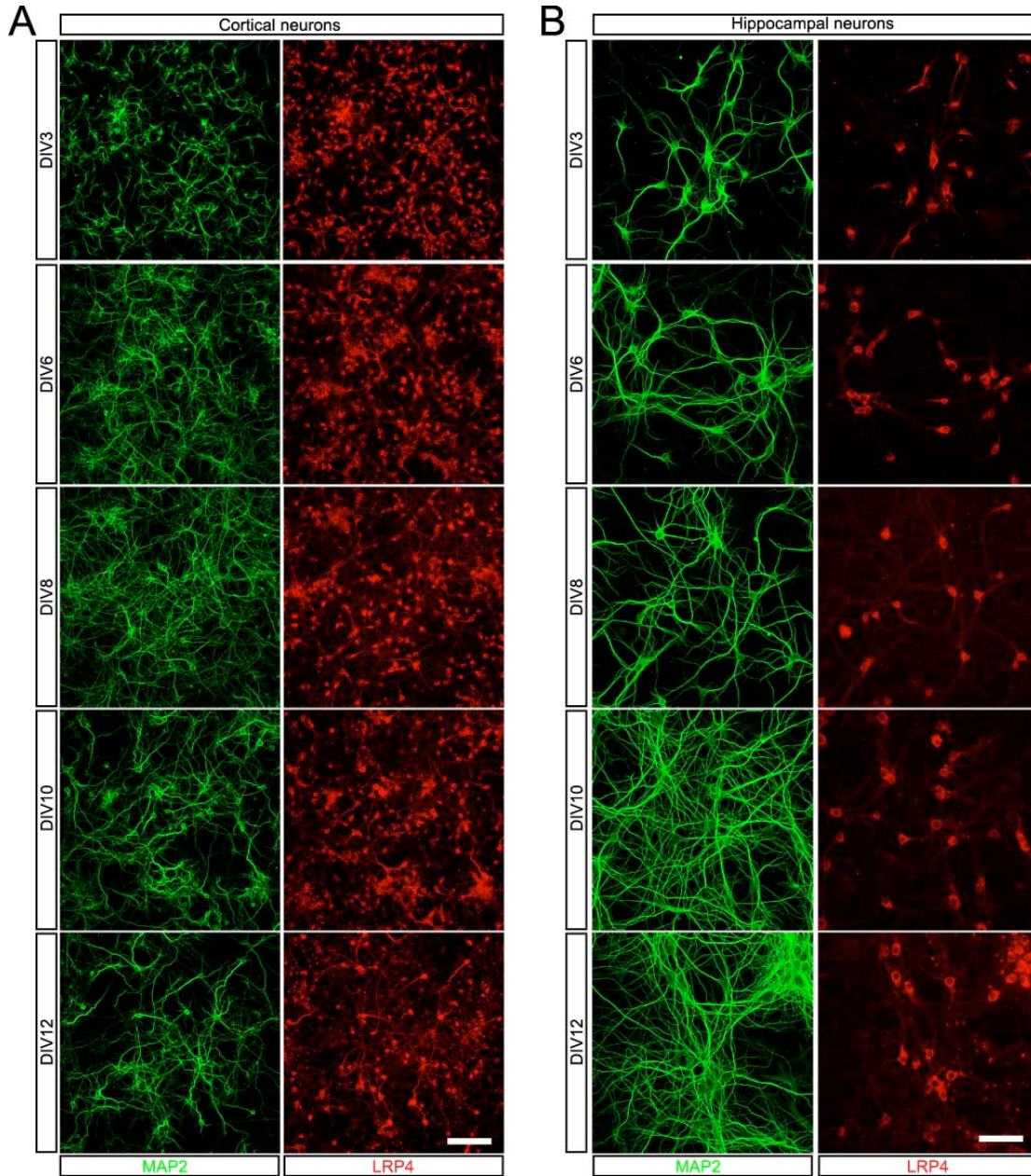


**Figure 3.13. Endogenous LRP4 expression in dissociated cultures from the embryonic cerebral cortex and hippocampus**

Dissociated cells from the E14 cortex (A) and E16 hippocampus (B) at different days *in vitro* (DIV) labeled for LRP4 (red) and MAP2 (green). Note that LRP4 is present in neurons of all the stages analyzed (DIV3, 6, 8, 10 and 12). Scale bars: 100  $\mu$ m (A; B).

### 3.3.1 LRP4 is localized in somas, dendrites and axons of cultured hippocampal neurons

In order to more precisely determine the subcellular distribution of LRP4, I stained dissociated cells from the E16 hippocampus with antibodies that specifically label either the dendritic or the axonal processes of neurons. To this end, hippocampal neurons were cultured *in vitro* until day 12 (DIV12) and stained for MAP2 and the axonal marker, Tau. I observed abundant, punctate LRP4 staining on the neuronal cell bodies and the proximal, MAP2-positive dendrites. Some

punctate staining was also evident on Tau-positive axons and growth cones at some distance from the cell body (Figure 3.14).

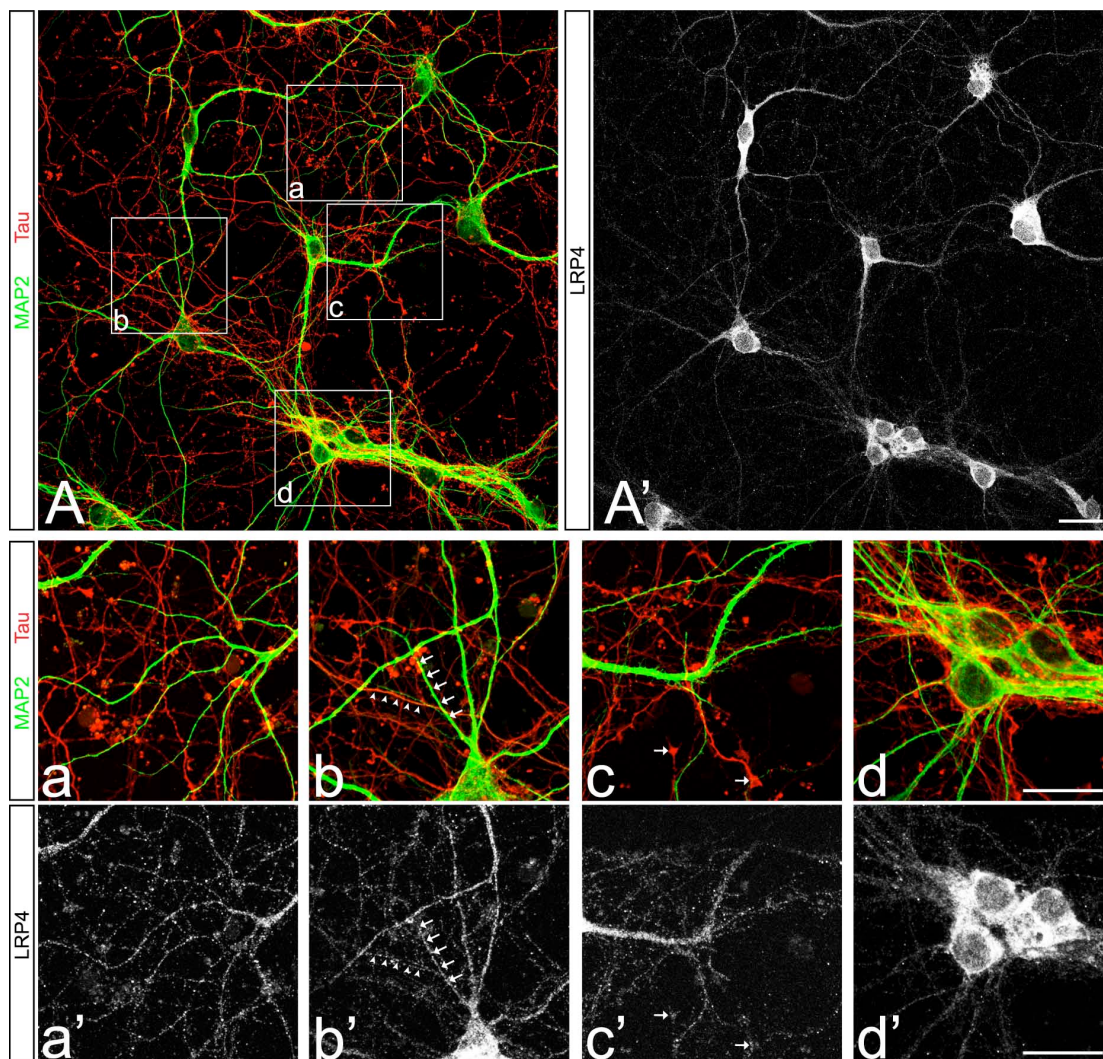


**Figure 3.14. Distribution of LRP4 in hippocampal neuronal cultures**

(A-A') E16 hippocampal neurons cultured for two weeks. Immunostaining for MAP2 (green), Tau (red) and LRP4 (white). Scale bar 50  $\mu$ m. (a-d') Enlarged images of the cells in pictures A and A' (white boxed areas). (b-b') MAP2 labeled dendrites are positive for LRP4 (white arrows) and Tau labeled axons are also positive for LRP4 (white arrowheads). (c-c') Tau-labeled growth cones show LRP4 immunoreactivity (white arrows). (d-d') Neuronal cell bodies also show immunoreactivity for LRP4. Scale bar 20  $\mu$ m.

The presence of LRP4 in neurons *in vitro* was confirmed by Western blotting using protein lysates from dissociated cortical and hippocampal cultures in which the full-length 250 kDa band was detected (Figure 3.15).



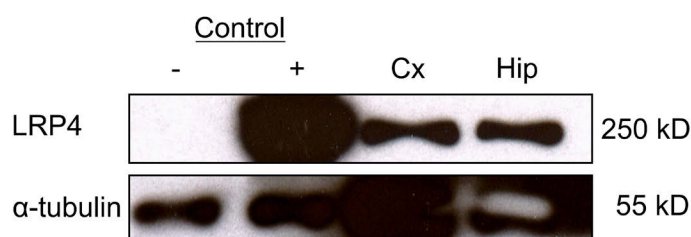


**Figure 3.15. LRP4 protein is present in lysates from cortical and hippocampal neurons**

Western blotting of protein lysates from cortical (Cx) and hippocampal (Hip) neurons of DIV1 probed with anti-LRP4 antibodies. Lysates from HEK293 cells transfected with full-length mouse LRP4 (+ control) and untransfected HEK293 cells (- control) were used to determine the specificity of the antisera. Anti- $\alpha$ -tubulin antibodies were used as loading control. The antibodies reacted with a band of 250 kDa, corresponding to the molecular mass of LRP4.

These results are in agreement with the distribution of LRP4 in the hippocampus of adult mouse brain tissue where LRP4 is localized in somas and processes of hippocampal neurons of the CA1-CA3 regions (**Figure 3.10**).

### 3.3.2 Both glutamatergic and GABAergic neurons express LRP4

To determine if LRP4 is present in both glutamatergic and GABAergic neurons I immunolabeled hippocampal neurons with antibodies specific for these neuronal subtypes. Thus, glutamatergic neurons were labeled with CamKII, a well-established marker for glutamatergic neurons (Jones et al., 1994), whereas GABAergic neurons were identified by an antibody against GABA (Sloviter and Nilaver, 1987). I detected LRP4 in both neuronal types (**Figure 3.16**), suggesting that it might be involved in the development of both excitatory and inhibitory neurons.



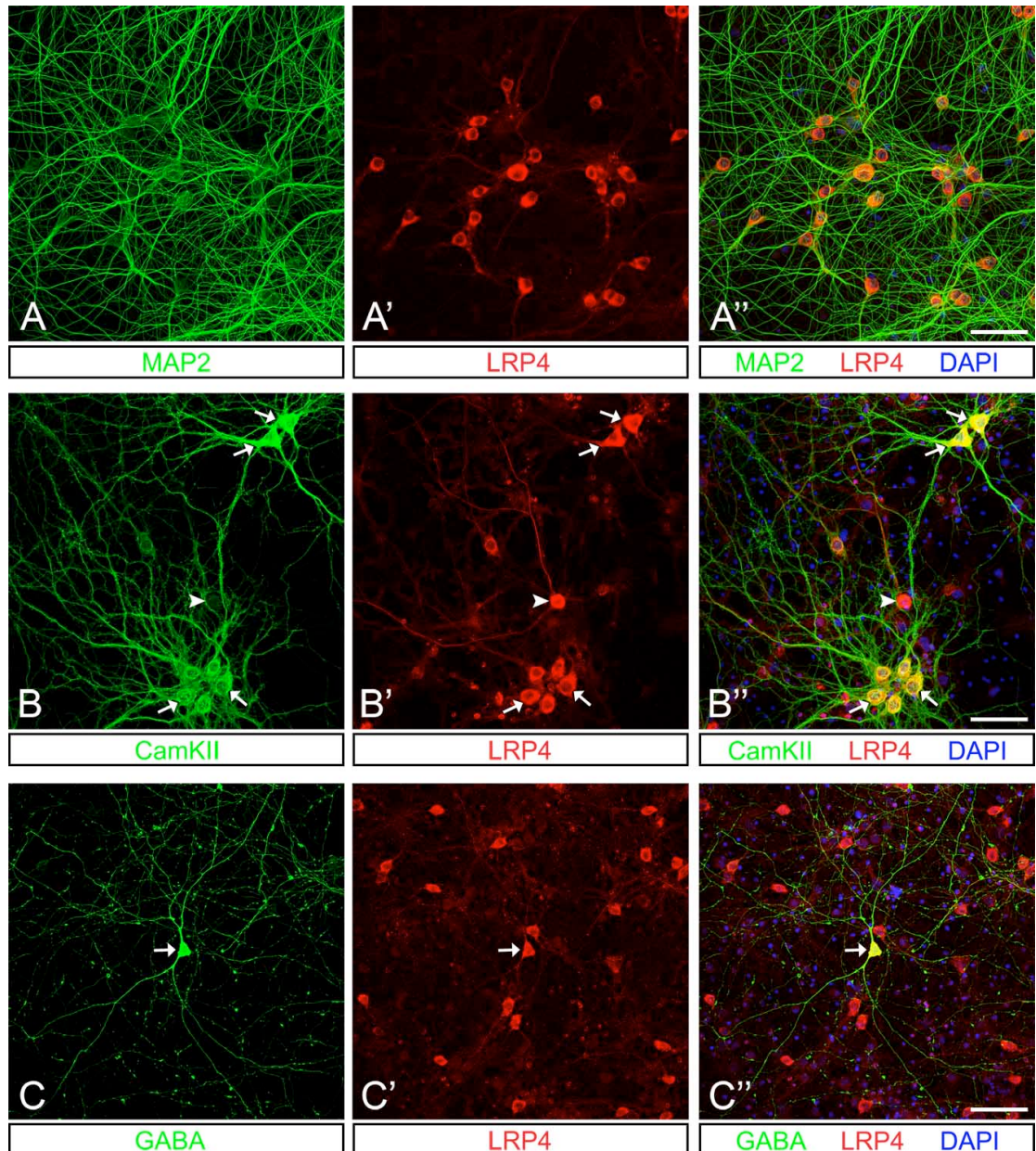


**Figure 3.16. LRP4 is present in both glutamatergic and GABAergic neurons**

(A-A'') E16 hippocampal neurons fixed after 17 days in culture. Immunostaining for MAP2 (green channel) and LRP4 (red channel). Nuclei are stained with DAPI (blue channel). Note that all the MAP2-labeled cells are immunoreactive for LRP4. (B-B'') E16 hippocampal neurons after 17 days in culture. Immunostaining for CamKII (green channel), LRP4 (red channel) and DAPI nuclear staining (blue channel). Note that LRP4 is expressed in CamKII positive neurons (white arrows). However, not all LRP4-labeled cells are positive for CamKII (white arrowhead). (C-C'') E16 hippocampal neurons after 17 days in culture. Immunostaining for GABA (green channel), LRP4 (red channel) and DAPI nuclear staining (blue channel). GABA positive neurons are immunoreactive for LRP4 (white arrow). Scale bars: 50  $\mu$ m.

### 3.3.3 LRP4 in astrocytes

To verify the results obtained from the immunostaining performed in the adult mouse cortex where I showed that the levels of LRP4 in astrocytes were below the detection limits (**Figure**

3.9), I co-immunostained hippocampal cultures with antibodies against GFAP,  $\beta$ III-tubulin and LRP4. As expected,  $\beta$ III-tubulin positive neurons showed high levels of LRP4 in both their somas and processes (Figure 3.17). In contrast, LRP4 levels in GFAP-labeled astrocytes were below the detection limits (Figure 3.17). These results show that in these cultures LRP4 is mainly expressed by neurons rather than glial cells, confirming my previous *in vivo* results.

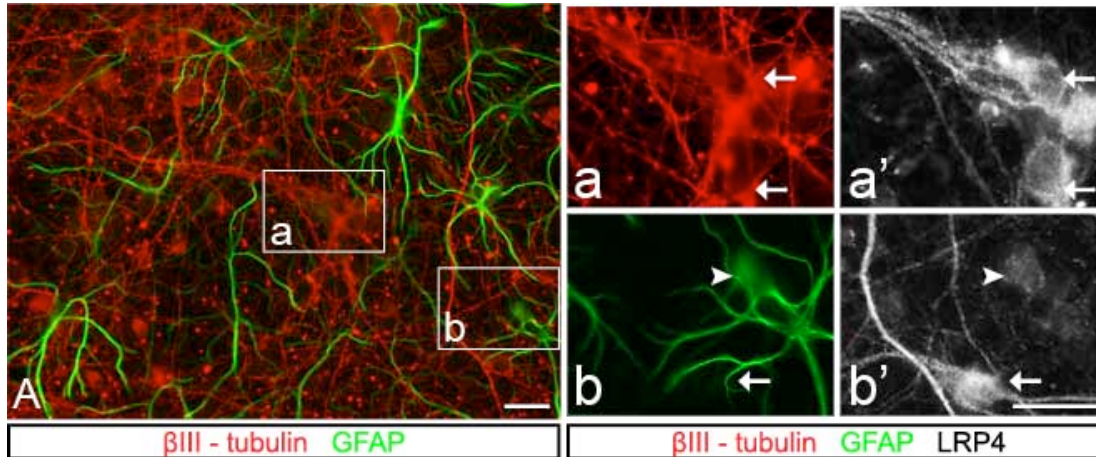


**Figure 3.17. LRP4 is present in astrocytes in low levels**

(A) Dissociated cells from the E16 hippocampus after 8 DIV labeled for  $\beta$ III-tubulin (red channel), GFAP (green channel) and LRP4 (white channel). Note that LRP4 is highly expressed in  $\beta$ III-tubulin positive neurons (arrows in a' and b'), whereas LRP4 levels in GFAP positive astrocytes are close to the limits of detection (arrowhead in b'). Scale bars: 50  $\mu$ m (A), 10  $\mu$ m (a-b').

### 3.4 Function of LRP4 in neuronal cultures

Previous studies have shown that at the NMJ muscle membrane-associated LRP4 was necessary and sufficient for presynaptic differentiation and the establishment of synaptic contacts between  $\alpha$ -motoneurons and skeletal muscle fibers (Wu et al., 2012; Yumoto et al., 2012; Kim et al., 2008). To investigate the function of LRP4 in neuronal cultures, I performed *in vitro* gain- and loss-of-function experiments and analyzed their effects on synaptogenesis and dendritic arborization.

#### 3.4.1 Overexpression of LRP4 in neurons

To overexpress LRP4 in neuronal cultures of the cortex and the hippocampus, the full-length cDNA of mouse LRP4 was cloned into the pcDNA3.1(-) vector downstream the CMV promoter. In order to exclusively overexpress LRP4 in neurons I replaced the CMV promoter by the neuron-specific synapsin-1 (SYN) promoter, generating the plasmid pSYN-LRP4. Syn-1 is a phosphoprotein that regulates the formation of synaptic vesicles and has a high level of early transcription in primary hippocampal neurons (Kügler et al., 2001; Gascón et al., 2008). I co-transfected cortical and hippocampal neurons on DIV3 with the pSYN-LRP4 plasmid and a second vector encoding a synapsin-driven eGFP-actin fusion protein (SYN-eGFP:actin), which



allowed me to observe spine-like protrusions enriched with GFP:actin monomers (Fischer et al., 1998; Gascón et al., 2008). I next confirmed the presence of LRP4 protein in the co-transfected cells (eGFP:actin positive) by immunocytochemistry and observed exclusive expression in neurons (**Figure 3.18**).

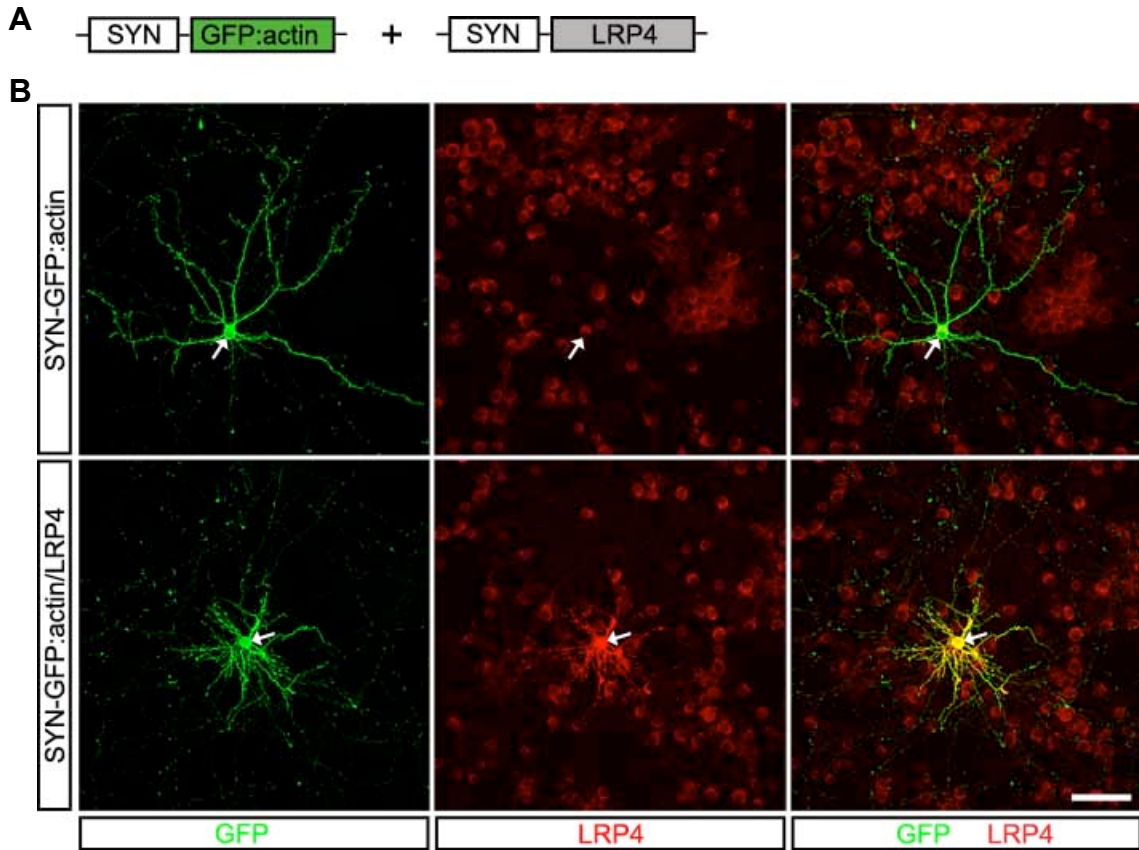


**Figure 3.18. Constructs for expression of GFP:actin and LRP4 in neurons in vitro**

(A) Constructs encoding the GFP:actin fusion protein and for LRP4 ORF. Transgene expression is driven by the synapsin (SYN) promoter. (B) E14 cortical cultures transfected with either GFP:actin encoding plasmid (upper set of pictures) or double transfected with GFP:actin and LRP4 encoding plasmids (lower set of pictures). Immunostaining for eGFP (green channel) and LRP4 (red channel) reveals that in the case of the double transfection the neuron is transfected with both plasmids. Scale bars: 50 μm.

### 3.4.2 Overexpression of LRP4 affects dendritic development and synapse formation in vitro

The pSYN-LRP4 plasmid was used in order to overexpress LRP4 in cortical and hippocampal neurons. By using the transfection reagent Lipofectamine 2000 and only 0.5 μg of DNA a low efficiency of transfection was achieved that allowed me to analyze the morphological characteristics of individual neurons surrounded by non-transfected neurons. Interestingly, overexpression of LRP4 led to a prominent change of the dendritic morphology, i.e. an increased number of primary dendrites and a reduced length of the dendritic branches (**Figure 3.19**). Morphometric analysis revealed a significantly increased number of primary dendrites ( $13.87 \pm$

1.64 in cortical,  $p<0.01$ ;  $13.03 \pm 1.32$  in hippocampal,  $p<0.001$ ) in neurons overexpressing LRP4 compared to the neurons transfected with the SYN-GFP:actin plasmid alone ( $7.54 \pm 1.65$  in cortical;  $6.39 \pm 0.37$  in hippocampal). I also observed a decreased primary dendritic length in both cortical and hippocampal neurons ( $49 \pm 6.48 \mu\text{m}$  in cortical,  $p<0.001$ ;  $43.47 \pm 10.64 \mu\text{m}$  in hippocampal,  $p<0.01$ ) compared to control neurons ( $112 \pm 10.26 \mu\text{m}$  in cortical;  $133.1 \pm 24.17 \mu\text{m}$  in hippocampal). Thus, overexpression of LRP4 reduces the length of primary dendrites while increasing the number of dendritic branches in cortical and hippocampal neurons. I did not observe an effect of the LRP4 overexpression on the length and arborization of axonal processes extended by cortical and hippocampal neurons in culture (data not shown).

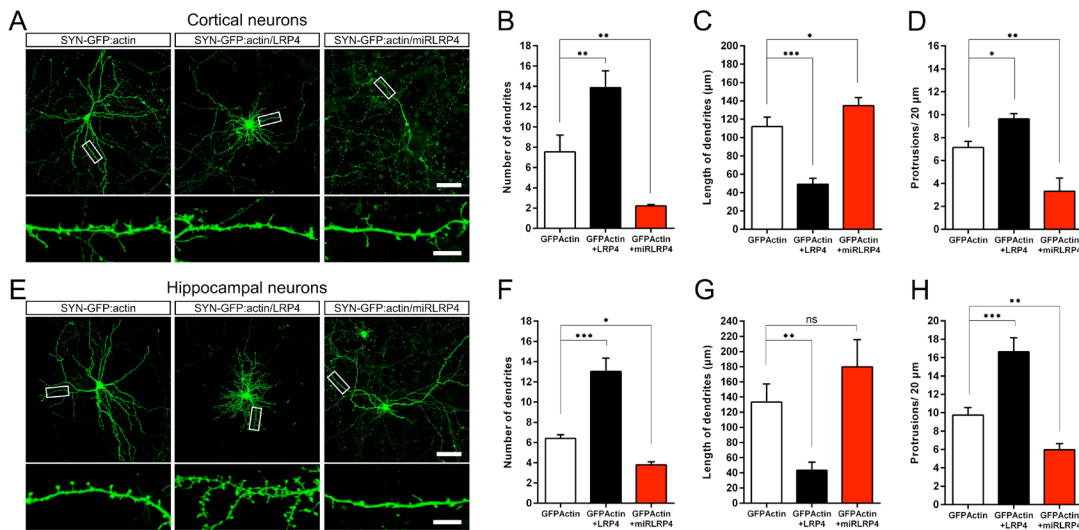


**Figure 3.19. LRP4 affects the number and length of dendrites and the number of spines in cultured cortical and hippocampal neurons**

Representative examples of dissociated cells from the E14 cerebral cortex after 10 DIV (A) and the E16 hippocampus after 12 DIV (E) co-transfected with pSYN-GFP:actin and additionally with either pSYN-LRP4 or with pCAG-miLRP4 at DIV3. Enlarged images of dendritic segments are shown to illustrate the dendritic protrusions. Histograms depict the number of primary dendrites (B, F), the length of the primary dendrites (C, G) and the density of spines/protrusions (D, H) in cortical (upper panels) and hippocampal (lower panels) neurons. Note that overexpression of LRP4 significantly increased the number of primary dendrites (B, F; black bars) and the density of spines/protrusions (D, H; black bars) and decreases the dendritic length (C, D; black bars) in both cortical and hippocampal neurons. In contrast, knockdown of LRP4 significantly decreased the number of primary dendrites (B, F; red bars) and spines/protrusions (C, G; red bars) and significantly increased the dendritic length in cortical (C; red bar) but not in hippocampal (G; red bar) neurons. Data are shown as mean  $\pm$  SD from three independent experiments,  $n = 15$ -25 cortical neurons per condition/experiment;  $n = 5$ -10 hippocampal neurons per condition/experiment. \* $p<0.05$ , \*\* $p<0.01$ , \*\*\* $p<0.001$ , One-way ANOVA with Dunnett's posthoc test. Scale bars: 50  $\mu\text{m}$  (A and E), and 10  $\mu\text{m}$  (insets in A and E).

### 3.4.3 Time lapse analysis of E14 cortical neurons overexpressing LRP4

Previous studies have demonstrated that at the NMJ LRP4 is required for the transformation of the highly motile growth cone to a much more stable presynaptic terminal (Wu et al., 2012; Yumoto et al., 2012). To investigate the mechanism of how LRP4 overexpression influenced dendritic arbor formation, I performed time-lapse video microscopy of neurons transfected with an RFP-encoding vector (pCAG-RFP) alone or in combination with the pSYN-LRP4 vector (**Figure 3.20**). Cells were transfected on DIV3 and imaging started 2-3 days after transfection and lasted for 8 hours. Following single dendrites from either control or LRP4 overexpressing cortical neurons over time, revealed that within a few hours after LRP4 overexpression, dendritic extension stopped (**Figure 3.20**). Neither extension nor retraction of dendritic processes was observed after LRP4 overexpression and the dendrites appeared rather immobile. This behavior might be similar to what has been reported for  $\alpha$ -motoneurons at the NMJ, where LRP4 expression arrested motor axon growth (Wu et al., 2012; Yumoto et al., 2012). Thus, my results suggest a similar role of LRP4 in process extension in  $\alpha$ -motoneurons and in CNS dendrites.

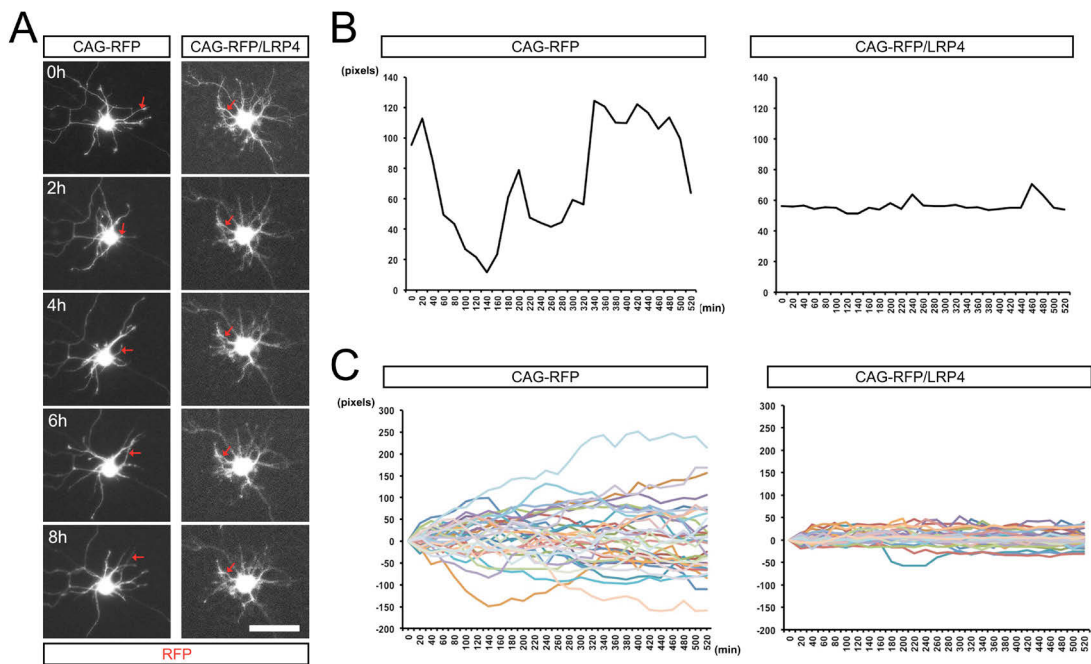


**Figure 3.20. Overexpression of LRP4 in cultured cortical neurons reduced the dynamics of the primary dendrite growth**

(A) Fluorescence micrographs of representative examples of neurons from the E14 cerebral cortex (DIV5-6) co-transfected with pCAG-RFP and pSYN-LRP4 or the empty pCAG-RFP control vector and live-imaged for 8 hours two days after transfection. Red arrows indicate single dendritic processes followed over the imaging time. (B) Graphs representing the mobility of the two dendrites indicated by red arrows in panel A. The x axis represents the time in minutes and the y axis represents the length of each dendrite (2.016 pixels/ $\mu\text{m}$ ). While dendrites of neurons transfected with the control vector were highly dynamic, overexpression of LRP4 resulted in a reduced motility and a stop of dendrite growth. (C) Overlay of the motility analysis of 35 (control) and 37 (overexpression) dendritic processes from 3 independent

experiments. Note that some dendrites decrease in length while the majority increases whereas after LRP4 overexpression, neither shrinkage nor growth was observed. Scale bar: 50  $\mu\text{m}$  (A).

#### 3.4.4 Overexpression of LRP4 increases the number of synapses

To investigate if LRP4 levels affect the formation of synapse-like specializations, I first determined the density of dendritic protrusions in both cortical and hippocampal neurons overexpressing LRP4 and compared them to wildtype neurons (**Figure 3.21**). I observed an increase in the density of spine-like processes in hippocampal as well as in cortical cultures after neuron-specific overexpression of LRP4 ( $9.64 \pm 0.46/20 \mu\text{m}$  in cortical,  $p < 0.05$ ;  $16.64 \pm 1.53/20 \mu\text{m}$  in hippocampal neurons,  $p < 0.001$ ) compared to neurons transfected with pSYN-GFP:actin ( $7.14 \pm 0.53/20 \mu\text{m}$  in cortical;  $9.74 \pm 0.8/20 \mu\text{m}$  in hippocampal neurons). This increase in spine density was accompanied by a simultaneous increase in the number of puncta labeled by antibodies against presynaptic proteins, including bassoon ( $1.93 \pm 0.54/\mu\text{m}$  in hippocampal, compared to  $1.05 \pm 0.04/\mu\text{m}$  in control cultures,  $p < 0.05$ ) and synaptobrevin2 (SV2,  $1.47 \pm 0.42/\mu\text{m}$  in cortical, compared to  $0.87 \pm 0.02/\mu\text{m}$  in control cultures,  $p < 0.05$ ). Moreover, antibodies against the postsynaptic PSD95 protein showed a similar increase in puncta ( $1.1 \pm 0.1/\mu\text{m}$  in hippocampal, compared to  $0.66 \pm 0.12/\mu\text{m}$  in control cultures,  $p < 0.01$ ).

In summary, these results demonstrate that overexpression of LRP4, in addition to its effect on dendritic morphology, increases the density of spines and of synapse-like specializations in embryonic cortical and hippocampal neurons *in vitro*.

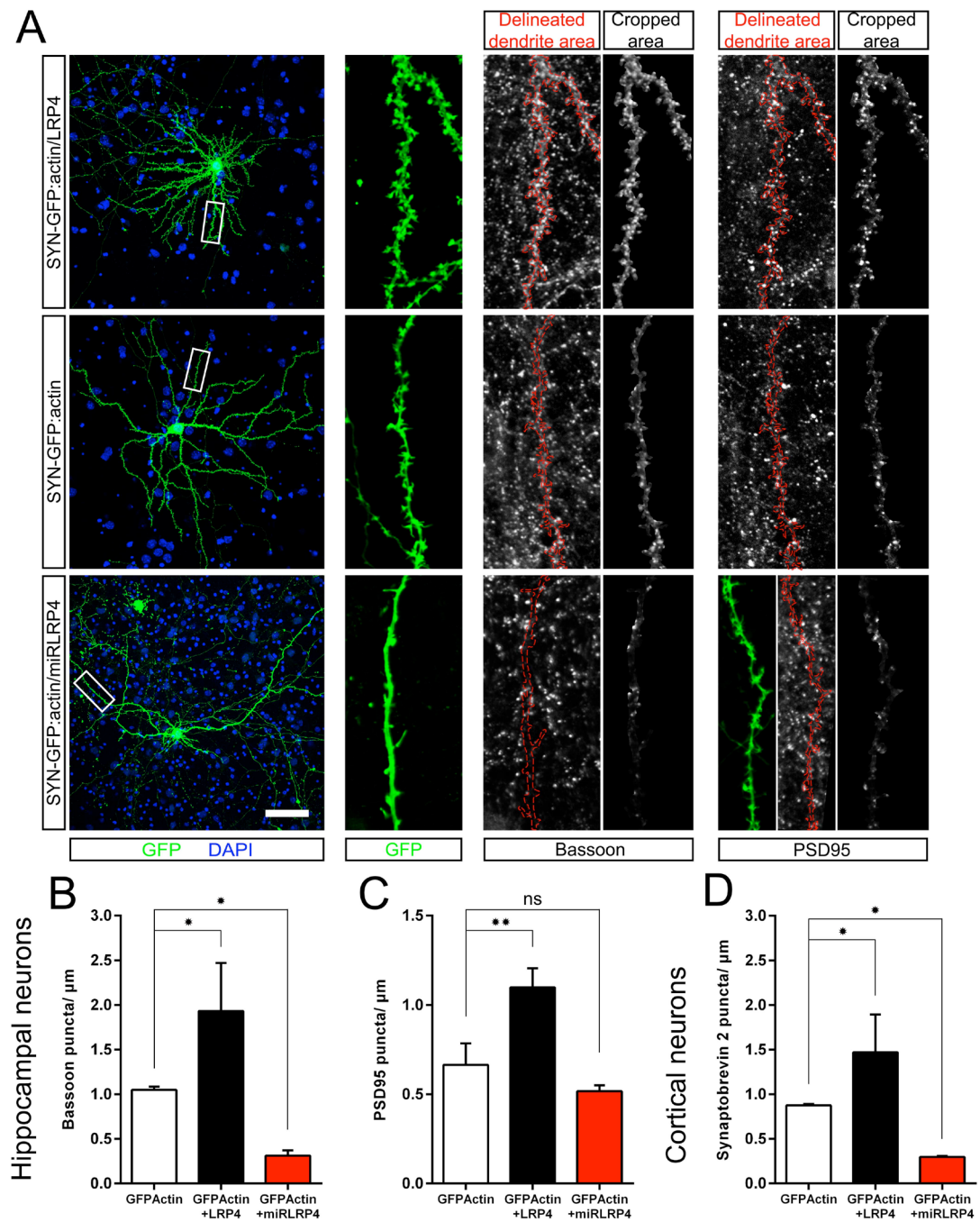


**Figure 3.21. LRP4 affects the number of pre- and post-synaptic specializations in neuronal cultures.**

(A) Representative examples of dissociated cells from the E16 hippocampus co-transfected with pSYN-GFP:actin and either pSYN-LRP4, pCAG-miRLRP4 or only the pSYN-GFP:actin as control. Enlarged images of single confocal planes of individual dendritic segments are shown. The dendrite was redrawn in red from the GFP signal in order to visualize the close association of the dendritic spine-like protrusions and the bassoon and PSD95 puncta, respectively. Note that changes in the expression levels of LRP4 affected the number of pre- and post-synaptic puncta. The number of synapse-like specializations was only altered in the dendrites of the transfected neurons. The cropped areas show the synaptic specializations directly overlapping with the dendrite of the transfected cell (as indicated by the red line) without the synaptic specializations of the surrounding area (representing non-transfected neurons). This allowed



distinguishing the synaptic specializations directly associated with the dendrite of the transfected neurons from those of untransfected neurons and represents a more direct visualization of the number of synaptic specializations associated with a particular dendritic segment. Quantitative analysis of the number of bassoon (B) and PSD95 (C) puncta associated with the dendrites of hippocampal neurons and the number of synaptobrevin2 puncta (D) associated with the dendrites of cortical neurons revealed a significant increase of bassoon (B; black bar), PSD95 (C; black bar) and synaptobrevin2 (D; black bar) in all neurons after LRP4 overexpression. In contrast, knockdown of LRP4 led to a significant decrease in the number of bassoon (B; red bar) and synaptobrevin2 (D; red bar) puncta, without affecting the number of PSD95 puncta (C; red bar). Data show mean  $\pm$  SD from three independent experiments;  $n = 5-7$  cortical neurons per condition/experiment;  $n = 5-8$  hippocampal neurons per condition/experiment. \* $p < 0.05$ , \*\* $p < 0.01$ , One-way ANOVA test with Dunnett's posthoc test. Scale bar: 50  $\mu$ m.

### 3.4.5 Generation of microRNAs for the knockdown of LRP4 in vitro

The experiments detailed above indicated that increased expression of LRP4 in cortical and hippocampal neurons promotes the formation of synapse-like specializations. However, this does not necessarily imply that basal endogenous levels of LRP4 are required for synaptogenesis. To analyze this, I examined the consequence of LRP4 loss-of-function. For this reason, I cloned four different microRNAs (mir1232, mir1544, mir6854 and mir7072; **Figure 3.22**) targeting the open reading frame (ORF) or the 3' UTR of *lrp4* mRNA into the pcDNA6.2<sup>TM</sup>-GW vector (pcDNA6.2<sup>TM</sup>-GW-miR). To reduce possible off-target effects, the microRNAs were designed with the help of the miRNA designer software from Invitrogen. Additionally, a BLAST search with all sequences was performed to confirm the absence of similar sequences in other mRNA transcripts. To test the efficiency of RNA interference, HEK cells were co-transfected with the pCMV-LRP4 construct plus the pcDNA6.2<sup>TM</sup>-GW-miR plasmid or the pcDNA<sup>TM</sup>6.2-GW/EmGFP as a control. Cells were collected 72 hours after transfection and total protein was extracted. Western blotting identified mir1232 and mir1544 as most effective in reducing LRP4 protein levels (**Figure 3.22**).

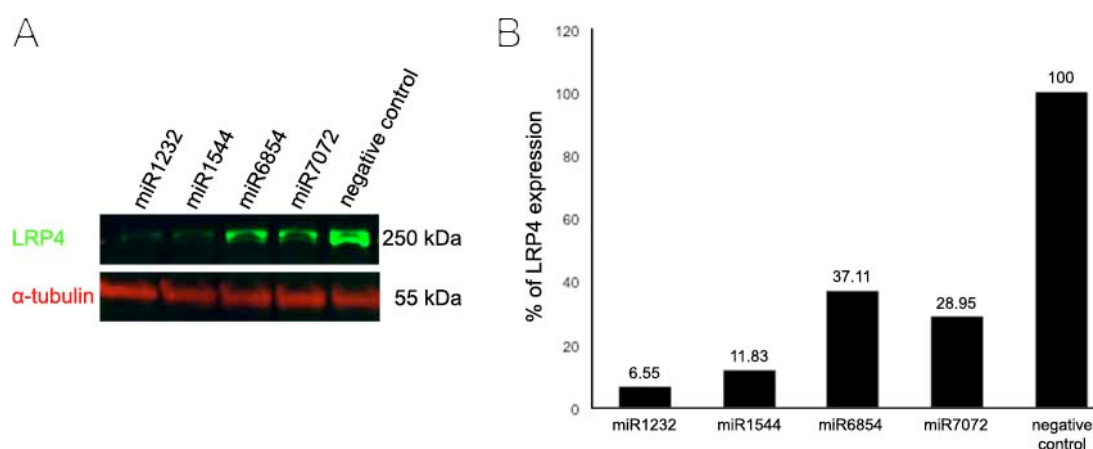


**Figure 3.22. Generation and test of microRNAs targeting LRP4**

(A) Test of knock down efficiency of the microRNAs. HEK293 cells were co-transfected with pCMV-LRP4 and either the microRNA plasmids or the empty vector as a negative control. Note that miR1232 and miR1544 led to a significant knock down of LRP4, whereas miR6854 and miR7072 were not as



effective in reducing LRP4 levels. (B) Quantification of the LRP4 expression levels using an ImageJ plugin. Note that miR1232 and miR1544 can knock down LRP4 with an efficiency of almost 95% and 90%, respectively.

To enhance knock down of LRP4, these two microRNAs were then chained together with the RFP cDNA sequence in a CAG-driven-promoter expression vector (CAG-miRLRP4-RFP) and subsequently used for transfections in cortical and hippocampal neurons. As a control for the transfections, we used the pCAG-RFP vector lacking the microRNA sequences (**Figure 3.23**). Immunostaining of cortical neurons confirmed the effectiveness of the microRNAs in reducing LRP4 protein levels. At the same time these experiments also further confirmed the specificity of the antibody (**Figure 3.23**).

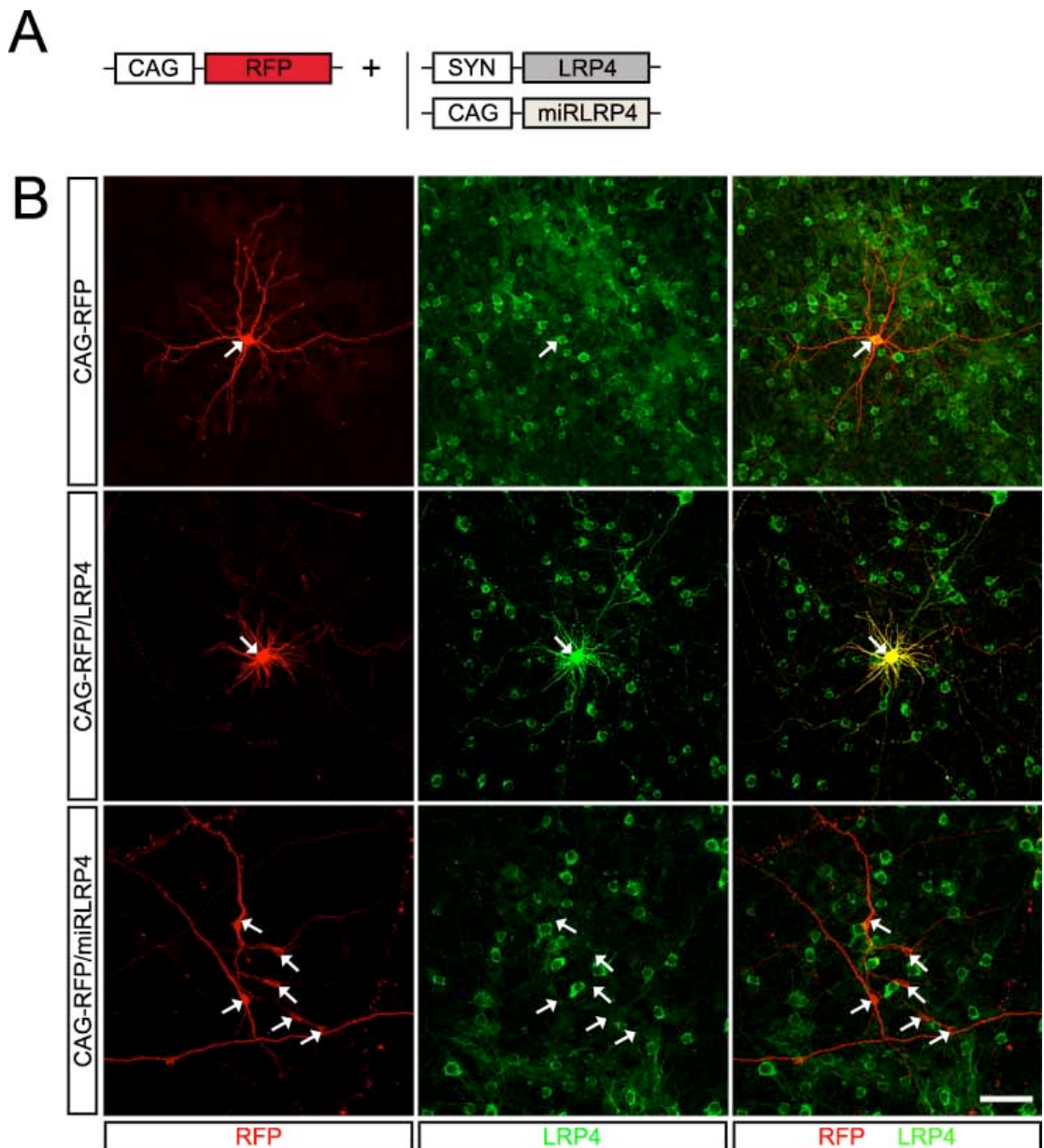


**Figure 3.23. Constructs for expression of RFP, LRP4 and miRLRP4**

(A) Constructs encoding RFP, LRP4 and miRLRP4 (the miR1232 and miR1544 chained together). Transgene expression is driven by the CAG promoter, besides the LRP4 expression that is driven by the synapsin (SYN) promoter. (B) E14 cortical cultures transfected with RFP encoding construct (upper set of pictures). Immunostaining for RFP (red channel) and LRP4 (green channel) shows the endogenous levels of LRP4 in the transfected neuron (white arrow). Double transfected cortical neurons with RFP and LRP4 encoding constructs (middle set of pictures). Immunostaining for RFP (red channel) and LRP4 (green channel) shows that the neuron is transfected with both plasmids (white arrow). Cortical neurons transfected with miRLRP4 encoding construct (lower set of pictures). Immunostaining for RFP (red channel) and LRP4 (green channel) reveals that the neurons that are transfected with the miRLRP4 do not show immunoreactivity for LRP4. Scale bars: 50  $\mu$ m.

### 3.4.6 Knockdown of LRP4 affects dendritic development and synapse formation *in vitro*

In order to test the effects of down regulation of LRP4 *in vitro*, I co-transfected primary cortical and hippocampal neurons at DIV3 with pSYN-GFP:actin in combination with either the pCAG-miRLRP4-RFP or with the pCAG-RFP vector as control. The effect was analyzed 7-9 days post transfection. I quantified the number and length of dendrites and the density of spines and synapses. Neurons transfected with pSYN-GFP:actin and pCAG-RFP had a morphology that was indistinguishable from untransfected neurons (data not shown), demonstrating that the transfection and the expression of a transgene itself did not influence neuronal morphology. In contrast, knockdown of LRP4 in cortical and hippocampal neurons led to a significant decrease in the number of primary dendrites extending from the neuron soma ( $2.22 \pm 0.14$  in cortical,  $3.8 \pm 0.3$  in hippocampal,  $p < 0.01$  and  $p < 0.05$ , respectively) and to a decrease in the density of spine-like protrusions ( $3.33 \pm 1.13 / 20 \mu$ m in cortical and  $5.97 \pm 0.65 / 20 \mu$ m in hippocampal neurons,  $p < 0.01$ ; **Figure 3.19**). In addition, the density of puncta labeled by antibodies against presynaptic proteins was decreased (bassoon:  $0.31 \pm 0.06 / \mu$ m in hippocampal,  $p < 0.05$ ; SV2:  $0.3 \pm 0.009 / \mu$ m in cortical,  $p < 0.05$ ), whereas the density of PSD95 puncta was not significantly affected ( $0.52 \pm 0.03 / \mu$ m,  $p = 0.1807$ ; **Figure 3.21**). The length of the primary dendrites was also significantly increased in cortical neurons ( $134.7 \pm 8.88 \mu$ m,  $p < 0.05$ ), but was not significantly affected in hippocampal neurons ( $179.8 \pm 35.85 \mu$ m,  $p = 0.1158$ ; **Figure 3.19**).

These results demonstrate that LRP4 knockdown has the opposite effect on dendritic process number, dendritic length and density of synaptic puncta compared to the overexpression of LRP4. Overall, these results confirm a role of LRP4 in regulating dendritic development and synapse formation in cortical and hippocampal neurons *in vitro*. The results also reveal that hippocampal and cortical neurons react differently to LRP4 knockdown.

### 3.4.7 Knockdown of LRP4 reduces the number of direct presynaptic partners in dissociated neuronal cultures

Our results indicated that LRP4 knockdown significantly reduces the number of synapses and spine-like protrusions in hippocampal and cortical neurons. Therefore, I next investigated to which extent LRP4-loss-of-function affected the integration of neurons into a neuronal network. To this end, I used a rabies virus-mediated monosynaptic tracing technique (Wickersham et al., 2007b) which allows the visualization of all neurons presynaptic to a transfected neuron. Briefly, cortical neurons in culture were transfected with a retroviral vector encoding the EnvA-receptor TVA, the rabies virus glycoprotein G, which is responsible for retrograde transport of the virus across synapses and with the fluorescence reporter construct *DsRedExpress2* (**Figure 3.24**). This makes neurons susceptible to subsequent primary infection by the G-deficient, eGFP-encoding EnvA-pseudotyped rabies virus (RABV) and capable of retrograde transfer of the virus to the immediate presynaptic partner cells (Wickersham et al., 2007a). The schemes B and C in **Figure 3.24** depict the general strategy for monosynaptic tracing of presynaptic partners of neurons *in vitro*. Delivery of G and TVA-encoding plasmid together with either pCAG-RFP or pCAG-miRLRP4-RFP followed by RABV infection resulted in the appearance of double reporter-positive neurons (starter cells), indicating that they had received both the plasmids and the virus (**Figure 3.24 D**, white arrows). I also observed cells expressing only eGFP but not RFP, indicating transsynaptic transmission of RABV from the starter neurons to their presynaptic partners (**Figure 3.24 D**). Further analysis showed that the number of direct presynaptic partners of LRP4 knockdown neurons was significantly lower when compared to control neurons (**Figure 3.24 E**). These results demonstrate that LRP4 is necessary for the establishment of neuron-to-neuron synaptic contacts and, therefore, has an important role in the integration of neurons into neuronal circuits in cultured CNS neurons.

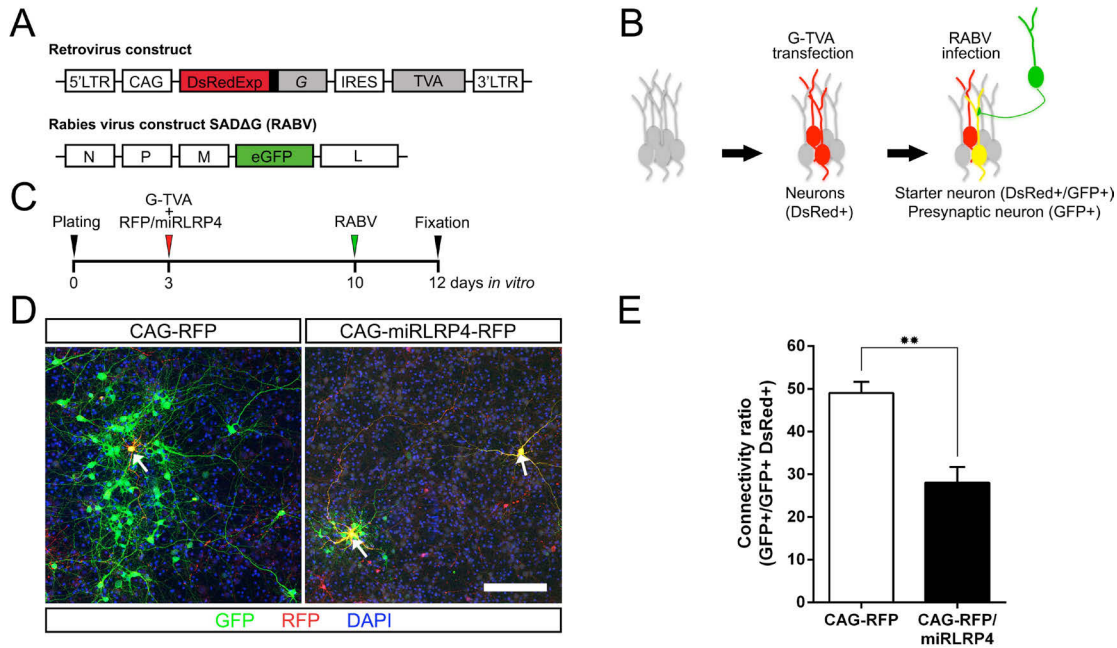


**Figure 3.24. Knockdown of LRP4 in dissociated neuronal cultures decreases the number of presynaptic partners**

(A) Schematic representation of the RABV and Glyco-TVA constructs used to investigate the number of functional presynaptic connections after LRP4 knockdown. (B) Experimental design for tracing monosynaptic connections in cortical neuronal cultures via consecutive delivery of G- and TVA-expression construct and RABV. (C) Timeline of the experimental protocol. (D) Representative examples of cortical neurons from E14 embryos after 12 DIV co-transfected with the G/TVA encoding vector and either pCAG-RFP (left panel) or pCAG-miRLRP4-RFP (right panel), followed by RABV infection. Arrows: double-transduced starter neurons. Note that the number of GFP+ cells surrounding a GFP+/RFP+ (starter) neuron is lower after knockdown of LRP4. (E) Ratio of RABV-traced cells versus GFP/RFP double positive starter neurons in control and knockdown conditions. The number of direct presynaptic partners is reduced to approximately 50% in neurons after knockdown of LRP4. Data show mean  $\pm$  SD from three independent experiments. (\*\* $p < 0.01$ , unpaired t-test with Welch's correction). Scale bar: 100  $\mu$ m.

### 3.5 TM-agrin is required for the LRP4-mediated effect on dendritic development

At the neuromuscular junction, LRP4 is the agrin receptor (Zhang et al., 2008b; Kim et al., 2008). To test if an interaction of agrin with LRP4 is also required for the effects on dendrite morphology, I first confirmed that the two proteins colocalized in the CA1 region of the adult mouse hippocampus using specific antibodies (**Figure 3.25**). Since agrin has been shown to be concentrated at CNS synapses (Mann and Kröger, 1996; Koulen et al., 1999; Ksiazek et al., 2007), the colocalization of agrin and LRP4 further supports the idea that LRP4 accumulates at CNS synapses. Since previous studies have shown that the transmembrane form of agrin (TM-agrin) is expressed in hippocampal neurons (Burgess et al., 2000; Neumann et al., 2001), our results also demonstrate a colocalization of LRP4 with this particular agrin isoform at CNS

synapses. To further analyze the colocalization, cells isolated from the E14 cerebral cortex were cotransfected with the pCAG-RFP and the pSYN-LRP4 vectors on DIV2 and subsequently with pSYN-GFP:actin and pSYN-TMagrin on DIV3. Analysis of the sites of neuronal contacts by confocal microscopy revealed that TM-agrin was highly concentrated at contact sites between dendrites overexpressing LRP4 and axons overexpressing TM-agrin (**Figure 3.25**, panel B). In contrast, neurons overexpressing TM-agrin did not concentrate at the site of contact to neurons in which LRP4 had been knocked down by transfection with the LRP4 miRNAs (**Figure 3.25**, panel C). These results show an influence of LRP4 on TM-agrin localization in neurons. They also suggest that LRP4 directly interacts with TM-agrin in neurons and might be involved in aggregating TM-agrin at the contact sites.

To determine if agrin is involved in the LRP4-mediated effects on dendritic growth, I analyzed the response of dendrites of cortical neurons to LRP4 overexpression in the presence or absence of anti-agrin antibodies (**Figure 3.25**). These antibodies were generated against the 95 kDa C-terminal fragment of mouse agrin, which has been shown to be responsible for LRP4 binding and acetylcholine receptor (AChR) aggregation at the NMJ (Eusebio et al., 2003). Preimmune serum did not have any effect on the number and length of primary dendrites (data not shown). In contrast, treatment of neurons overexpressing LRP4 with anti-agrin antibodies reduced the number of primary dendrites ( $5.46 \pm 0.65$  compared to  $10.27 \pm 0.32$  in untreated cultures,  $p < 0.001$ ) and increased their length ( $105.9 \pm 12.47 \mu\text{m}$  compared to  $33.97 \pm 1.21 \mu\text{m}$  in untreated cultures,  $p < 0.0001$ ) but had no detectable effect on untransfected neurons (data not shown). Thus, addition of anti-agrin antibodies reversed the effect of LRP4 overexpression suggesting that agrin is involved in the effects mediated by LRP4 on the dendritic morphology of CNS neurons *in vitro*.

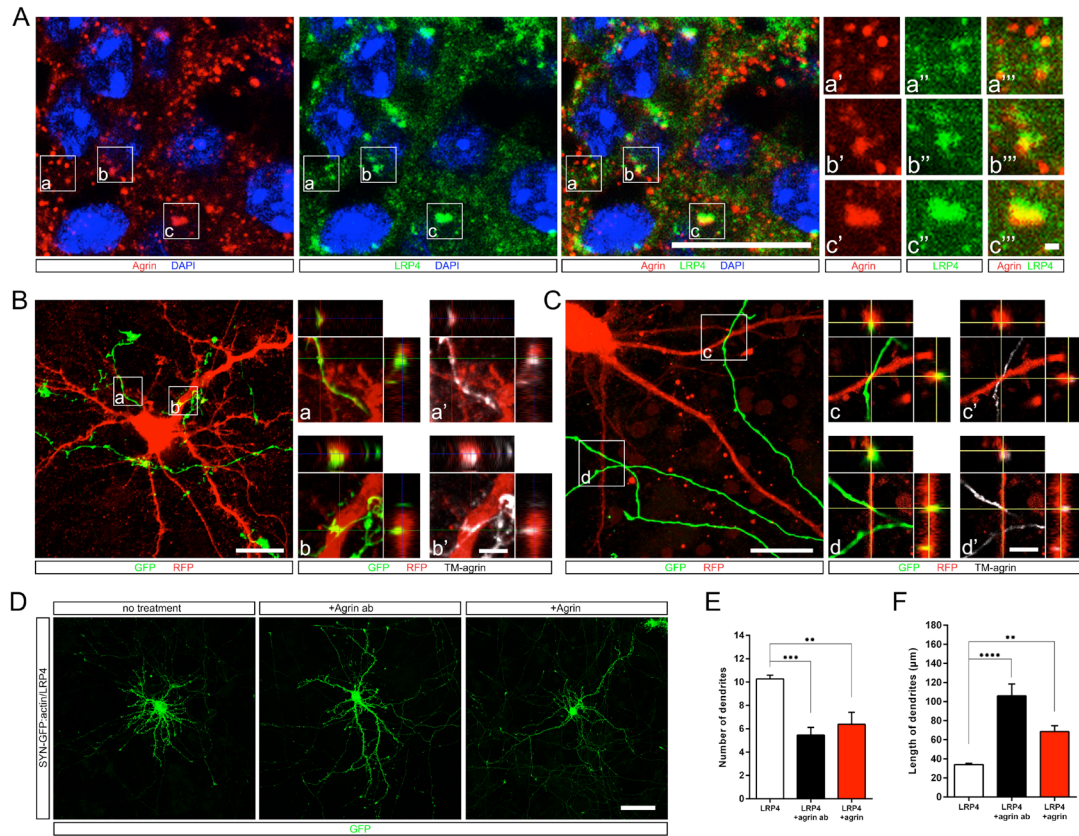


**Figure 3.25 Colocalization and functional interaction of LRP4 and the transmembrane form of agrin on dendrites in vitro**

(A) Agrin (red channel) and LRP4 (green channel) staining of the CA1 region of the hippocampus. Note that many but not all agrin-positive puncta colocalized with LRP4 puncta. (B) Representative example of E14 cortical neurons sequentially co-transfected with pCAG-RFP and pSYN-LRP4 on DIV3 (in red) and pSYN-GFP:actin and pSYN-TM-agrin on DIV4 (in green). Note that TM-agrin is concentrated at contact sites between dendrites overexpressing LRP4 and axons overexpressing TM-agrin (insets a and b; a' and b' represent orthogonal projections), indicating that LRP4 and TM-agrin from two different cells might interact. (C) Representative example of E14 cortical neurons sequentially co-transfected with pCAG-miLRP4-RFP on DIV3 (in red) and pSYN-GFP:actin and pSYN-TM-agrin on DIV4 (in green). Note that TM-agrin is not concentrated at contact sites between dendrites of neurons in which LRP4 expression has been knocked down and axons overexpressing TM-Agrin (insets c and d; c' and d' represent orthogonal projections). (D) Representative examples of dissociated cells from the E14 cortex co-transfected with pSYN-GFP:actin and pSYN-LRP4. Neurons were treated with the soluble C-terminal 125 kDa (A4B8) chicken agrin fragment or cultured in the presence of anti-agrin antibodies. Note that in the presence of anti-agrin antibodies as well as in the presence of the soluble agrin fragment ameliorates the dendritic phenotype caused by LRP4 overexpression. (E-F) Quantification of the number (E) and length (F) of primary dendrites extending from cortical neurons overexpressing LRP4 after treatment with the soluble C-terminal agrin fragment (red bars) or with anti-agrin antibodies (black bars). Note that treatment with either the antibodies or with soluble agrin significantly decreased the number (E) and increased the length (F) of primary dendrites compared to transfected neurons in the absence of antibodies or agrin. Data show mean  $\pm$  SD from three independent experiments,  $n = 10$  neurons per condition/experiment. \* $p < 0.05$ , \*\* $p < 0.01$ , \*\*\* $p < 0.001$ , \*\*\*\* $p < 0.0001$  One-way ANOVA with Dunnett's posthoc test. Scale bars: 50  $\mu\text{m}$  (A and D), 25  $\mu\text{m}$  (B and C), 10  $\mu\text{m}$  (insets in B and C) and 2  $\mu\text{m}$  (insets in A).



### 3.6 LRP4-mediated effects on dendritic development are ameliorated by soluble agrin and are independent of MuSK

The effect of anti-agrin antibodies on dendrite growth suggested that an interaction of LRP4 with TM-agrin is necessary for the formation of a normal dendritic arbor. To confirm this, I investigated whether a soluble C-terminal fragment of agrin, which is able to bind to LRP4 but is not anchored to the cell membrane, interferes with the interaction of LRP4 with TM-agrin for example by competing with the agrin binding site on the LRP4 protein. To this end, I analyzed the effects of LRP4 overexpression (using the pSYN-GFP:actin and pSYN-LRP4) in the presence or absence of the C-125 fragment (A4B8 isoform) of chick agrin (Tsim et al., 1992; Pevzner et al., 2012). Chick agrin is known to function in mouse tissue *in vitro* and *in vivo* (Moll et al., 2001). Cultures were fixed 3-4 days after transfection and agrin addition and morphometric analysis was performed as described above. The presence of the soluble agrin fragment led to a decrease in the number ( $6.37 \pm 1.03$  compared to  $10.27 \pm 0.32$  in untreated cultures,  $p < 0.01$ ) and an increase in the length ( $68.48 \pm 6.2 \mu\text{m}$  compared to  $33.97 \pm 1.21 \mu\text{m}$  in untreated cultures,  $p < 0.01$ ) of primary dendrites of neurons overexpressing LRP4 compared to neurons transfected with the empty vector (**Figure 3.25**). Thus, the presence of soluble agrin ameliorated the effect of LRP4 overexpression and mimicked the effect of the anti-agrin antibodies, resulting in a dendritic morphology that resembled that of control neurons. Thus, the soluble isoform of agrin rescued the LRP4-mediated effects on dendritic arborization in cortical neurons similar to anti-agrin antibodies. This strongly suggests that an interaction of LRP4 with TM-agrin is required for normal dendritic arborization of cortical neurons. Furthermore, the equivalent effects of the anti-agrin antibodies and the soluble agrin fragment suggests that the membrane association of agrin is required for the LRP4-mediated changes in dendritic morphology of cortical neurons.

At the NMJ, the effect of agrin and LRP4 on synapse formation is mediated by the tyrosine kinase MuSK (Glass et al., 1996). Since MuSK is also expressed by CNS neurons and concentrated at synapses (Ksiazek et al., 2007) we investigated whether it is also involved in the agrin/LRP4-mediated effect on dendritic arbor formation by analyzing the effect of LRP4 overexpression in hippocampal neurons from MuSK knockout mice (DeChiara et al., 1996). Hippocampal neurons from MuSK<sup>+/+</sup>, MuSK<sup>+/-</sup> and MuSK<sup>-/-</sup> mice were co-transfected with the pSYN-LRP4 plasmid and pSYN-GFP:actin or with only the pSYN-GFP:actin vector as control (**Figure 3.26**). Overexpression of LRP4 in wildtype, MuSK<sup>+/-</sup> and MuSK<sup>-/-</sup> neurons resulted in an increased number and decreased length of primary dendrites as detailed above in

neurons from all three genotypes (**Figure 3.26**). Thus, the absence of MuSK did not affect the LRP4-induced changes in dendritic morphology.

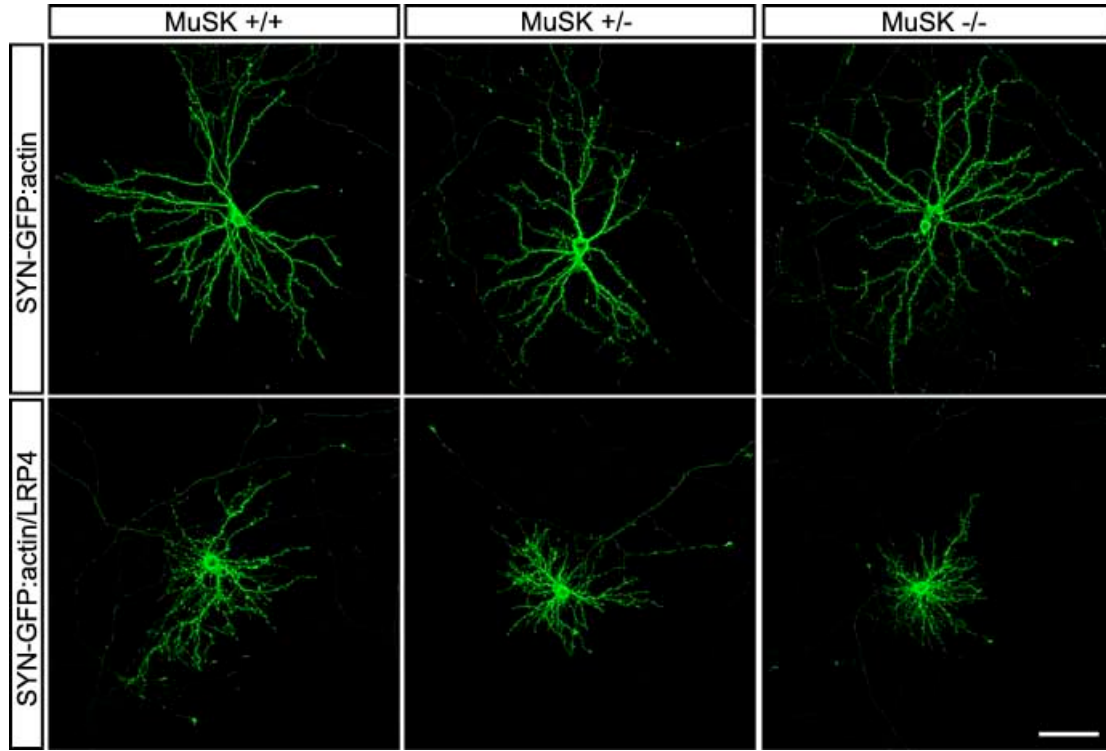


**Figure 3.26. Overexpression of LRP4 in MuSK+/+, MuSK+/- and MuSK-/- hippocampal neurons**

Representative examples of dissociated cells from the E18 hippocampus of MuSK+/+, MuSK+/- and MuSK-/- mice co-transfected with SYN-GFP:actin and SYN-LRP4 plasmids (lower panel/set of pictures) or with SYN-GFP:actin plasmid alone as a vector control (upper panel/set of pictures). Note that the dendritic phenotype caused by LRP4 overexpression is observed in all the three genotypes, thus indicating that is independent of MuSK expression (Scale bar 50  $\mu$ m).

Taken together, these results demonstrate that LRP4 regulates dendrite growth in CNS neurons through interaction with TM-agrin, in a MuSK-independent manner, suggesting that different pathways are initiated by LRP4 in CNS neurons and at the NMJ.



## 4 Discussion

LRP4 is a single-pass transmembrane protein with important functions in bone homeostasis, limb patterning, kidney formation, and placode development (Ahn et al., 2013; Choi et al., 2013; Johnson et al., 2005; Karner et al., 2010). In the nervous system, the function of LRP4 has been best characterized at the neuromuscular junction where it serves as a receptor for the extracellular matrix protein agrin. Upon agrin binding, LRP4 activates the tyrosine kinase MuSK which subsequently induces a signaling cascade resulting in the formation of most, if not all, postsynaptic specializations (Wu et al., 2010). LRP4 expressed by skeletal muscle fibers also acts retrogradely to induce the differentiation of the presynaptic terminal (Wu et al., 2012; Yumoto et al., 2012). Consequently, reduced function of LRP4 causes serious neuromuscular deficits, as indicated for example by the effects of anti-LRP4 autoantibodies in myasthenia gravis (Pevzner et al., 2012; Higuchi et al., 2011; Zhang et al., 2012), and by LRP4 knockout mice, which die at birth due to lack of neuromuscular junctions and therefore respiratory musculature failure (Weatherbee et al., 2006). These and other results have established a fundamental role of LRP4 during NMJ formation, maintenance and function. This thesis examines the physiological role of LRP4 in the CNS. Specifically, I focused on analyzing the distribution of LRP4 in different areas of the CNS and the function of LRP4 during synapse formation, spine development, dendrite outgrowth and branching in primary cortical and hippocampal neurons. My results reveal a widespread distribution of LRP4 in many, but not all, CNS neurons and a prominent function in dendritic arborization and synaptogenesis.

In this study, the expression pattern of LRP4 in the CNS was determined. For this purpose, two polyclonal antibodies targeting different regions of the protein (one against an intracellular and one against a juxtamembrane extracellular epitope) were generated in rabbits. These antibodies were used together with the two commercially available antibodies throughout my study. In principle, all the four sera gave similar results in the initial control experiments performed to test their selectivity and specificity. First, all four antibodies were able to specifically and efficiently recognize LRP4 upon overexpression in HEK293 cells by immunocytochemistry. Confirming the immunocytochemistry results, LRP4 protein was detectable as a 250 kDa band in Western blotting using lysates from HEK293 cells upon overexpression of LRP4. All four antibodies were also able to detect endogenous LRP4 at neuromuscular junctions from adult mouse skeletal muscle by immunohistochemistry. The specificity of the antibodies was tested using competition experiments *in vivo* in which the antibodies were preincubated with an excess of the respective peptide against which the antibody was generated and subsequently used for immunostaining of the NMJs. Furthermore, specificity was demonstrated by the absence of LRP4 staining upon

usage of microRNAs specifically designed to knock down LRP4 (see paragraph 2.1). These data collectively established the specificity and selectivity of the antisera for LRP4 in immunohistochemistry and Western blotting.

#### 4.1 Expression of LRP4 in the murine brain

The antisera were subsequently used to investigate – for the first time – the localization and distribution of the LRP4 protein in the adult murine brain. Previous studies reported a widespread *lrp4* mRNA expression in the rat CNS and a concentration of LRP4 protein in the synaptosomal protein preparation (Tian et al., 2006; Gomez et al., 2014). Accordingly, endogenous LRP4 was detectable as a 250 kDa band in membrane fractions isolated from adult mouse cortex, hippocampus, cerebellum and olfactory bulb (see **Figure 3.7**). Moreover, and consistent with previous *in situ* hybridization data in the adult rat brain (Tian et al., 2006), I demonstrated that LRP4 is highly expressed in neuronal populations distributed in the cortex, hippocampus, cerebellum and olfactory bulb from the adult mouse brain. Both the commercial and the generated-in-house antibodies against the intracellular region of LRP4 revealed an equivalent distribution in the mouse brain. Interestingly, the distribution of LRP4 in the mouse brain did not appear to be homogeneous, but apparently was enriched in specific neuronal subpopulations. These included neurons from all cortical layers, pyramidal neurons of the CA1 and CA3 hippocampal regions, cerebellar Purkinje neurons and mitral cells of the olfactory bulb. Moreover, the colocalization of LRP4 and agrin at CNS synapses demonstrates a concentration of LRP4 at interneuronal synapses and makes a functional cooperation of the two proteins in the CNS possible, similar to what has previously been described at the NMJ (Kim et al., 2008; Zhang et al., 2008).

Interestingly, LRP4 protein was not detected in adult-born neuroblasts of the subgranule zone (SGZ) of the dentate gyrus. Similarly, LRP4 is absent in the other well-known neurogenic niche of the adult murine brain, the subependymal zone (SEZ). These data indicate that the expression of LRP4 is restricted to the neurons generated during embryonic or early postnatal development. Consistently, Burk et al. (Burk et al., 2012) observed no *lrp4* mRNA expression in neuroblasts migrating along the rostral migratory stream to the olfactory bulb. Unlike neurons that are born in the embryo, adult-born generated neurons of the SGZ and SEZ have to synaptically integrate into preexisting mature and functional networks and little is known about the molecular signals and mechanisms underlying this integration. The absence of LRP4 expression in adult neural stem cells of both the neurogenic niches might suggest that LRP4 is not required for their survival and synaptic integration into the preexisting neuronal networks of the hippocampus and olfactory bulb. However, one interesting observation is the distribution of LRP4 in the mitral

cell layer of the olfactory bulb, a cell population that represents the main synaptic target for newly arriving interneurons (Ming and Song, 2011). Likewise, LRP4 is highly expressed in the CA3-pyramidal neurons of the hippocampus, another cell population where adult-born granule cells of the dentate gyrus send their mossy fibers and therefore their synaptic outputs (Toni et al., 2008). Related to these results is that agrin is strongly expressed in neuronal precursors in the RMS, OB and hippocampus (O'Connor et al., 1994; Cohen et al., 1997). Taken together, the distribution of LRP4 in the MCL of the OB and the CA3 hippocampal region and the distribution of agrin in the respective synaptic partners could suggest an interaction of the two proteins that may be sufficient for synaptogenesis in the CNS, similar to what was previously observed at the NMJ (Kim et al., 2008; Zhang et al., 2008).

In contrast to its expression in neurons, we were not able to detect LRP4 protein in glial cells using immunohistochemistry in the adult murine cortex or in primary neuronal cultures. This demonstrates that the effects I observed are due to neuronal LRP4. However, our results do not completely rule out an influence of glial cells.

## 4.2 The role of LRP4 in dendrite formation

In this study, the effect of LRP4 on the dendritic arborization of cortical and hippocampal neurons *in vitro* was investigated. To this end, I used constructs specifically designed to overexpress and knockdown LRP4 in hippocampal and cortical neurons. Both neuronal types responded to LRP4 overexpression by changes in dendritic arborization with an increased number of primary dendrites extending from the neuronal cell body, that were significantly shorter when compared to control neurons. A knockdown of LRP4 in the neurons had the opposite effect, i.e. fewer, but significantly longer, dendritic processes were generated and the density of synapse-like specializations was decreased. LRP4-deficient mice rescued from perinatal death by re-expression of LRP4 in the neuromuscular system as well as mice with a selective loss of the intracellular and the transmembrane domains showed a significantly decreased density of dendritic spines in the CA3-hippocampal region, consistent with my results, but had no gross anatomical abnormalities in the prenatal and adult hippocampus, cortex and cerebellum (Gomez et al., 2014; Pohlkamp et al., 2015). Thus, lack of LRP4 does not lead to a general reduction in the number of CNS neurons. Consistently, we did not observe an increase of apoptotic or dying cells in our cultures after overexpression or knockdown of LRP4.

With regard to the dendritic phenotype, it is currently unclear why similar changes in dendritic morphology were not observed in LRP4-deficient brains *in vivo*. One possible explanation for the discrepancy between our *in vitro* data and the *in vivo* data is the activation of redundant or compensatory mechanisms *in vivo*, which ameliorate the dendritic phenotype observed *in vitro*.

Compensatory activity within the family of LRP proteins has been suggested during limb development (Li et al., 2010). Potential candidates with compensatory activity could be LRP1 which, like LRP4, is concentrated in the PSD fraction (May et al., 2004) or LRP10, which is structurally almost identical to LRP4 (Brodeur et al., 2012; Lane-Donovan et al., 2014).

Time-lapse video microscopy of neurons overexpressing LRP4 and control neurons revealed that within a few hours after LRP4 overexpression, dendritic extension stopped and the dendrites appeared rather stable, without extending or retracting. Thus, overexpression of LRP4 in neurons caused a severe reduction in dendrite process extension. The reduction of growth speed after LRP4 overexpression appears to be similar to what has been reported as a function of LRP4 at the NMJ, i.e. the transformation of a highly motile growth cone into a stable presynaptic terminal (Wu et al., 2012; Yumoto et al., 2012). Accordingly, in LRP<sup>-/-</sup> mice the  $\alpha$ -motoneuron growth cone continues to grow along the muscle fiber and never develops into a presynaptic terminal (Weatherbee et al., 2006). Thus, LRP4 overexpression might have similar functional consequences in dendritic growth of hippocampal and cortical neurons as it has in axons of  $\alpha$ -motoneurons.

### 4.3 The role of LRP4 in spine and synapse formation

In this study, the effect of LRP4 on spinogenesis and synapse formation was also investigated. I observed that a decreased LRP4 expression in cultured cortical and hippocampal neurons lead to a reduced density of spine-like protrusions and dendrite-associated synapse-like specializations, including bassoon-, synaptobrevin2- and PSD95 puncta. In contrast, overexpression of LRP4 had the opposite effect, i.e. increased densities of spine-like protrusions and synapse-like specializations. The knockdown effects of LRP4 in spine density and synapse number are in agreement with the reduced number of spines on dendrites *in vivo* (Gomez et al., 2014; Pohlkamp et al., 2015). However, it is unknown if the reduced spine density observed *in vivo* was due to a direct effect of LRP4 on neurons or indirectly caused by affecting glial cells. Our knockdown and overexpression experiments were designed to exclusively affect neurons, but not glial cells. In addition to this, we were not able to detect LRP4 in glial cells neither *in vivo* nor *in vitro* based on our immunochemical studies. Taken together, it appears likely that the effect observed *in vitro* in our culture system and also *in vivo* by other laboratories (Gomez et al., 2014; Pohlkamp et al., 2015) is, at least in large parts, caused by neuron-derived LRP4. Although we cannot exclude a role of glial cell-derived LRP4 during CNS development, our results strongly suggest that the cognitive deficits, altered LTP and reduced spine density previously observed in the hippocampus of adult mice with LRP4-deficient brains (Gomez et al., 2014) involve neuron-derived LRP4 rather than glia cell-derived.

Little is known about the cellular and molecular mechanisms underlying dendrite extension and branching in the CNS. Dendritogenesis is a highly dynamic process that is influenced by synaptic activity as well as by signals from the immediate environment (Cheng and Poo, 2012; Dong et al., 2014). The opposite effects of LRP4 overexpression and knockdown on dendrite number, length and on synapses opens the possibility that all three effects might depend on each other. One possibility is that the reduced density of synapses induced by LRP4 knockdown causes a reduction in the number of primary dendrites and an increase in dendritic length, whereas the overexpression of LRP4 causes an increase in synaptic density which results in a subsequent decrease in dendritic mobility and an increased number of shorter dendrites. Thus, the effect on dendritic arborization may be secondary to differences in synapse number. Alternatively, synapse formation and dendritic arbor formation could be independently caused by changes in LRP4 expression. This hypothesis is consistent with the changes observed in LRP4-deficient brains, which exhibit a reduction in synaptic density without a significant change in the dendritic arborization (Gomez et al., 2014; Pohlkamp et al., 2015). Interestingly, neurons in the brain of agrin<sup>-/-</sup> mice, in which the perinatal lethality has been rescued by motoneuron-specific expression of agrin, also develop fewer synapses and shorter dendrites (Ksiazek et al., 2007), suggesting that the LRP4-mediated effect on dendritic morphology might be caused by an interaction of LRP4 with agrin.

#### 4.4 Agrin and LRP4 might act together to regulate dendritic development

At the NMJ, the interaction of LRP4 with agrin is crucial for synaptogenesis (Wu et al., 2010). In our culture system, I observed that the inhibition of the LRP4-agrin interaction by anti-agrin antibodies or the addition of a soluble C-terminal agrin fragment reversed the effects of LRP4 overexpression. The most likely interpretation of these results is that both treatments interfered with the agrin-LRP4 interaction by either blocking the agrin binding to LRP4 (antibodies) or by competing with the ligand-binding site of LRP4 (soluble agrin fragment). The comparable effects of both treatments on the LRP4-overexpression-mediated effects in CNS neurons suggest TM-agrin as one potential binding partner for LRP4 in the CNS. Thus, LRP4-TM-agrin interactions might shape the dendritic morphology and influence the formation of synapses in cultured neurons of the CNS. My results also suggest an important role of the membrane anchor of TM-agrin in the LRP4 overexpression-mediated effects, since the soluble LRP4-binding part of agrin interfered with the changes in dendritic morphology. In contrast, the same soluble agrin fragment can bind to LRP4 and induce AChR aggregation *in vitro* in primary muscle cultures (Pevzner et al., 2012). Thus, the transmembrane anchor might locally stabilize the agrin-LRP4 interaction, securing a continuous presence of TM-agrin at synapses. A soluble agrin fragment

has previously been shown to induce both dendritic elongation and dendritic branching in hippocampal cultures, whereas the cultured hippocampal neurons depleted of agrin extended shorter dendrites compared to controls (Mantych and Ferreira, 2001). Our results might therefore suggest that the effect of soluble agrin is mediated by LRP4.

At the NMJ agrin binding to LRP4 activates the tyrosine kinase MuSK. Since MuSK is also present in the CNS (Ksiazek et al., 2007) and mice after MuSK knockdown exhibit deficits in memory consolidation and LTP (Garcia-Osta et al., 2006) similar to those observed in mice expressing a truncated LRP4 protein which lacks the intracellular- and the transmembrane domain (LRP4<sup>ECD/ECD</sup>; Choi et al., 2013; Pohlkamp et al., 2015) the hypothesis was raised that MuSK and LRP4 functionally interact to maintain normal synapse function also in the CNS. Interestingly, the effects of LRP4 overexpression on dendritic branching did not depend on MuSK. This does not exclude an interaction of LRP4 with MuSK in adult neurons or glial cells, but suggests that the molecular mechanism of synapse formation in the CNS might differ from that at the NMJ.

#### 4.5 Functional consequences of LRP4 knockdown in CNS neurons

Using a rabies virus-mediated monosynaptic tracing technique (Wickersham et al., 2007), I demonstrated that the number of functional presynaptic partners after LRP4 knockdown was significantly reduced. This technique depends on the presence of functional synapses and, thus, our results suggest that the reduction of synapse-like specializations after miRNA-mediated LRP4 knockdown is paralleled by a reduced number of functional synaptic inputs to the transduced neuron. Since the rabies virus can only be transported in a retrograde manner, from the postsynaptic to the presynaptic neuron, our results also suggest that LRP4 has a retrograde effect from the postsynaptic dendrites to the presynaptic terminals. Whether a similar activity of LRP4 also occurs at the axon terminal cannot be analyzed by this technique and, thus, remains to be determined. Interestingly, synapses were reduced by 30% in agrin-deficient brains (Ksiazek et al., 2007), suggesting overlapping and possibly interdependent functions of LRP4 and agrin in synapse formation at the NMJ and in the CNS.

#### 4.6 Conclusions and future prospects

The present study focuses mostly on the cerebral cortex and hippocampus. However, LRP4 has a widespread expression pattern in the CNS, including neuronal populations outside the forebrain, such as the Purkinje cells of the cerebellum or ganglion cells in the retina. It is therefore conceivable that LRP4 generally regulates dendritogenesis and synapse formation in other regions of the brain beyond the cerebral cortex and the hippocampus. This study provides the first indication for a function of LRP4 in dendritic branching and synapse formation in the

developing CNS, opening up avenues for elucidating the underlying molecular mechanism in other regions of the CNS. Considering that defects in dendrite formation and synapse development or maintenance are crucial in neurodevelopmental disorders such as schizophrenia, Down's syndrome and autism spectrum disorders (Caroni et al., 2012), it will be interesting to further elucidate the molecular contribution of LRP4 in pathologically altered brains.

## 5 Bibliography

- Ahn, Y., C. Sims, J.M. Logue, S.D. Weatherbee, and R. Krumlauf. 2013. Lrp4 and Wise interplay controls the formation and patterning of mammary and other skin appendage placodes by modulating Wnt signaling. *Development*. 140:583–93.
- Arimura, N., and K. Kaibuchi. 2007. Neuronal polarity: from extracellular signals to intracellular mechanisms. *Nat. Rev. Neurosci.* 8:194–205.
- Attardo, A., J.E. Fitzgerald, and M.J. Schnitzer. 2015. Impermanence of dendritic spines in live adult CA1 hippocampus. *Nature*. 523:592–596.
- Bardehle, S., M. Krüger, F. Buggenthin, J. Schwausch, J. Ninkovic, H. Clevers, H.J. Snippert, F.J. Theis, M. Meyer-Luehmann, I. Bechmann, L. Dimou, and M. Götz. 2013. Live imaging of astrocyte responses to acute injury reveals selective juxtavascular proliferation. *Nat. Neurosci.* 16:580–586.
- Brodeur, J., C. Thériault, M. Lessard-Beaudoin, A. Marcil, S. Dahan, and C. Lavoie. 2012. LDLR-related protein 10 (LRP10) regulates amyloid precursor protein (APP) trafficking and processing: evidence for a role in Alzheimer’s disease. *Mol. Neurodegener.* 7:31.
- Burgess, R.W., W.C. Skarnes, and J.R. Sanes. 2000. Agrin isoforms with distinct amino termini: Differential expression, localization, and function. *J. Cell Biol.* 151:41–52.
- Burk, K., A. Desoeuvre, C. Boutin, M.A. Smith, S. Kroger, A. Bosio, M.-C. Tiveron, and H. Cremer. 2012. Agrin-Signaling Is Necessary for the Integration of Newly Generated Neurons in the Adult Olfactory Bulb. *J. Neurosci.* 32:3759–3764.
- Caceres, A., G. Banker, O. Steward, L. Binder, and M. Payne. 1984. MAP2 is localized to the dendrites of hippocampal neurons which develop in culture. *Brain Res.* 315:314–318.
- Caroni, P., F. Donato, and D. Muller. 2012. Structural plasticity upon learning: regulation and functions. *Nat. Rev. Neurosci.* 13:478–490.
- Chen, W.J., J.L. Goldstein, and M.S. Brown. 1990. NPXY, a sequence often found in cytoplasmic tails, is required for coated pit-mediated internalization of the low density lipoprotein receptor. *J. Biol. Chem.* 265:3116–3123.
- Cheng, P., and M. Poo. 2012. Early Events in Axon/Dendrite Polarization. *Annu. Rev. Neurosci.* 35:181–201.



- Choi, H.Y., M. Dieckmann, J. Herz, and A. Niemeier. 2009. Lrp4, a novel receptor for dickkopf 1 and sclerostin, is expressed by osteoblasts and regulates bone growth and turnover in vivo. *PLoS One*. 4(11): e7930.
- Choi, H.Y., Y. Liu, C. Tennert, Y. Sugiura, A. Karakatsani, S. Kröger, E.B. Johnson, R.E. Hammer, W. Lin, and J. Herz. 2013. APP interacts with LRP4 and agrin to coordinate the development of the neuromuscular junction in mice. *eLife* 2013;2:e00220.
- Cohen, N.A., W.E. Kaufmann, P.F. Worley, and F. Rupp. 1997. Expression of agrin in the developing and adult rat brain. *Neuroscience*. 76:581–596.
- DeChiara, T.M., D.C. Bowen, D.M. Valenzuela, M. V Simmons, W.T. Poueymirou, S. Thomas, E. Kinetz, D.L. Compton, E. Rojas, J.S. Park, C. Smith, P.S. DiStefano, D.J. Glass, S.J. Burden, and G.D. Yancopoulos. 1996. The receptor tyrosine kinase MuSK is required for neuromuscular junction formation in vivo. *Cell*. 85:501–512.
- Deshpande, A., M. Bergami, A. Ghanem, K.-K. Conzelmann, A. Lepier, M. Götz, and B. Berninger. 2013. Retrograde monosynaptic tracing reveals the temporal evolution of inputs onto new neurons in the adult dentate gyrus and olfactory bulb. *Proc. Natl. Acad. Sci. U. S. A.* 110:E1152–61.
- Dietrich, M.F., L. van der Weyden, H.M. Prosser, A. Bradley, J. Herz, and D.J. Adams. 2010. Ectodomains of the LDL receptor-related proteins LRP1b and LRP4 have anchorage independent functions in vivo. *PLoS One*. 5(4): e9960.
- Dong, X., K. Shen, and H.E. Bülow. 2014. Intrinsic and Extrinsic Mechanisms of Dendritic Morphogenesis. *Annu. Rev. Physiol.* 77:271-300.
- Dotti, CG., C.A. Sullivan, and G.A. Banker. 1988. The establishment of polarity by hippocampal neurons in culture. *J. Neurosci.* 8:1454–1468.
- Drögemüller, C., T. Leeb, B. Harlizius, I. Tammen, O. Distl, M. Höltershinken, A. Gentile, A. Duchesne, and A. Eggen. 2007. Congenital syndactyly in cattle: four novel mutations in the low density lipoprotein receptor-related protein 4 gene (LRP4). *BMC Genet.* 8:5.
- Duchesne, A., M. Gautier, S. Chadi, C. Grohs, S. Floriot, Y. Gallard, G. Caste, A. Ducos, and A. Eggen. 2006. Identification of a doublet missense substitution in the bovine LRP4 gene as a candidate causal mutation for syndactyly in Holstein cattle. *Genomics*. 88:610–621.

- Eusebio, A., F. Oliveri, P. Barzaghi, and M.A. Ruegg. 2003. Expression of mouse agrin in normal, denervated and dystrophic muscle. *Neuromuscul. Disord.* 13:408–415.
- Ferraro, E., F. Molinari, and L. Berghella. 2012. Molecular control of neuromuscular junction development. *J. Cachexia. Sarcopenia Muscle.* 3:13–23.
- Fischer, M., S. Kaech, D. Knutti, and A. Matus. 1998. Rapid actin-based plasticity in dendritic spines. *Neuron.* 20:847–854.
- Garcia-Osta, A., P. Tsokas, G. Pollonini, E.M. Landau, R. Blitzler, and C.M. Alberini. 2006. MuSK expressed in the brain mediates cholinergic responses, synaptic plasticity, and memory formation. *J. Neurosci.* 26:7919–7932.
- Gascón, S., J.A. Paez-Gomez, M. Díaz-Guerra, P. Scheiffele, and F.G. Scholl. 2008. Dual-promoter lentiviral vectors for constitutive and regulated gene expression in neurons. *J. Neurosci. Methods.* 168:104–112.
- Gautam, M., P.G. Noakes, L. Moscoso, F. Rupp, R.H. Scheller, J.P. Merlie, and J.R. Sanes. 1996. Defective neuromuscular synaptogenesis in agrin-deficient mutant mice. *Cell.* 85:525–535.
- Gesemann, M., V. Cavalli, A.J. Denzer, A. Brancaccio, B. Schumacher, and M.A. Ruegg. 1996. Alternative splicing of agrin alters its binding to heparin, dystroglycan, and the putative agrin receptor. *Neuron.* 16:755–767.
- Glass, D.J., D.C. Bowen, T.N. Stitt, C. Radziejewski, J. Bruno, T.E. Ryan, D.R. Gies, S. Shah, K. Mattsson, S.J. Burden, P.S. DiStefano, D.M. Valenzuela, T.M. DeChiara, and G.D. Yancopoulos. 1996. Agrin acts via a MuSK receptor complex. *Cell.* 85:513–523.
- Gomez, A.M., R.C. Froemke, and S.J. Burden. 2014. Synaptic plasticity and cognitive function are disrupted in the absence of Lrp4. *Elife.* 3:1–16.
- Harris, K.M., and S.B. Kater. 1994. Dendritic spines: cellular specializations imparting both stability and flexibility to synaptic function. *Annu Rev Neurosci.* 17:341–371.
- Harris, K.M. 1999. Structure, development, and plasticity of dendritic spines. *Curr. Opin. Neurobiol.* 9:343–348.
- Hering, H., and M. Sheng. 2001. Dendritic spines: structure, dynamics and regulation. *Nat. Rev. Neurosci.* 2:880–888.

- Herz, J., and H.H. Bock. 2002. Lipoprotein receptors in the nervous system. *Annu Rev Biochem.* 71:405-434.
- Higuchi, O., J. Hamuro, M. Motomura, and Y. Yamanashi. 2011. Autoantibodies to low-density lipoprotein receptor-related protein 4 in myasthenia gravis. *Ann. Neurol.* 69:418-422.
- Jacque, C.M., C. Vinner, M. Kujas, M. Raoul, J. Racadot, and N.A. Baumann. 1978. Determination of glial fibrillary acidic protein (GFAP) in human brain tumors. *J. Neurol. Sci.* 35:147-155.
- Jande, S.S., S. Tolnai, and D.E. Lawson. 1981. Immunohistochemical localization of vitamin D-dependent calcium-binding protein in duodenum, kidney, uterus and cerebellum of chickens. *Histochemistry.* 71:99-116.
- Jennings, C.G., S.M. Dyer, and S.J. Burden. 1993. Muscle-specific trk-related receptor with a kringle domain defines a distinct class of receptor tyrosine kinases. *Proc. Natl. Acad. Sci. U. S. A.* 90:2895-2899.
- Johnson, E.B., R.E. Hammer, and J. Herz. 2005. Abnormal development of the apical ectodermal ridge and polysyndactyly in Megf7-deficient mice. *Hum. Mol. Genet.* 14:3523-3538.
- Johnson, E.B., D.J. Steffen, K.W. Lynch, and J. Herz. 2006. Defective splicing of Megf7/Lrp4, a regulator of distal limb development, in autosomal recessive mulefoot disease. *Genomics.* 88:600-609.
- Jones, E.G., G.W. Huntley, and D.L. Benson. 1994. Alpha calcium/calmodulin-dependent protein kinase II selectively expressed in a subpopulation of excitatory neurons in monkey sensory-motor cortex: comparison with GAD-67 expression. *J. Neurosci.* 14:611-629.
- Jones, G., T. Meier, M. Lichtsteiner, V. Witzemann, B. Sakmann, and H.R. Brenner. 1997. Induction by agrin of ectopic and functional postsynaptic-like membrane in innervated muscle. *Proc. Natl. Acad. Sci. U. S. A.* 94:2654-2659.
- Kaech, S., and G. Banker. 2006. Culturing hippocampal neurons. *Nat. Protoc.* 1:2406-2415.
- Karner, C.M., M.F. Dietrich, E.B. Johnson, N. Kappesser, C. Tennert, F. Percin, B. Wollnik, T.J. Carroll, and J. Herz. 2010. Lrp4 regulates initiation of ureteric budding and is crucial for kidney formation - a mouse model for cenani-lenz syndrome. *PLoS One.* 5(4): e10418.

- Kim, N., A.L. Stiegler, T.O. Cameron, P.T. Hallock, A.M. Gomez, J.H. Huang, S.R. Hubbard, M.L. Dustin, and S.J. Burden. 2008. Lrp4 Is a Receptor for Agrin and Forms a Complex with MuSK. *Cell*. 135:334–342.
- Koulen, P., L.S. Honig, E.L. Fletcher, and S. Kröger. 1999. Expression, distribution and ultrastructural localization of the synapse-organizing molecule agrin in the mature avian retina. *Eur. J. Neurosci*. 11:4188–4196.
- Kriegstein, A.R., and M.A. Dichter. 1983. Morphological classification of rat cortical neurons in cell culture. *J. Neurosci*. 3:1634–1647.
- Kröger, S., and J.E. Schröder. 2002. Agrin in the developing CNS: new roles for a synapse organizer. *News Physiol. Sci*. 17:207–212.
- Ksiazek, I., C. Burkhardt, S. Lin, R. Seddik, M. Maj, G. Bezakova, M. Jucker, S. Arber, P. Caroni, J.R. Sanes, B. Bettler, and M.A. Ruegg. 2007. Synapse loss in cortex of agrin-deficient mice after genetic rescue of perinatal death. *J. Neurosci*. 27:7183–7195.
- Kügler, S., L. Meyn, H. Holzmüller, E. Gerhardt, S. Isenmann, J.B. Schulz, and M. Bähr. 2001. Neuron-specific expression of therapeutic proteins: evaluation of different cellular promoters in recombinant adenoviral vectors. *Mol. Cell. Neurosci*. 17:78–96.
- Lane-Donovan, C., G.T. Philips, and J. Herz. 2014. More than Cholesterol Transporters: Lipoprotein Receptors in CNS Function and Neurodegeneration. *Neuron*. 83:771–787.
- Lein, E.S., M.J. Hawrylycz, N. Ao, M. Ayres, A. Bensinger, A. Bernard, A.F. Boe, M.S. Boguski, K.S. Brockway, E.J. Byrnes, L. Chen, L. Chen, T.-M. Chen, M.C. Chin, J. Chong, B.E. Crook, A. Czaplinska, C.N. Dang, S. Datta, N.R. Dee, A.L. Desaki, T. Desta, E. Diep, T.A. Dolbeare, M.J. Donelan, H.-W. Dong, J.G. Dougherty, B.J. Duncan, A.J. Ebbert, G. Eichele, L.K. Estin, C. Faber, B.A. Facer, R. Fields, S.R. Fischer, T.P. Fliss, C. Frensley, S.N. Gates, K.J. Glattfelder, K.R. Halverson, M.R. Hart, J.G. Hohmann, M.P. Howell, D.P. Jeung, R.A. Johnson, P.T. Karr, R. Kawal, J.M. Kidney, R.H. Knapik, C.L. Kuan, J.H. Lake, A.R. Laramee, K.D. Larsen, C. Lau, T.A. Lemon, A.J. Liang, Y. Liu, L.T. Luong, J. Michaels, J.J. Morgan, R.J. Morgan, M.T. Mortrud, N.F. Mosqueda, L.L. Ng, R. Ng, G.J. Orta, C.C. Overly, T.H. Pak, S.E. Parry, S.D. Pathak, O.C. Pearson, R.B. Puchalski, Z.L. Riley, H.R. Rockett, S.A. Rowland, J.J. Royall, M.J. Ruiz, N.R. Sarno, K. Schaffnit, N. V Shapovalova, T. Sivisay, C.R. Slaughterbeck, S.C. Smith, K.A. Smith, B.I. Smith, A.J. Sodt, N.N. Stewart, K.-R. Stumpf, S.M. Sunkin, M.

- Sutram, A. Tam, C.D. Teemer, C. Thaller, C.L. Thompson, L.R. Varnam, A. Visel, R.M. Whitlock, P.E. Wohnoutka, et al. 2007. Genome-wide atlas of gene expression in the adult mouse brain. *Nature*. 445:168–176.
- Li, Y., B. Pawlik, N. Elcioglu, M. Aglan, H. Kayserili, G. Yigit, F. Percin, F. Goodman, G. Nürnberg, A. Cenani, J. Urquhart, B.D. Chung, S. Ismail, K. Amr, A.D. Aslanger, C. Becker, C. Netzer, P. Scambler, W. Eyaid, H. Hamamy, J. Clayton-Smith, R. Hennekam, P. Nürnberg, J. Herz, S.A. Temtamy, and B. Wollnik. 2010. LRP4 Mutations Alter Wnt/ $\beta$ -Catenin Signaling and Cause Limb and Kidney Malformations in Cenani-Lenz Syndrome. *Am. J. Hum. Genet.* 86:696–706.
- Longair, M.H., D.A. Baker, and J.D. Armstrong. 2011. Simple neurite tracer: Open source software for reconstruction, visualization and analysis of neuronal processes. *Bioinformatics*. 27:2453–2454.
- Mann, S., and S. Kröger. 1996. Agrin is synthesized by retinal cells and colocalizes with gephyrin. *Mol. Cell. Neurosci.* 8:1–13.
- Mantych, K.B., and A. Ferreira. 2001. Agrin differentially regulates the rates of axonal and dendritic elongation in cultured hippocampal neurons. *J. Neurosci.* 21:6802–6809.
- May, P., A. Rohlmann, H.H. Bock, K. Zurhove, J.D. Marth, E.D. Schomburg, J.L. Noebels, U. Beffert, J.D. Sweatt, E.J. Weeber, and J. Herz. 2004. Neuronal LRP1 functionally associates with postsynaptic proteins and is required for normal motor function in mice. *Mol. Cell. Biol.* 24:8872–8883.
- McConville, J., and A. Vincent. 2002. Diseases of the neuromuscular junction. *Curr. Opin. Pharmacol.* 2:296–301.
- McMahan, U.J. 1990. The agrin hypothesis. *Cold Spring Harb. Symp. Quant. Biol.* 55:407–418.
- Ming, G. li, and H. Song. 2011. Adult Neurogenesis in the Mammalian Brain: Significant Answers and Significant Questions. *Neuron*. 70:687–702.
- Moll, J., P. Barzaghi, S. Lin, G. Bezakova, H. Lochmüller, E. Engvall, U. Müller, and M.A. Ruegg. 2001. An agrin minigene rescues dystrophic symptoms in a mouse model for congenital muscular dystrophy. *Nature*. 413:302–307.
- Mori, T., K. Tanaka, A. Buffo, W. Wurst, R. Kühn, and M. Gotz. 2006. Inducible gene deletion in astroglia and radial glia - A valuable tool for functional and lineage analysis. *Glia*. 54:21–34.

- Mullen, R.J., C.R. Buck, and A.M. Smith. 1992. NeuN, a neuronal specific nuclear protein in vertebrates. *Development*. 116:201–211.
- Nakamura, T., M.C. Colbert, and J. Robbins. 2006. Neural crest cells retain multipotential characteristics in the developing valves and label the cardiac conduction system. *Circ. Res.* 98:1547–1554.
- Nakayama, M., D. Nakajima, T. Nagase, N. Nomura, N. Seki, and O. Ohara. 1998. Identification of high-molecular-weight proteins with multiple EGF-like motifs by motif-trap screening. *Genomics*. 51:27–34.
- Neumann, F.R., G. Bittcher, M. Annies, B. Schumacher, S. Kröger, and M.A. Ruegg. 2001. An alternative amino-terminus expressed in the central nervous system converts agrin to a type II transmembrane protein. *Mol. Cell. Neurosci.* 17:208–225.
- Nitkin, R.M., M. a. Smith, C. Magill, J.R. Fallon, Y.M. Yao, B.G. Wallace, and U.J. McMahan. 1987. Identification of agrin, a synaptic organizing protein from Torpedo electric organ. *J. Cell Biol.* 105:2471–2478.
- Noctor, S.C., V. Martínez-Cerdeño, and A.R. Kriegstein. 2007. Contribution of intermediate progenitor cells to cortical histogenesis. *Arch. Neurol.* 64:639–642.
- O'Connor, L.T., J.C. Lauterborn, C.M. Gall, and M.A. Smith. 1994. Localization and alternative splicing of agrin mRNA in adult rat brain: transcripts encoding isoforms that aggregate acetylcholine receptors are not restricted to cholinergic regions. *J. Neurosci.* 14:1141–1152.
- Ohazama, A., E.B. Johnson, M.S. Ota, H.J. Choi, T. Porntaveetus, S. Oommen, N. Itoh, K. Eto, A. Gritli-Linde, J. Herz, and P.T. Sharpe. 2008. Lrp4 modulates extracellular integration of cell signaling pathways in development. *PLoS One*. 3(12): e4092.
- Parrish, J.Z., K. Emoto, M.D. Kim, and Y.N. Jan. 2007. Mechanisms that regulate establishment, maintenance, and remodeling of dendritic fields. *Annu. Rev. Neurosci.* 30:399–423.
- Parrish, J.Z., M.D. Kim, Y.J. Lily, and N.J. Yuh. 2006. Genome-wide analyses identify transcription factors required for proper morphogenesis of Drosophila sensory neuron dendrites. *Genes Dev.* 20:820–835.
- Pereda, A.E. 2014. Electrical synapses and their functional interactions with chemical synapses. *Nat. Rev. Neurosci.* 15:250–63.

- Pevzner, A., B. Schoser, K. Peters, N.C. Cosma, A. Karakatsani, B. Schalke, A. Melms, and S. Kröger. 2012. Anti-LRP4 autoantibodies in AChR- and MuSK-antibodynegative myasthenia gravis. *J. Neurol.* 259:427–435.
- Pohlkamp, T., M. Durakoglugil, C. Lane-Donovan, X. Xian, E.B. Johnson, R.E. Hammer, and J. Herz. 2015. Lrp4 Domains Differentially Regulate Limb/Brain Development and Synaptic Plasticity. *PLoS One.* 10:e0116701.
- Pradidarcheep, W., W.T. Labruyère, N.F. Dabhoiwala, and W.H. Lamers. 2008. Lack of specificity of commercially available antisera: better specifications needed. *J. Histochem. Cytochem.* 56:1099–1111.
- Punga, A.R., and M.A. Ruegg. 2012. Signaling and aging at the neuromuscular synapse: lessons learnt from neuromuscular diseases. *Curr. Opin. Pharmacol.* 12:340–346.
- Qiu, S., K.M. Korwek, and E.J. Weeber. 2006. A fresh look at an ancient receptor family : Emerging roles for low density lipoprotein receptors in synaptic plasticity and memory formation. *Neurobiol Learn Mem.* 85:16–29.
- Rimer, M., I. Mathiesen, T. Lømo, and U.J. McMahan. 1997. gamma-AChR/epsilon-AChR switch at agrin-induced postsynaptic-like apparatus in skeletal muscle. *Mol. Cell. Neurosci.* 9:254–263.
- Schlessinger, J. 2000. Cell signaling by receptor tyrosine kinases. *Cell.* 103:211–225.
- Schröder, J.E., M.R. Tegeler, U. Großhans, E. Porten, M. Blank, J. Lee, C. Esapa, D.J. Blake, and S. Kröger. 2007. Dystroglycan regulates structure, proliferation and differentiation of neuroepithelial cells in the developing vertebrate CNS. *Dev. Biol.* 307:62–78.
- Shen, C., W.-C. Xiong, and L. Mei. 2015. LRP4 in neuromuscular junction and bone development and diseases. *Bone.* 80:101-108.
- Sheng, M., and E. Kim. 2011. The postsynaptic organization of synapses. *Cold Spring Harb. Perspect. Biol.* 3(12):a005678.
- Simon-Chazottes, D., S. Tutois, M. Kuehn, M. Evans, F. Bourgade, S. Cook, M.T. Davisson, and J.L. Guénet. 2006. Mutations in the gene encoding the low-density lipoprotein receptor LRP4 cause abnormal limb development in the mouse. *Genomics.* 87:673–677.
- Sloviter, R.S., and G. Nilaver. 1987. Immunocytochemical localization of GABA-, cholecystokinin-, vasoactive intestinal polypeptide-, and somatostatin-like

- immunoreactivity in the area dentata and hippocampus of the rat. *J. Comp. Neurol.* 256:42–60.
- Stuart, G., N. Spruston, B. Sakmann, and M. Hausser. 1997. Action potential initiation and back propagation in neurons of the mammalian central nervous system. *Trends Neurosci.* 20:125–131.
- Threadgill, R., K. Bobb, and A. Ghosh. 1997. Regulation of dendritic growth and remodeling by Rho, Rac, and Cdc42. *Neuron.* 19:625–624.
- Tian, Q.B., T. Suzuki, T. Yamauchi, H. Sakagami, Y. Yoshimura, S. Miyazawa, K. Nakayama, F. Saitoh, J.P. Zhang, Y. Lu, H. Kondo, and S. Endo. 2006. Interaction of LDL receptor-related protein 4 (LRP4) with postsynaptic scaffold proteins via its C-terminal PDZ domain-binding motif, and its regulation by Ca<sup>2+</sup>/calmodulin-dependent protein kinase II. *Eur. J. Neurosci.* 23:2864–2876.
- Tintignac, L.A., H.-R. Brenner, and M.A. Ruegg. 2015. Mechanisms Regulating Neuromuscular Junction Development and Function and Causes of Muscle Wasting. *Physiol. Rev.* 95:809–852.
- Toni, N., D.A. Laplagne, C. Zhao, G. Lombardi, C.E. Ribak, F.H. Gage, and A.F. Schinder. 2008. Neurons born in the adult dentate gyrus form functional synapses with target cells. *Nat. Neurosci.* 11:901–907.
- Tsim, K.W., M.A. Ruegg, G. Escher, S. Kröger, and U.J. McMahan. 1992. cDNA that encodes active agrin. *Neuron.* 8:677–689.
- Walz, W. 2000. Controversy surrounding the existence of discrete functional classes of astrocytes in adult gray matter. *Glia.* 31:95–103.
- Weatherbee, S.D., K. V Anderson, and L.A. Niswander. 2006. LDL-receptor-related protein 4 is crucial for formation of the neuromuscular junction. *Development.* 133:4993–5000.
- Wickersham, I.R., S. Finke, K.-K. Conzelmann, and E.M. Callaway. 2007a. Retrograde neuronal tracing with a deletion-mutant rabies virus. *Nat. Methods.* 4:47–49.
- Wickersham, I.R., D.C. Lyon, R.J.O. Barnard, T. Mori, S. Finke, K.K. Conzelmann, J.A.T. Young, and E.M. Callaway. 2007b. Monosynaptic Restriction of Transsynaptic Tracing from Single, Genetically Targeted Neurons. *Neuron.* 53:639–647.



- Wu, H., Y. Lu, C. Shen, N. Patel, L. Gan, W.C. Xiong, and L. Mei. 2012. Distinct roles of muscle and motoneuron LRP4 in neuromuscular junction formation. *Neuron*. 75:94–107.
- Wu, H., W.C. Xiong, and L. Mei. 2010. To build a synapse: signaling pathways in neuromuscular junction assembly. *Development*. 137:1017–1033.
- Yang, X., S. Arber, C. William, L. Li, Y. Tanabe, T.M. Jessell, C. Birchmeier, and S.J. Burden. 2001. Patterning of muscle acetylcholine receptor gene expression in the absence of motor innervation. *Neuron*. 30:399–410.
- Yumoto, N., N. Kim, and S.J. Burden. 2012. Lrp4 is a retrograde signal for presynaptic differentiation at neuromuscular synapses. *Nature*. 489:438–442.
- Zhang, B., C. Liang, R. Bates, Y. Yin, W.-C. Xiong, and L. Mei. 2012. Wnt proteins regulate acetylcholine receptor clustering in muscle cells. *Mol. Brain*. 5:7.
- Zhang, B., S. Luo, Q. Wang, T. Suzuki, W.C. Xiong, and L. Mei. 2008. LRP4 Serves as a Coreceptor of Agrin. *Neuron*. 60:285–297.
- Zhang, W., A.S. Coldefy, S.R. Hubbard, and S.J. Burden. 2011. Agrin binds to the N-terminal region of Lrp4 protein and stimulates association between Lrp4 and the first immunoglobulin-like domain in muscle-specific kinase (MuSK). *J. Biol. Chem*. 286:40624–40630.
- Zong, Y., B. Zhang, S. Gu, K. Lee, J. Zhou, G. Yao, D. Figueiredo, K. Perry, L. Mei, and R. Jin. 2012. Structural basis of agrin-LRP4-MuSK signaling. *Genes Dev*. 26:247–258.



## 6 Appendix

### 6.1 Appendix 1: List of abbreviations

**AChR:** acetylcholine receptor

**CAG:** chicken- $\beta$ -actin

**cDNA:** complementary deoxyribonucleic acid

**CMV:** cytomegalovirus

**CNS:** central nervous system

**DAPI** (4',6-diamidino-2-phenylindole)

**Dcx:** doublecortin

**DIV:** day *in vitro*

**E:** embryonic day

**eGFP:** enhanced green fluorescent protein

**G:** rabies virus glycoprotein

**GABA:** g-amino-butyric acid

**GFAP:** glial fibrillary acidic protein

**HEK:** human embryonic kidney

**kD:** kilo Daltons

**LRP4:** low-density lipoprotein receptor-related protein 4

**MAP2:** microtubule associated protein 2

**mRNA:** messenger ribonucleic acid

**MuSK:** muscle specific tyrosine kinase

**NMJ:** neuromuscular junction

**PFA:** paraformaldehyde

**RABV:** EnvA-pseudotyped rabies virus

**RFP:** red fluorescent protein

**SEZ:** subependymal zone

**SYN:** synapsin

**SV2:** synaptobrevin2

**TM:** transmembrane

**TVA:** tumor virus A

**WB:** Western blotting

**$\mu$ m:** micrometer



## 6.2 Appendix 2: List of figures

- Figure 1.1** Stages of neuronal polarization
- Figure 1.2** Morphology of dendritic spines
- Figure 1.3** Structure of the chemical synapse
- Figure 1.4** A working model for the agrin/LRP4/MuSK signaling pathway at the NMJ
- Figure 1.5** The LDL receptor family
- Figure 1.6** Domain structure of LRP4
- Figure 1.7** The agrin/LRP4/MuSK complex at the NMJ
- Figure 3.1** Test of antibody specificity using transiently transfected HEK293 cells with full length LRP4
- Figure 3.2** Test of antibody specificity using transiently transfected HEK293 cells with extracellular LRP4
- Figure 3.3** Analysis of antibody specificity in Western blotting
- Figure 3.4** Analysis of LRP4 localization at the adult NMJ and antibody specificity
- Figure 3.5** Test of antibody specificity – antibody antigen competition experiment
- Figure 3.6** *lrp4* mRNA is present in the murine brain and eyes during development and in adult stages
- Figure 3.7** LRP4 protein is present in the adult mouse brain
- Figure 3.8** Distribution of LRP4 in the neurons of the adult murine cortex
- Figure 3.9** Distribution of LRP4 in astrocytes of the adult murine cortex
- Figure 3.10** Distribution of LRP4 in the adult murine hippocampus
- Figure 3.11** Overview of LRP4 distribution in the adult-born neurons
- Figure 3.12** Distribution of LRP4 in the adult murine cerebellum
- Figure 3.13** Endogenous LRP4 expression in dissociated cultures from the embryonic cerebral cortex and hippocampus
- Figure 3.14** Distribution of LRP4 in hippocampal neuronal cultures
- Figure 3.15** LRP4 protein is present in lysates from cortical and hippocampal neurons
- Figure 3.16** LRP4 is present in both glutamatergic and GABAergic neurons
- Figure 3.17** LRP4 is present in astrocytes in low levels
- Figure 3.18** Constructs for expression of GFP:actin and LRP4 in neurons *in vitro*
- Figure 3.19** LRP4 affects the number and length of dendrites and the number of spines in cultured cortical and hippocampal neurons
- Figure 3.20** Overexpression of LRP4 in cultured cortical neurons reduces the dynamics of the primary dendrite growth

**Figure 3.21** LRP4 affects the number of pre- and post-synaptic specializations in neuronal cultures

**Figure 3.22** Generation and test of microRNAs targeting LRP4

**Figure 3.23** Constructs for expression of RFP, LRP4 and miRLRP4

**Figure 3.24** Knockdown of LRP4 in dissociated neuronal cultures decreases the number of presynaptic partners

**Figure 3.25** Colocalization and functional interaction of LRP4 and the transmembrane form of agrin on dendrites *in vitro*

**Figure 3.26** Overexpression of LRP4 in MuSK<sup>+/+</sup>, MuSK <sup>+/-</sup> and MuSK <sup>-/-</sup> hippocampal neurons

### **6.3 Appendix 3: List of tables**

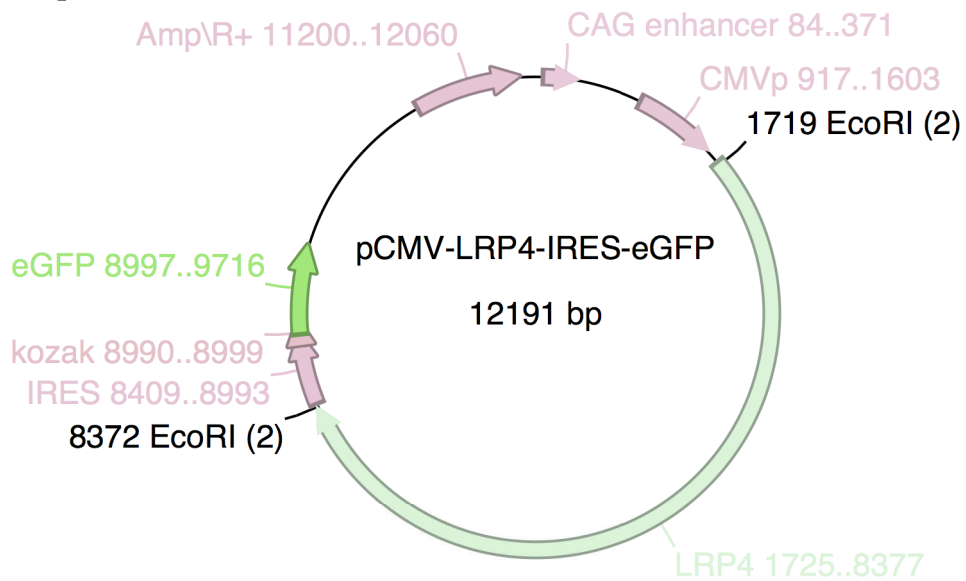
<b>Table 1</b>	Primary antibodies
<b>Table 2</b>	Secondary antibodies
<b>Table 3</b>	Buffers and solutions
<b>Table 4</b>	Media for cells and bacteria culture
<b>Table 5</b>	Prokaryotic and eukaryotic cell lines



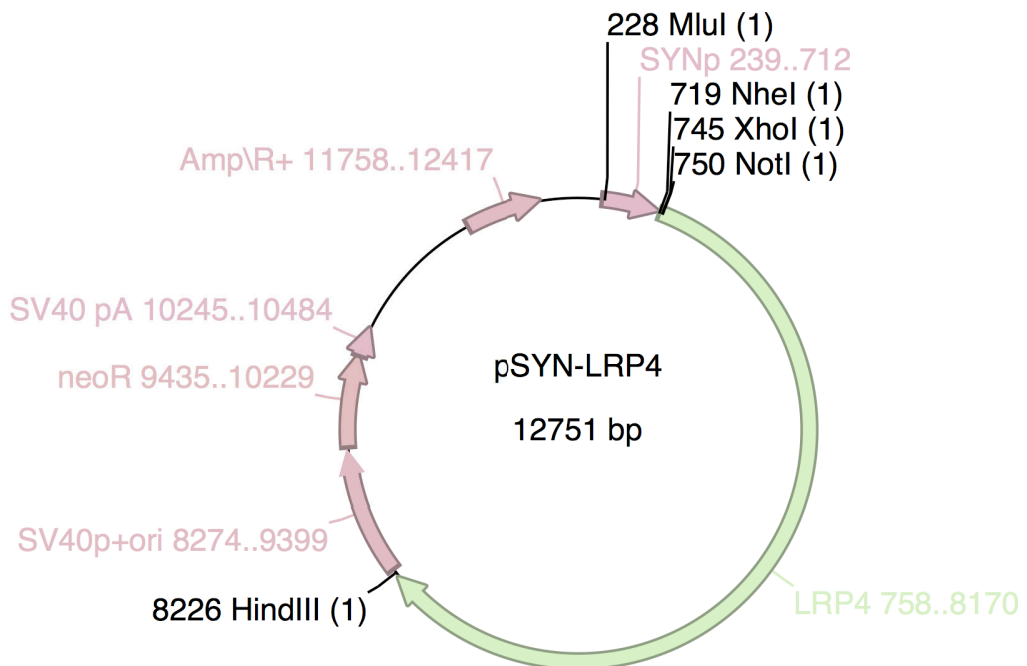


## 6.4 Appendix 3: Plasmid maps

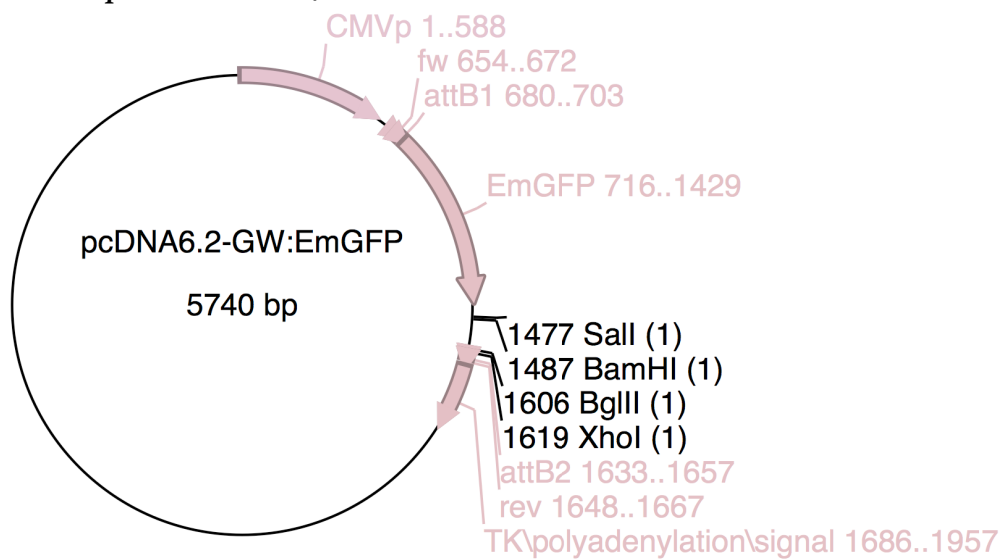
### 6.4.1 pCMV-LRP4-IRES-eGFP



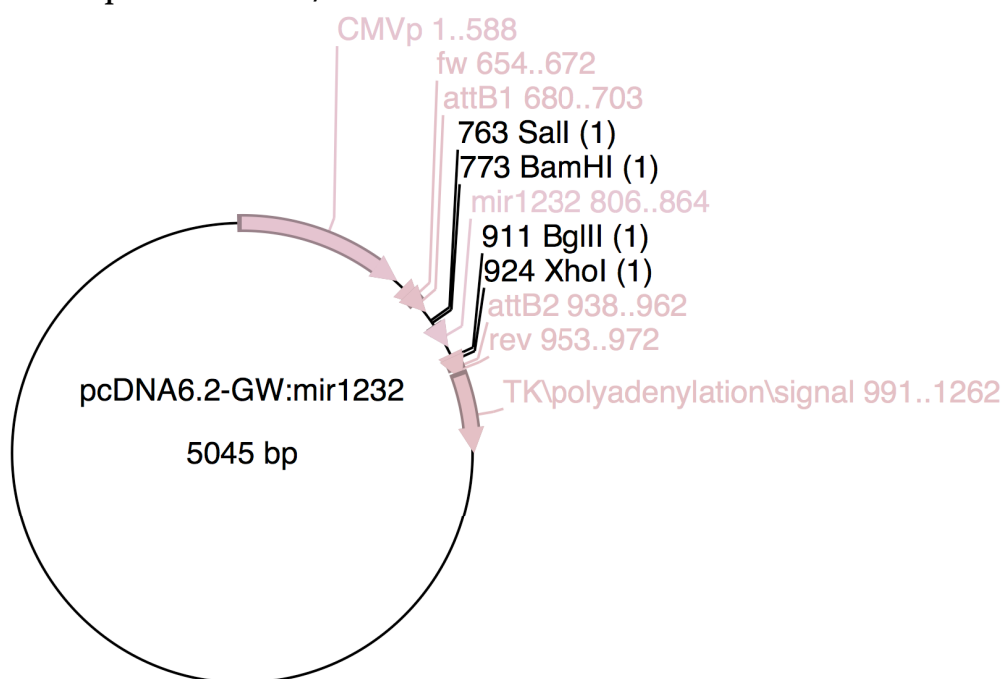
### 6.4.2 pSYN-LRP4



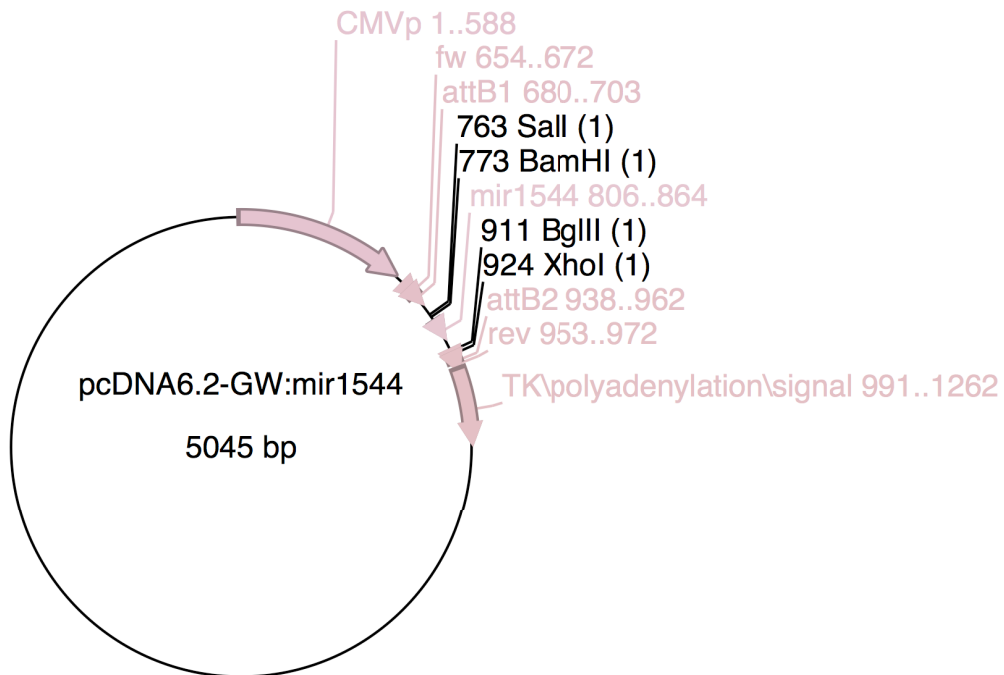
### 6.4.3 pcDNA6.2-GW/EmGFP



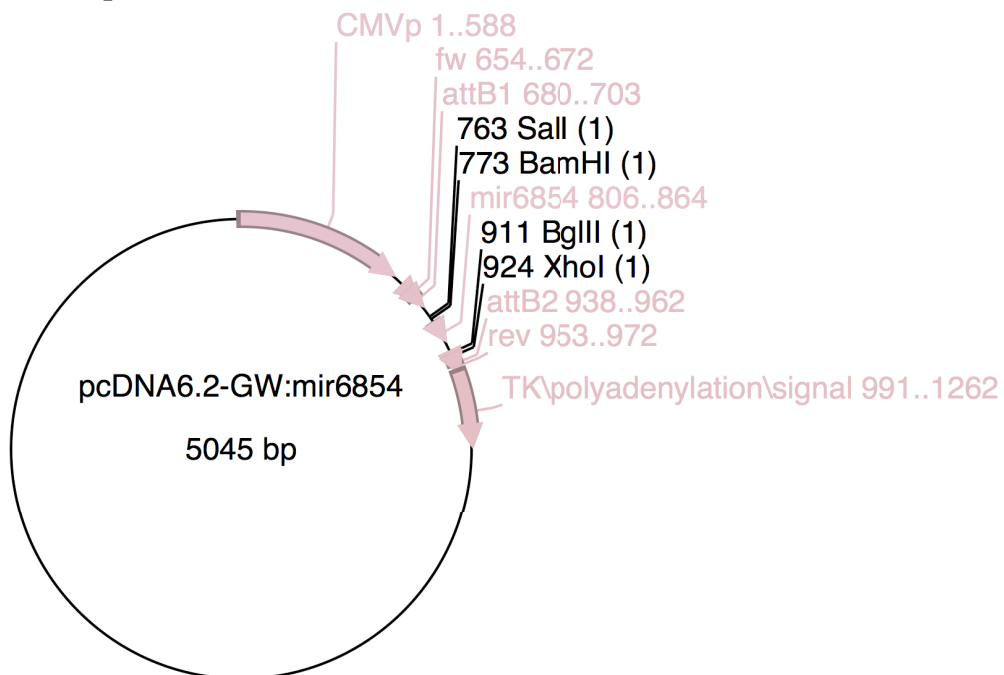
### 6.4.4 pcDNA6.2-GW/mir1232



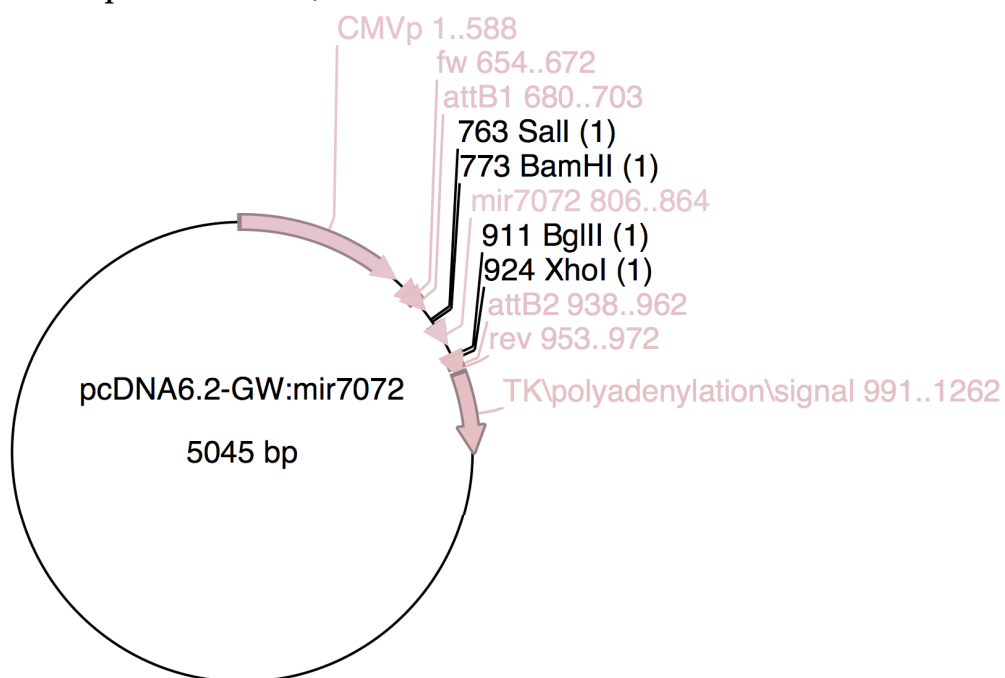
## 6.4.5 pcDNA6.2-GW/mir1544



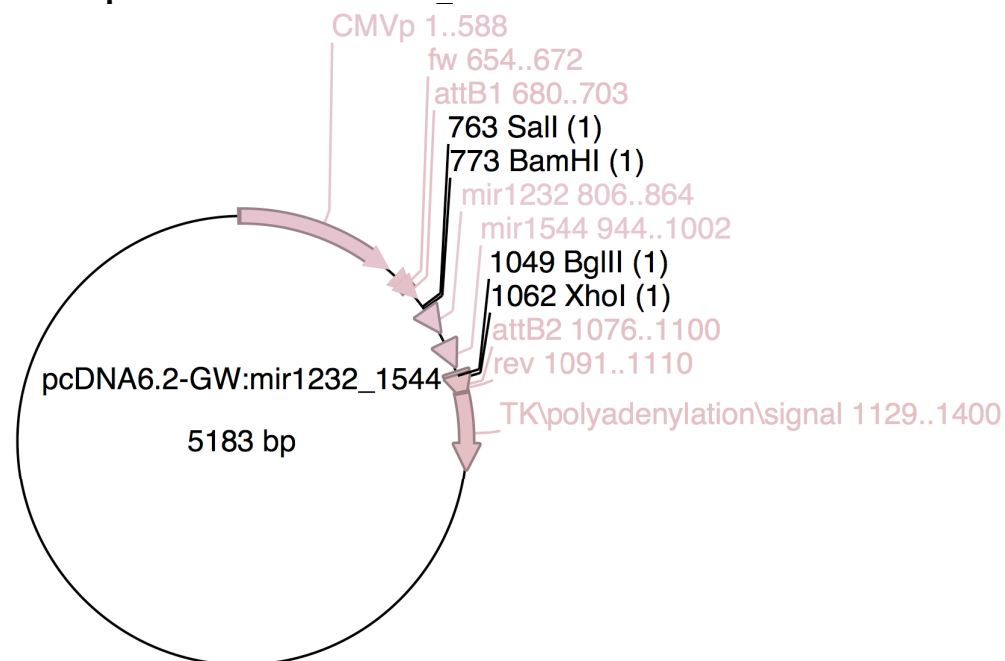
## 6.4.6 pcDNA6.2-GW/mir6854



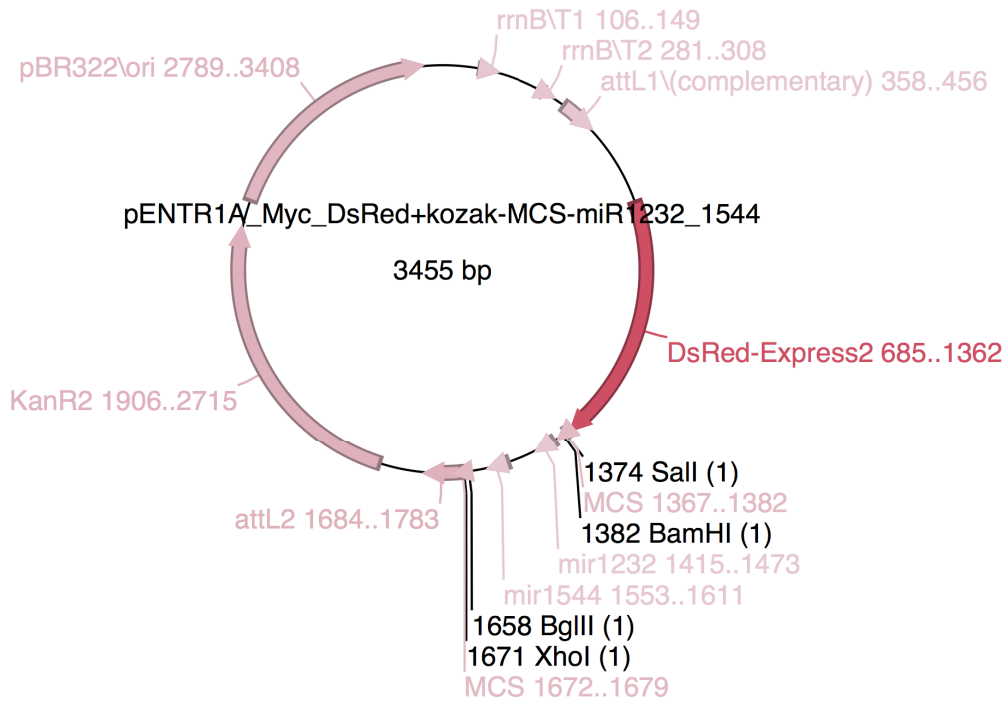
#### 6.4.7 pcDNA6.2-GW/mir7072



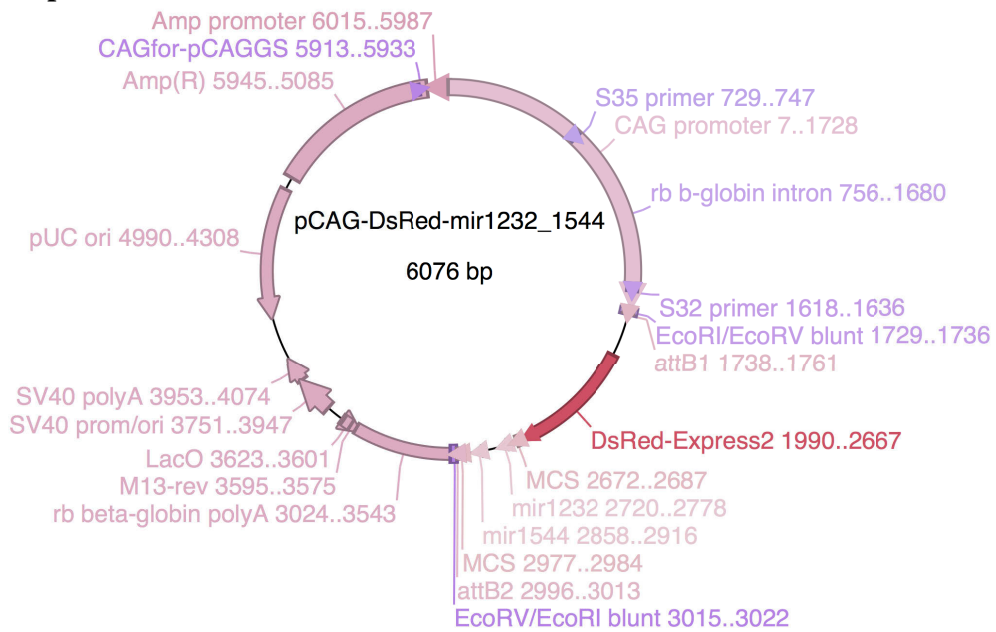
#### 6.4.8 pcDNA6.2-GW/mir1232\_1544



#### 6.4.9 pENTR1A\_mir1232\_1544



#### 6.4.10 pCAG-miR-RFP





## List of publications

This dissertation will be published as follows:

1. **Andromachi Karakatsani**, Anna Schick, Elisa Murenu, Georgios Kalamakis, Yina Zhang, Alexander Ghanem, Karl-Klaus Conzelmann, Markus A. Rüegg, Sergio Gascon\*, Stephan Kröger\*. “*LRP4 regulates dendritic arborization and synapse formation in central nervous system neurons.*” In preparation.

Other publications:

2. Yina Zhang, Shuo Lin, **Andromachi Karakatsani**, Markus A. Rüegg, Stephan Kröger. “*Differential regulation of AChR clustering in the polar and equatorial region of murine muscle spindles.*” Eur J Neurosci. 2015 Jan;41(1):69-78.

3. Yina Zhang, Marta Wesolowski, **Andromachi Karakatsani**, Veit Witzemann, Stephan Kröger. “*Formation of cholinergic synapse-like specializations at developing murine muscle spindles.*” Dev Biol. 2014 Sep 15;393(2):227-235.

4. Hong Y Choi, Yun Liu, Christian Tennert, Yoshie Sugiura, **Andromachi Karakatsani**, Stephan Kröger, Eric B Johnson, Robert E Hammer, Weichun Lin, Joachim Herz. “*APP interacts with LRP4 and agrin to coordinate the development of the neuromuscular junction in mice.*” eLife 2013;2:e00220.

5. Alexandra Pevzner, Benedikt Schoser, Katja Peters, Nicoleta-Carmen Cosma, **Andromachi Karakatsani**, Berthold Schalke, Arthur Melms, Stephan Kröger. “*Anti-LRP4 autoantibodies in AChR- and MuSK-antibody-negative myasthenia gravis.*” J Neurol. 2012 Mar;259(3):427-435.





## Acknowledgements

The path toward this dissertation has been long and circuitous, with enjoyable, but often intense and tempestuous moments. My accomplishment would lose merit if I did not thank a number of wonderful individuals for being part of this journey and making this thesis possible.

First and foremost I would like to thank Stephan Kröger for giving me the opportunity to pursue a PhD in his laboratory. I am very grateful for his support, patience and encouragement at all times. Also I thank him for giving me the freedom to explore my project by my own and guiding me when I was losing focus.

I am thankful to Hans Straka for being my supervisor from the Faculty of Biology and for all his support and guidance during my TAC meetings; to Magdalena Götz and Joachim Graw for their thoughtful feedback and advice; to Karl-Klaus Conzelmann for providing me with rabies virus; to Markus Rüegg and Wilko D. Altmann for sharing antibodies. I would also like to extend my gratitude to Carmen Ruiz de Almodóvar for her support, patience and help during the last months.

I am truly grateful to Sergio Gascon for following my project with great interest, for his constant intellectual and experimental help with my project, and, most importantly, for being an amazing and patient friend.

A cordial thank you to all the members of the lab; Yina Zhang for being my companion-in-arms through this journey; Alex Pevzner and Nicoleta Carmen Cosma for sharing interesting ideas and long philosophical discussions; Katja Peters, Martina Bürkle and Tatiana Simon-Ebert (neighbor lab) for their technical assistance. Also, a thank you to Julia Meltoranta, Anna Schick, Marta Wesolowska, and Christiane Gasperi for all the scientific discussions and for having a great lab atmosphere. Without their support and kindness working in the lab would have been a lot more different. I would also like to thank Lana Polero and Suada Ajanovic for helping me with the paperwork issues. A great thank you to all the people in the present lab here in Heidelberg; Severino Urban, Robert Luck, Heike Adler, Laura Castro, Isidora Paredes, Aida Freire, Nathalie Tisch, Patricia Himmels and Xiaohong Wang for all the support and the warm and friendly atmosphere during the last months of the PhD. Last, but not least, many thanks to Enric and Wilson for the long writing nights at the lab – stress is better when shared.

Luckily, along the way I met wonderful friends who gave me a sense of family and belonging and helped me settle in a new and foreign culture. A heart-felt thank you to my friends Elisa, Sofia, Aditi, Francesca, and Felipe for being always there for me.

Lastly, I would like to thank those people who have been instrumental in their support and encouragement. A hearted thank you to my parents for instilling in me the ethics of hard work

---

## Acknowledgements

---

and patiently supporting me in every single decision I make. To my sister and brother for always believing in me. Above all, a heart-felt thank you to my soul mate, Giorgos, for being a source of happiness and strength, and patiently walking this way by my side.

Andromachi.

## Curriculum Vitae

### PERSONAL DATA

---

Name: Andromachi Karakatsani  
Date of Birth: 04. June 1986  
Nationality: Greek  
Email Address: [Andy.Kara@med.uni-muenchen.de](mailto:Andy.Kara@med.uni-muenchen.de)

### EDUCATION

---

6/2004: **HIGH SCHOOL DIPLOMA** with “Honours of Excellence” from the Greek Minister of Education.  
9/2004-9/2008: **DIPLOMA STUDIES**, Department of Molecular Biology & Genetics (MBG), Democritus University of Thrace, Greece.  
10/2008-6/2009: **DIPLOMA THESIS**, Department of Molecular Biology & Genetics (MBG), Democritus University of Thrace (ASS. PROF. MARIA GRIGORIOU).  
7/2009-present: **PHD STUDIES**, Institute of Physiological Genomics of Ludwig Maximilians University (LMU), Munich (PROF. Dr. STEPHAN KRÖGER).

### RESEARCH EXPERIENCE

---

11/2006-6/2007: Practical training in basic techniques used in Molecular, Cellular and Developmental Biology under the supervision of Ass. Prof. Maria Grigoriou and Ass. Prof. Georgios Skavdis.  
2/2008-6/2009: Research scholar under the supervision of Ass. Prof. Maria Grigoriou at the laboratory of Molecular Biology of Development & Molecular Neurobiology, at MBG, Greece. Diploma thesis: “*Hepatoma Up – Regulated (hup) gene expression during mouse embryogenesis.*”  
7/2009-present: Research scholar under the supervision of Prof. Dr. Stephan Kröger at the Institute of Physiological Genomics of LMU, Munich. Ph.D. thesis: “*LRP4 regulates dendritic arborization and synapse formation in the central nervous system neurons.*”

### POSTERS & PRESENTATIONS

---

- 10<sup>th</sup> Göttingen Meeting of the German Neuroscience Society, 13-16 March 2013, Göttingen, Germany. Poster presented.
- 18<sup>th</sup> Edition of the International Student Congress of (bio) Medical Sciences, 9<sup>th</sup> June 2011, Groningen, The Netherlands. Poster presented. Best Poster in Neurology Session.
- 12<sup>th</sup> International Congress for Medical Students and Young Health Professionals, “Medicalis”, 12-15 May 2011, Cluj-Napoca, Romania. 2<sup>nd</sup> Prize at the Fundamental Science Oral Presentation section with the paper “*LRP4 is a possible autoantigene in seronegative myasthenia gravis.*”
- <interact> 2011 Ph.D. Symposium, 7<sup>th</sup> April 2011, Munich, Germany. Poster presented.
- 30<sup>th</sup> Scientific Conference of the Hellenic Society for Biological Sciences, 22-24 May 2008, Thessaloniki, Greece. Talk & Poster presented.